MICROCOPY RESOLUTION TEST CHART

NATIONAL BUREAU OF STANDARDS-1963-A

AD-A134796

Illinois Institute of Technology,   Chicago, Illinois 60616

UNDERSTANDING TRANSITION TO TURBULENCE IN SHEAR LAYERS

by

Mark V. Morkovin

May, 1983

iiT

DTIC
ELECTE
NOV 1 7 1983

A

DTIC FILE COPY

83   11   15   175

REPORT DOCUMENTATION PAGE	READ INSTRUCTIONS BEFORE COMPLETING FORM

1. REPORT NUMBER	2 GOVT ACCESSION NO.	3 RECIPIENT'S CATALOG NUMBER
AFOSR-TR- 83-0931	A134794	

4. TITLE (and Subtitle)	5. TYPE OF REPORT & PERIOD COVERED
UNDERSTANDING TRANSITION TO TURBULENCE IN SHEAR LAYERS	Final Oct. 1, 1976 to Dec. 31, 1982
	6 PERFORMING ORG. REPORT NUMBER

7. AUTHOR(s)	8. CONTRACT OR GRANT NUMBER(s)
Mark V. Morkovin	F49620-77-C-0013

9. PERFORMING ORGANIZATION NAME AND ADDRESS	10. PROGRAM ELEMENT PROJECT, TASK AREA & WORK UNIT NUMBERS
Illinois Institute of Technology Mechanical & Aerospace Engineering Chicago, Illinois 60616	61102F 2307/A4

11. CONTROLLING OFFICE NAME AND ADDRESS	12. REPORT DATE
Air Force Office of Scientific Research Building 410 Bolling AFB, D.C. 20332	May 1983
	13. NUMBER OF PAGES
	137

14. MONITORING AGENCY NAME & ADDRESS(if different from Controlling Office)	15. SECURITY CLASS. (of this report)
	Unclassified
	15a. DECLASSIFICATION DOWNGRADING SCHEDULE

16. DISTRIBUTION STATEMENT (of this Report)

Approved for public release; distribution unlimited.

17. DISTRIBUTION STATEMENT (of the abstract entered in Block 20, if different from Report)

18. SUPPLEMENTARY NOTES

19. KEY WORDS (Continue on reverse side if necessary and identify by block number)

Instabilities, transition to turbulence, turbulent-layer instability, shear layers, bifurcations, unstable Navier-Stokes solutions, flow instability mechanisms, vorticity distributions, linearized instability theory, compressibility effects on stability, role of disturbances in transition, free-stream disturbances, transition-conditioned design, receptivity of boundary layers to sound, self-excitation in boundary layers, boundary layers, free shearflows.

20. ABSTRACT (Continue on reverse side if necessary and identify by block number)

Critical examination of experimental, analytical and numerical research on shear-flow instabilities evolving into turbulence led to a conceptual framework consistent with reliable observations. Mechanically driven shear
(continued)

DD FORM 1473 EDITION OF 1 NOV 65 IS OBSOLETE
1 JAN 73

layers fall into four classes , (Fig 0-1): (a) boundary layers, (b) confined duct flows, (c) free shear layers, and (d) flows in annuli between cylinders driven by the rotation of the inner cylinder. These classes correspond to distinct, initially rather homogeneous vorticity distributions. Each instability restructures these distributions; it dehomogenizes them spatially, while the very slow viscous effects smooth the largest gradients. The restructuring continues even after the shear layers become turbulent.

The major mechanisms causing the restructuring are described physically: viscous tuning in wall TS waves, inflectional instability, centrifugal instability, subharmonic vortex amalgamation, vorticity stretching and rotating, and cross-flow instability in three-dimensional layers. The first three and the last cause the initial instabilities, while all may be active in secondary and higher instabilities.

The sequences of instabilities leading to transition to turbulence in flow classes (a) - (d) are strikingly different. Conversion from (c) to (a) by adding one wall stabilizes the flow greatly; the flow may remain laminar for Reynolds numbers far exceeding Re_{cr} (the Re for which it becomes unstable to vanishing disturbances). Adding a second, fully confining wall to obtain category (b) often brings about transition at low Re_{tr} values, not explicable by any existent theory. To account for this anomaly as well as observations in free shear layers at higher Re, a working hypothesis is required which allows for development of very rapid instabilities from more slowly evolving nonequilibrium vorticity configurations.

The other factor essential to reconciliation of such observations is the forcing role of disturbances in the environment, largely neglected by theorists. Classes (a) - (c) comprise open, through-flow systems penetrated by invariably unknown mixtures of vorticity disturbances from upstream and pressure fluctuations from all directions. This controlling factor, ever present in flows common in technology, makes the onset of turbulence much more erratic than in the closed systems (d). On the other hand, deliberately induced special disturbances provide a measure of control over the onset and the initial structure of turbulence (which, after all, can be either friend or foe).

In applications, theoretical tools are pragmatically restricted to linear analyses of the first restructuring. The linear tools for diagnostics and possible aid in design for Re larger than Re_{cr} are reviewed and evaluated. The importance of existence of transitions in which the instability mechanisms have not yet been identified (such as for distributed roughness) is stressed.

UNDERSTANDING TRANSITION TO TURBULENCE IN SHEAR LAYERS - 1983

Mark V. Morkovin

F I G U R E S

INTRODUCTION

This Final Report on AFOSR Contract F49620-77-C-0013 deals with
the perspective and main issues of the problem of shear-flow instabi-
lities and transition to turbulence as relevant to modern aerodynami-
cally conditioned technology. The objective is to provide a "feel" for
the instability phenomena and the transition field as a whole. Such
perspective should be especially useful when approaching questions of
further development and research in the field. The specialist who is
interested in the experimental and partly theoretical documentation of
these ideas, or in the details of important experiments of the past,
will find them in the associated Technical Report, a comprehensive
monograph entitled: "Guide to Experiments on Instability and Laminar-
Turbulent Transition in Shear Layers". Of necessity, the Final Report
must refer to the Guide for the substantiation of the statements and
viewpoints presented here. In a certain sense it can also be considered
as an introduction for the prospective user of the Guide.

Instabilities in turbulence

The knowledge of shear turbulence is still a rapidly developing
subject, even though it has been over a hundred years since turbulence
was identified by Osborne Reynolds. Modern instrumentation and data
processing opened up a new perception of turbulence a dozen years ago,
when conditional sampling of flows became possible. It turns out that
most of the so-called coherent turbulent structures (that emerged as the
key new concept beyond Reynolds averaging) originate during the last of
the sequence of instabilities. When the work on the Guide began late in
1976, such a relation between sequences of instabilities and turbulence
was merely a conjecture among a few specialists. The idea was first
stated publically, for the clearer special case of mixing layers, at a
NASA conference in 1972. It was becoming more evident, however, that
the unifying key to the mechanisms in the transition processes, as
within turbulence itself, is the behavior of distributions of vorticity.

The transition process is now identified as a sequence of instabilities and restructuring of the rather homogeneous initial vorticity distribution in the original laminar shear layer. Evidently the self-interaction of the vorticity fields continues once the state of turbulence, with its characteristic transport processes, has been established. Instabilities have not ceased.

Forced transition and receptivity

These sequences are described, in terms as physical as possible, in the 0.02 Sections of the Report. They are strongly conditioned by the geometry of the shear layer and by the nature and strength of the flow disturbances in the environment. The so-called "natural" transition turns out to be "forced" or "controlled" by the specific environmental disturbances in the through-flow systems prevalent in nature and technology.

The mechanisms whereby the external disturbances become internalized as unsteady vorticity disturbances from which the restructuring of the whole distribution grows are collectively characterized as the receptivity of the shear layers. During the preparation of the Guide a mode of receptivity to external unsteady pressure fields in boundary layers was identified and documented by M. Nishioka and the author. It is believed to dominate in external flows around shaped bodies. However, receptivity to ambient vorticity fields, the remnants of older turbulence from upstream origins, remains one of the two most difficult problems in transition. The other is the identification of the mechanism through which distributed roughness leads to transition. How smooth does a surface have to be to remain laminar at high Reynolds numbers, for instance in the highly accelerated regions of airfoils or circular cylinders?

Control of the nonunique paths to turbulence?

Instabilities arise because, as Reynolds number increases, the highly nonlinear flows possess many possible local vorticity configurations. Nor is the specific sequence of instabilities for a given

geometry unique. Improved knowledge about the mechanisms of receptivity and about efficient ways of tripping the layer should also make it possible to modify for various pragmatic reasons the path of the evolution to turbulence. This implies partial control of the energetic coherent structures, at least during the early stages of turbulence.

Such a surmise may seem more likely for free shear layers -- jets, wakes, mixing layers. For these, the receptivity to unsteady pressure gradients at the lines of separation, where the layers are born, is extremely efficient and can be used for control at distance across streamlines. Whatever controlled unsteady vorticity is created at the trailing edges becomes immediately amplified by the powerful inflectional instability of the shear layer. This is a very effective combination, which fuels most flow-conditioned acoustic resonances, including organ pipes and destructive resonances in heat exchangers. Additional ways of influencing aero-acoustic noise of jets and the mixedness in fuels may possibly be found in studying the control processes. Turbulence, after all, can be friend or foe, depending on the nature of the objectives. Twenty people died in Sonora, PA from pollution effects some thirty years ago when the atmosphere was not sufficiently turbulent. And Prandtl showed the value of turbulence when he dramatically decreased the drag of a sphere by making its boundary layer turbulent.

Besides the obvious need for optimal tripping in boundary layers (not yet mastered) to preempt laminar stall in its various guises, controlling coherent structures in boundary layers may seem farfetched. Yet, a tentative consensus is developing among researchers that the turbulent boundary layers commonly studied in the laboratories do not achieve sufficiently high Reynolds numbers to escape the heavy imprint of the original mode of transition. The suspicion is growing that the specific manner in which turbulent spots are seeded may lead to turbulent skin friction which is not necessarily minimal. Since conducting research and development tests on turbulent boundary layers at very high Reynolds numbers runs into horrendous costs, it would be helpful if we could age the boundary layers artificially, with confidence in the

generality of the results. Automated multidimensional traversing, combined with state-of-the-art data processing, seems to make research on the relationship between the topographics of transition and the subsequent character of the turbulent boundary layer (especially the evolution of its large-scale structures and skin friction) nearly at hand. As of 1982 we can identify three distinct local geometries of breakdown to turbulence in smooth laminar boundary layers on convex bodies, but we know next to nothing about the seeding rates of turbulent spots. The thesis of Savas (1979) has unsettled past views on the growth and interaction of turbulent spots; that topic should therefore be part of any effort along the above lines.

Conceptual and theoretical background

As we discover more facets to the transition processes, many previously contradictory experiments become reconcilable in terms of hidden, previously unsuspected parameters. A researcher, interested in instability theory, may attack his problem with ad hoc assumptions, facilitating the next difficult step forward, without worrying about the overall harmony in the field or consistency with the sea of experimental literature. For a critical interpreter of the body of experimental results, consistency of the overall framework of concepts stands as a first prerequisite. Unexplained exceptions depreciate the reliability of judgment in the context of transition. Examples of classes of transition for which we still do not have rational explanations are cited in the missing-link Section 0.03.07.

Beyond that, two discordant strains from the general trend in stability theory run through the interpretations of the specific cases in the Guide. In fairness, it should be mentioned that the need for a different view arose in studying through-flow systems like those in Figs 0-1a,b,c , most of which are characterized by a streamwise growing scale $\delta(x)$, and consequently by $Re(x)$. To date, little theory aims at these more complex systems.

It is the experimental facts and recent numerical investigations that force the author to stray from the fold. Further progress in our understanding seemed thwarted without the following working hypothesis: There exist processes, rapid with respect to the normal flow evolution which are identifiable as instabilities and yet develop without passing through an equilibrium. In fact, several competing instabilities commonly overlap spatially and proceed simultaneously in free shear layers at higher Reynolds numbers. (At high Re, saturation has little meaning until the free flow has gone through the instability on its largest scale.) The numerical experimentation by Orszag and coworkers on duct and pipe flows and the plane Couette flow also document the possibility of instability in absence of an equilibrium. The instabilities in all such cases are rapid, i.e. inviscid in nature.

The other partially discordant view is on the dominance in through-flow systems of the role of environmental disturbances, as already mentioned. The long standing paradox of early transition in wall-confined through-flows cannot be explained except through finite initial disturbances. In recent years, there have been some helpful theoretical contributions on the associated linearized receptivity problems. In fact, because in wall layers the initial instability is the slowest, i.e. the rate-controlling bottleneck on the road to transition, quantitative linear theories constitute the chief tools for diagnostics and whatever judicial estimates of transition situations we can make. Usage of linearized computer codes, of course, has to be buttressed by theoretico-empirical qualitative understanding.

This qualitative understanding itself is based on the mathematical structure of each problem and on associated detail experimental experience, the subject matter of the Guide. A glance at the subtitles in the Contents will show the recurrent linkage between theory, concept, and experiment. In particular, the 0.04 Sections illustrate the character of the available linearized information and its judicial application. The collection of charts and their illustrated usage should

particularly benefit the development engineer as well as an engineering graduate student. Although theoretical concepts of necessity enter this report and the Guide, the reader need not understand all details at first reading. It is hoped that the account is sufficiently descriptive to provide the needed broader background of understanding. The theoretically inclined reader, on the other hand, may also find some nuggets for thought -- the challenge of critically appraised experimental information.

0.01   HOW TO DESCRIBE THE TRANSITION PROCESS?

There is no generally accepted definition of the onset of tur-
bulence in a flow; even definitions of turbulence itself differ. The
point of view adopted in the Guide rests on modern interpretations of
the classical concepts of turbulence, e.g. Liepmann (1979) and Lumley
(1981), and on the practical need for repeatable, operational identifi-
cation of the transition phenomena in the field or laboratory. Without
a consistent point of view, applicable to all the observations in
mechanically driven shear flows, there could be no sensible account of
these challenging phenomena.

0.01.01   Instabilities, onset of turbulence and its identification

As the Reynolds number increases in a given class of flows, the
continuously distributed vorticity in the base shear layer undergoes
successive instabilities, i.e. transformations into increasingly more
complex spatial and temporal patterns of vorticity concentrations. In
two-dimensional instabilities, the initial growth rate of the unsteady
vorticity is usually exponential even though the total vorticity is
preserved (like heat) during these essentially dehomogenizing processes.
At some stage of a sequence of instabilities, the dehomogenized, spotty,
three-dimensional flow becomes operationally indistinguishable from our
perception of classical high-Re turbulence as defined by four key syn-
dromes: Stewart (1969), Tennekes and Lumley (1972, pp 1-3). Of the
four syndromes: irregularity (disorder), three-dimensional vorticity
(eddying), diffusion in excess of molecular transport (mixing), and
dissipation, the first three can be diagnosed by a careful experimenter.
Local onset of smaller-scale turbulent diffusion can often be identified
positively by visualization techniques.

The irregularity syndrome - apparent randomness of motion - represents strange behavior in continuum mechanics and requires instrumentation capable of characterizing stochastic functions. Single sensors at a point disclose broad-band spectra which testify to a sufficiently large range of scales of motion in the turbulence (range of possible cascades). In a sense, large range of scales represents a large number of degrees of freedom in the fluid system, Liepmann (1979). Some researchers call the disorder syndrome "chaotic behavior" and present intriguing evidence that even nonfluid nonlinear systems with large enough degrees of freedom exhibit chaotic behavior in time; in fluid mechanics, however, turbulence is not the only field that can be chaotic. In the free stream of wind tunnels, Chapter 3, at least two sensors are needed to separate random irrotational velocity-pressure fields (which reach across mean streamlines) from the turbulent vorticity-velocity fields (which, to the first order, are convected along mean streamlines).

Ideally, to document the transition process for a given flow, an experimenter should (1) describe the salient features of the successive instabilities (changes in vorticity patterns), and (2) identify the local onset of turbulence by clearcut operational criteria based on as many of the turbulence syndromes as possible. Ideally, to understand the process we should (a) relate all the observed instability characteristics to classes of solutions of Navier-Stokes equations or to classes of solutions of admissibly simplified equations, and (b) clarify the role of external disturbances and, when the role is deemed important, identify the mechanisms through which the influence is exerted (disturbance receptivity); see A.17 of the Guide.

It is the objective of the Guide to report on the current status of the experimental evidence of transition processes and their conceptual understanding for all the major classes of mechanically driven shear layers. Organized recognition of our shortcomings with respect to the ideal described above, and discussion of their causes may perhaps provide a framework for further desirable focused research.

0.01.02   Plan of the Guide

Historically the motivation for transition research came from the needs of practical applications. Fig 0-1 presents four schematic views of some of the conditions which lead to transition in simpler external and internal through-flow systems, in a mixed free-layer system, and in a closed Couette flow system. The Guide will ultimately address all the issues lurking in Fig 0-1, and more. For the present, the figure makes clear that we should first examine instability and transition phenomena in order of increasing complexity and stress the generic aspects of each case in order to build up a broad conceptual base. This is attempted in Chapter 1 for free shear layers and in Chapter 2 for wall layers. The conceptual aspects of the underlying differential equations - the basic mechanisms of the phenomena - are sketched in Appendix A. An engineer rusty on handling of complex notation and eigenvalue problems can refer to Appendix B for illustration of the techniques on simplest instructive examples.

We study in detail, first qualitatively and then more quantitatively, selected evocative experiments from the research literature. In Chapter 1 we first focus on the behavior of the simple laminar mixing layers which illustrate many conceptual lessons. Various aspects of wakes, jets, and vortex rings are then taken up; at each step they provide reinforcement or contrast to the growing body of concepts. Case by case, we also consider the idealizations which more or less satisfactorily reproduce some of the features of the experiments. We note limitations of both the experiments and theoretical models, and establish a list of recurring research themes and controversial open questions. The chapter ends with two thought-provoking experiments on instability in free shear layers which are turbulent (!) at their origin.

The learning process continues in Chapter 2 with respect to wall layers. A graduated series of experiments, across categories of flows and instabilities, concretely illustrates key aspects and special features of wall-conditioned instabilities and transition. Feedback interaction between unsteady pressure gradients and vorticity is seen to

account for the subtle viscous destabilization in inviscidly stable wall layers. Similarities and contrasts between cross-flow instabilities, Gortler instability, and Taylor instability in Couette flow, and the associated paths to turbulence are discussed in some depth.

Accounts of transition occasioned by discrete and distributed roughness, by laminar-turbulent bubbles, and by lateral (transverse) contamination pose further difficult theoretical and conceptual questions. The last effect is related to the curious happenings called turbulent spots, turbulent puffs, and turbulent slugs which coexist in close proximity with pristine laminar flow. The side-by-side coexistence in such transitional flows of laminar and turbulent regimes in a single system, as well as streamwise thickening of the shear layer, make it difficult to characterize the state of shear-layer systems by state variables appropriate for phase-space approach. (See Section A.19 for illustration of simple two-dimensional and three-dimensional phase spaces.)

The broad learning process concludes in Chapter 3 with otherwise inaccessible conceptualization of disturbances in the ambient fluid environment and with discussion of receptivity experiments.

The genesis of the Guide harkens back to the author's rather concise 1969 attempt to clarify transition phenomena in supersonic flows and to encouragement by Itiro Tani and Dietrich Küchemann to broaden and supplement that "Critical Evaluation." However, after many revisions the Guide deals principally with incompressible flows; the instabilities associated with variable density as encountered in aeronautics are confined to Appendix A, Sections A.07, A.08, A.10-A.15, and Chapter 10. Effects of stratification as contrasted with the effects of compressibility are not covered in the Guide. Surface-tension effects and multiple phase phenomena are also beyond its scope.

From the preceding account the reader should be aware of the central role of the basic material in Chapters 1 - 3 and Appendices A and B. With this broad background, the reader is prepared for the comprehensive presentation of detailed information and references on the separate categories of flows in the subsequent chapters. The conceptual

framework, the themes, and the issues identified in the first part of
the book and Appendices A and B now provide a cohesive approach to an
otherwise bewildering variety of observations. Some of these observa-
tions are undoubtedly incomplete and even wrong. In a guide, comments
are appropriate concerning the degree of experimental rigor and reli-
ability of given investigations, tempered with realization of the
unusual experimental difficulties. Throughout we also insert sporadic
remarks on experimental pitfalls and procedures occasioned by the
special nature of probing of potentially unstable systems. The spe-
cialized chapters in the more encyclopedic second part of the monograph
need not be studied consecutively. The last chapters return to appli-
cations: what perspective and philosphy have we gained from the study
of the simpler systems in the monograph?

The task of the Introduction is to provide a broad-brush perspec-
tive and a primary vocabulary for Chapters 1 - 3. It also includes
descriptive characterizations of key theoretical models and preliminary
comments on their correspondence with experimental conditions. An
engineer who wishes to understand instabilities needs some acquaintance
with the terminology and structure of relevant theories. One may then
appreciate the recent achievements in clarifying past contradictory
evidence on transition to turbulence in two-dimensional ducts as out-
lined in Section 0.02.06.

0.02   MAJOR CLASSIFICATIONS OF OBSERVED SEQUENCES OF INSTABILITIES

Many distinct features of shear layers govern the road to turbu-
lence, only some of which are evident from Fig 0-1. A given shear
system can in fact be classified in different overlapping categories.

The classification here emphasizes the nature of the sequence of
instabilities leading to transition; later we shall classify individual
instabilities according to their primary mechanisms, irrespective of
their order in the sequence. We first describe the early evolution with
Re of three contrasting types of shear layers; this brings in naturally
some of the important classifications and terminology of bifurcation
theory and linearized theory. The more speculative Section 0.02.06 on
experiments in Poiseuille flows describes some difficulties in applying
the classical concepts and illustrates working hypotheses and viewpoints
which are used throughout the Guide to interpret the mass of often
confusing, at times contradictory, experimental information.

A basic conceptual setting is essential to understanding of tran-
sition. Whenever possible it should have an underpinning of detail
theoretical treatment. The conceptual setting should be broad enough to
reconcile confirmed, seemingly contradictory experimental results. In
0.02 sections we focus on the conceptualization of the diverse sequences
of instabilities and examine their correspondence with key experimental
information. With the help of results from recent numerical experiments
we can probably "explain" hitherto paradoxical information on two-dimen-
sional Poiseuille and Couette flows if we allow a role for system dis-
turbances far more weighty than in the past. However, flow geometries
remain, for which conceptual links to the instability sequence and
transition have yet to be discovered.

0.02.01   Instabilities and bifurcations

The range of phenomena covered in the monograph is commonly be-
lieved to be describable within the framework of the "compressible
Navier-Stokes system of equations" for mass, momentum, entropy (energy),
and thermodynamic state, with scalar coefficients of viscosity and heat
conductivity, as defined, say, in Section 3.6 of Batchelor (1967).
(That section also describes the nature of approximations which yield
the useful idealizations of isentropic and incompressible flows.) It
should be reassuring that the exceedingly complex instabilities we
glimpse in our visualizations and point-measurements should be comput-
able, at least in principle, from a known set of equations, henceforth
called the generalized NS equations. Few fields enjoy as solid a bed-
rock of constitutive equations.

At any sufficiently low Reynolds number, Re, all solutions of the
NS equations for a given geometry tend in time to a <u>single basic flow</u>.
For instance, all unsteady flows around a steadily moving circular
cylinder approach steady, laterally symmetric solutions such as por-
trayed in Figures 6, 24, and 40-45 of Van Dyke's Album (1982). Simi-
larly, however initially perturbed they may be, the velocity fields
powered by steady rotation Ω of the inner cylinder in <u>Fig 0-1d</u> settle
down to the unique Couette distribution:

$$\frac{u(r)}{\Omega R_1} = \frac{R_2^2 - r^2}{R_2^2 - R_1^2} \cdot \frac{R_1}{r} \qquad \text{(\underline{0-1})}*$$

Such unique low-Re basic flows are said to possess <u>global stability</u>.

At some higher Re values, the flow fields may converge to different
equilibrium flows. Thus, in the first example the flows around cylin-
ders in the second range of Reynolds numbers converge to periodic,
laterally <u>antisymmetric</u> vorticity concentrations in the wake, decaying
slowly when x exceeds eight cylinder diameters (e.g. Fig. 97 in
Van Dyke's Album). The steady, parabolically diffusing wake fields
remain solutions of the NS equations; they are unstable and

yield the stage to the unsteady, periodic vortex-street solutions. Through the instability, the vorticity distributions become dehomogenized and unsteady, despite the steady symmetric boundary conditions.

The Couette flows, (0-01)*, no matter how carefully started, develop into steady formations of annular Taylor vortices as the rotation of the inner cylinder increases; see, for instance, Fig 0-1d and Figs. 127 and 128a of Van Dyke. As in wake vortex streets, through instability the vorticity field here is dehomogenized into structures with scales on the order of the shear layer thickness. However, the spatial periodicity takes place in the spanwise rather than streamwise direction and therefore does not bring about temporal periodicity. This seemingly simple difference causes major differences in the evolution of instabilities at higher Reynolds numbers between the classes of flows. The new flows are again solutions of the nonlinear NS equations and are said to have bifurcated from the basic-flow solutions. Even when we specify the numerical value of the Reynolds number, mathematical descrip-- tions of details of the wake vorticity or of the counterrotating Taylor vortices must rely on advanced computers. To be useful, the computer-generated information must be stored in a priori selected graphical or tabular representations, with pragmatic limits on accuracy.

At still higher Reynolds numbers, these new base flows in turn become unstable and bifurcate into still more complex flows-solutions. In wall layers the sequence of instabilities generally brings forth vorticity nonhomogeneities with increasingly finer scales with respect to the shear layer thickness. In free layers, instabilities may at times also aggregate vorticity concentrations and thus increase scales. At some stage of this parametric sequence (or branching sequences) of instabilities the new flow becomes sufficiently three-dimensional, diffusive, and irregular to be judged turbulent according to the syndromes of Section 0.01.01. Solutions of NS equations automatically satisfy the dissipation syndrome, of course. Viscosity also counteracts the dehomogenizing effects of the instabilities, primarily at the finest scales.

Instabilities and bifurcations are associated with the fact that for a given geometry, the number of possible flows-solutions of NS equations increases as Reynolds number increases. The number of scales (and frequencies) in the corresponding vorticity distributions also increases until the discrete wave-number or frequency spectra are augmented or replaced by energetic continuous spectra, characteristic of the disorder syndrome of turbulence. Sufficient evidence has accumulated in recent years showing that instabilities, i.e. restructuring of the vorticity distributions with new scales, continue to take place within the turbulent fields. On the largest scales, their presence is reflected in the emergence of so-called coherent turbulent structures. On the smallest scales, they represent a plausible model for the occurrence of fine-scale intermittency which led Kolmogoroff to reconsider his universal similarity theory in 1962. The propensity of even turbulent flows separating at sharp spanwise edges to couple with pressure oscillations may at times make the unstable coherent structures more regular and potentially destructive; see, for instance, Rockwell and Schachenmann (1982) whose fully developed turbulent pipe flow discharged through an annular cavity and led to a violent nonlinear instability built up through pressure feedback from the circular edge closing the cavity. Thus the concept of instability within turbulent flows has technological implication and can be extended empirically to the concept of control, as in playing of pipe organs.

The discussion in this section started with the idea of an orderly very slow variation of the basic parameter, Re. However, the start-up time or distance for the shear layer may be very short. Thus a circular jet issuing from a high-pressure nozzle is born at a high Reynolds number whether Re is based on the thickness of the thin separating boundary layer at the lip of the nozzle or on the diameter of the initial vorticity sheath; see Fig 0-1c. This jet offers an especially clear case where there are many competing instabilities taking place simultaneously at different rates and scales, with different symmetries and asymmetries. Here, and in the case of many secondary and tertiary

instabilities, it is difficult, if not impossible, to speak of true sequences of equilibrium flows and pure instabilities. Furthermore, the instability evolution in any realization of the flow depends on the relative strength of the initial disturbances which feed the different instability modes. Rapid restructuring of the vorticity distributions there is, indicative of instability phenomena, but the relevant equilibrium flows in the bifurcation approach remain elusive.

0.02.02   Linearized NS equations and theoretical Re_{cr}

One commonsense diagnostic test for stability of a solution-flow is to try to provoke its bifurcation to a new equilibrium solution-flow by introducing special testing disturbances. If at a given Re some vanishingly small disturbances can grow to finite amplitudes and thereby change the original base solution-flow, that solution-flow is said to be linearly unstable. It can be shown theoretically that in nonpathological cases, linearly unstable solutions correctly mimic the initial behavior of the nonlinear solutions. Mathematically, the test involves NS equations for the perturbations, linearized with respect to the base flow. The designation "vanishingly small" or "infinitesimal" implies that terms in the disturbances of higher than first power are initially negligible. The simplifications in having to solve only linear differential equations are enormous, even though it took decades to understand their asymptotically singular behavior for wall flows. In particular, for parallel base flows such as the two-dimensional Poiseuille flow, the critical value, Re_{cr}, above which some infinitesimal disturbances grow, can now be readily obtained on a computer. Three examples will illustrate the critical and postcritical behavior.

(1) Circular Couette flows, (0-1)*, of infinite axial extent, driven solely by the rotation of the inner cylinder of radius R_1, i.e. with $V = 0$ in Fig 0-1d, are linearly stable for $Re = V_1(R_2-R_1)/\nu < Re_{cr}$, with $Re_{cr} = 94.7$ when $R_1/R_2 = 0.8$ and $Re_{cr} = 185$ when $R_1/R_2 = 0.95$; see

DiPrima (1981). In experiments, the boundary conditions at the end
faces of the apparatus introduce z dependence of the basic flow. But
this departure from strictly parallel streamlines has minor effects on
the onset of instability when Re increases gradually. Except for a nar-
row range around Re_{cr}, experiments disclose steady nonlinear Taylor
vortices, such as in Fig 0-23a, once Re values exceed Re_{cr}.

(2) Parabolic velocity distributions

$$\frac{U}{U_c} = 1-(\frac{y}{h})^2; \qquad h=\text{duct half width, } U_c=\text{centerline velocity} \qquad (0\text{-}2)\star$$

in two-dimensional ducts of infinite extent in the spanwise z and
streamwise x directions are similarly stable with respect to arbitrary
infinitesimal disturbances for $Re = U_c h/\nu < Re_{cr} = 5772$. Damped pre-
critical and amplifying postcritical linearized solutions were studied
extensively, analytically and numerically. However, most authorities
considered them physically unrealizable because until the experiments of
Nishioka, Iida and Ichikawa (1975) all experimentalists lost laminar
flow before reaching Reynolds numbers in excess of 5500, short of Re_{cr}.
Unless special care is exercised, transition may set in at Re values as
low as 1000. Figure 0-4 of Carlson & WP (1982) displays a so-called
turbulent patch generated by an artificial disturbance at Re of 1000.
In the experiments of Carlson & WP, "natural"--i.e., spontaneous spots
without the experimenters' intervention--commonly occurred at Re of
about 1200. Obviously, we need to seek the physical and mathematical reasons
for the stark contrast in behavior of these Poiseuille flows vis-a-vis
the Couette flows (1).

(3) The linear Re_{cr} for even the idealized uniform two-dimensional
viscous flow around a perfect, smooth cylinder of infinite span remains
uncertain.

The only computations we have for (3) are for strictly parallel
base flows with empirically fitted wake velocity-defect shapes such as
$\exp(-ay^2)$ in Wazzan & OK (1973) . With b defined as the crossflow
distance y at which the velocity defect reduces to half its centerline

value, modern computers yield critical values of $2bU\infty/\nu$, slightly higher than 10, Wazzan & OK, and between 1 and 2, Nakaya (1976).

The fact that the base flows used in the wake approximations do not solve the NS equations probably depreciates the results per se less than the assumption of parallelism. Base streamlines, unchanging with x, do not fit the crucial initial conditions near the cylinder (or, for that matter, those near thin trailing edges of plates or airfoils). Receptivity to disturbances (see Sections 0.01.01 and A.17) as well as the initial spatial amplification characteristics of the wake are dominated by the conditions at and near the cylinder. However, to take such conditions into account is beyond the current state of our analytical and numerical techniques. At present, the search for at least approximate guidelines leads us to reduce the spatial dependence of the base flow properties to the sole cross-flow variable y, as was done by Wazzan & OK and Nakaya. Base flows with exact NS solutions dependent solely on y will be called purified flows.

We note that among the real flows of Fig 0-1 only the class of rotating flows (d) (without an upstream or downstream) falls strictly into the purified category and then only if we allow for an infinite axial extent.

0.02.03   Experimental linear Re_{cr} and the role of disturbances

For the flow around a circular cylinder, experimentalists often define a "spontaneous Re_{cr}" as that Re for which the near wake ceases to be symmetric and/or starts amplifying "spontaneously" in their facility. While "spontaneous Re_{cr}" values from 35 to 60 have been reported, depending on the finite span-to-diameter ratio, free-stream disturbances, slight mean-flow nonuniformity, vibrations, etc., values between 40 and 50 are commonly observed. Do free-stream disturbances and minute cylinder vibrations qualify as "vanishingly small disturbances" for the diagnostic test of linear instability? To qualify, the excitation should include the least stable (or the most unstable)

motions -- antisymmetric vorticity distributions in the critical fre-
quency band in the present case. Furthermore, as the excitation inten-
sity is reduced to zero, the amplitudes of the observed fluctuations
should decrease proportionately toward zero. This requirement makes
certain that the response does not have a nonlinear threshold. In a
threshold response, no amplified motion in the band of dangerous fre-
quencies would be sensed for excitations up to a finite, if small,
amplitude.

The only published careful diagnosis of this type for the cylinder
flow is presented in Fig. 6 of Nishioka and Sato (1978), reproduced here
as semi-logarithmic Fig 0-2. Cross-flow cylinder vibrations of ampli-
tudes of 4 and 8% of the cylinder diameter (d = 2mm) are seen to induce
proportionate, initially exponential amplifications in the streamwise x
direction at a Reynolds number of 30, well below their lowest Re of
"spontaneous" amplification, 48. We note that at higher Reynolds num-
bers the leveling of curves, such as seen in Fig 0-2 for x/d > 8, would
usually be ascribed ᴌo nonlinear effects. Here the relatively low
amplitudes and the unusual continued near-proportionality of the lower
curves suggest viscous dissipation and frequency detuning (as the mean
streamlines broaden) as the likely causes. Judging by the altogether
declining curve for the vibration amplitudes of 0.15d, nonlinear stresses
and a substantial change in the mean wake were probably responsible for
the decay here. Whatever the interpretation of the behavior for larger
x , the feature of importance to the test is the proportionate exponen-
tial growth of the two lower curves.

A priori, a distinction is in order between the theoretical test in
which the perturbation represents the self-excited solution of a homo-
geneous linear system and the experimental test for which the small-
amplitude response in Fig 0-2 is forced or driven by the nonhomogeneous
boundary conditions at the vibrating cylinder. The driven solution con-
sists of a linear superposition of some particular solution and homo-
geneous solutions, which together satisfy the appropriate initial and
boundary conditions. The validity of the experimental tests rests on
the assumption that in the driven solution, the particular part of the

response becomes dwarfed by the exponentially growing, homogeneous part of the response. Both cases should then lead to consistent results because the instability is judged by the growth of the homogeneous solution alone. Still, the difference is interesting: in the experimental test the amplitude of the homogeneous component is determined by the vibrator, while in the theoretical test the amplitude remains arbitrary. (We recall that in real flows, determination of the amplitude of the homogeneous component constitutes the essence of the problem of receptivity to any given class of physical disturbances.)

Since "spontaneous Re_{cr}" depends on environmental disturbances, the "spontaneous self-excitation" should also be a "driven response" due mainly to free-stream vorticity and pressure fluctuations. (For additional discussion of these superficially contradictory terms, see Section A.17.) Experimentally for $Re < 100$, there is no doubt that external acoustic pressure excitations indeed induce exponentially growing wake fluctuations, initially proportional to the driving amplitude of sound. This proportionality is understandably more difficult to demonstrate for the effect of free-stream turbulence.

In the light of the preceding discussion, the experiments of Nishioka and Sato (1978) and Fig 0-2 imply that Re_{cr} in the sense of linearized NS equations is somewhat below 30 for the cylinder flow, evidently distinct from their "spontaneous Re_{cr}" of 48. Why should there be a difference? Assuming, as is reasonable, that the measurements leading to the data of Fig 0-2 exclude the probability of a threshold effect at lower amplitudes, we must look to the uncontrolled environmental disturbances for a consistent explanation. Below Re of 48 the given low-Re facility may not have contained any asymmetric disturbances in the dangerous range of amplifiable frequencies. Or if they were present, their amplified response must have remained below the level of detectability of the experimental technique. Because of the importance of the concept of the linear Re_{cr}, further independent experimental elucidation of the details of the wake responses below the "Re_{cr} of spontaneous amplification" seems highly desirable.

Returning to statement (3) in Section 0.02.02, the wide spread of
inferred values of linear Re_{cr} (from 1-2 of Nakaya to 10+ of Wazzan &
OK, to 30- of Nishioka and Sato, to 40-50 of most of the "spontaneous"
amplifications) illustrates the uncertainty in cases of substantially
nonparallel flows, subject to mixtures of environmental disturbances.
On the other hand, the substantial nonparallelism may simultaneously
mitigate the postcritical impact of the instability on the flow field
-- by sharply confining its domain in x; see comments on the leveling
and decay of the fluctuations in Fig 0-2 in this section. There is
evidence, Desruelle (1983), that from the "spontaneous Re_{cr}" to Re of
90-100, the fluctuations in the cylinder wake simply decay without
further instabilities in x, presumably because of combined effects of
nonlinearity, viscosity and nonparallel detuning. Such detuning does
not occur in the purified cases of circular Couette flow (1) and two-
dimensional Poiseuille flow (2). Prediction of this qualitative differ-
ence in unstable behavior is beyond the power of current bifurcation
analyses which cannot handle nonparallelism in the streamwise direction.

---

*Note 1   Two recurrent themes. Two ideas in Section 0.02.03 become
recurrent themes throughout the Guide. The first was illustrated in the
interpretation of the Nishioka-Sato Fig 0-2 and of the nature of the
"spontaneous Re_{cr}" in the flow around circular cylinders. The view of
the manner in which observed, exponentially growing fluctuations in the
initial linearizable regime of instabilities can be proportional to
small external disturbances is generally applicable. It constitutes an
important tool in our pursuit of objectives (a) and (b) in Section
0.01.01. The second is the need for awareness of the possibility that
substantial differences from common expectations may take place in
qualitative precritical and postcritical behavior in streamwise non-
parallel flows. Streamwise variation of Reynolds number based on shear-
layer thickness may modify the criticality of instabilities.

0.02.04   Bifurcation theory: characterization and vocabulary

What in the NS equations could account for the strikingly different
postcritical behavior in the three flows discussed in the preceding sec-
tions? In our quest for Re_{cr} and the locally most amplified solution,
often called fundamental, we discarded all powers in the disturbance

fluctuations beyond the first. If, by cleverly operating on the NS equations we manage to obtain a differential equation in higher powers of a _single_ suitably defined nonlinear _amplitude_ A(t) associated with the fundamental mode, could the resulting so-called _weakly_ _nonlinear_ equations discriminate between the different postcritical behaviors? The answer is a qualified yes when we restrict ourselves to purified (parallel) flows like the Couette flow (1) and the two-dimensional Poiseuille flow (2) in Section 0.02.02. Generally, inclusion of terms up to and including third power can characterize the dominant trends of the nonlinear interactions of the fundamental solution (a) with the mean flow (_base-flow distortion_), (b) with its _second harmonic_ (usually loss of energy), and (c) with itself (_shape distortion, saturation_).

In his descriptive 1971 review Stuart discusses the Couette and Poiseuille flows as prototypes of nonlinear behavior in _rudimentary_ _supercritical_ and _subcritical_ bifurcations, respectively. In the Guide the adjective _rudimentary_ refers to bifurcations for which the solutions _remain_ adequately characterizable by a single measure of intensity (or energy), the amplitude A(t), after the bifurcation. (It is not commonly used in the literature but is needed inter alia to clarify the nature of possible secondary bifurcations in Poiseuille flow, Section 0.02.06.) Subcritical bifurcations are occasionally called inverted bifurcation for reasons clear from the contrast in sketches _Sk0.02.04a_ and _Sk0.02.04b_ of two rudimentary bifurcations.   At a given Reynolds or Taylor number the heavy lines in these diagrams represent stable equilibrium solutions of the homogeneous equations, characterized by the single amplitude A(t) as $t \to \infty$. (The Taylor number, $T = 2Re^2(R_2 - R_1)/(R_2 + R_1)$ is preferable to Reynolds number when Couette flows with different radii are compared.) The dashed lines indicate unstable equilibria; the _arrows_ mark the direction of _evolving solutions_ of the _homogeneous_ _system of equations_. The unperturbed basic flow corresponds to A = 0, the ORe axis, of course.

In rudimentary _subcritical systems_, instability can occur for Re < Re_{cr} when the perturbations exceed the threshold represented by the dashed curve BRe_{cr} in _Sk0.02.04a_. In the domain to the left of

Re_{min2D} (the minimum Reynolds number of instability of the fundamental mode) "one expects that the basic flow is globally asymptotically stable," Drazin & Reid (1981, p 374). In the domain of conditional instability, $Re_{min2D} < Re < Re_{cr}$, the perturbation amplitudes should either decay to nothing or evolve and converge to a new stable equilibrium along BC. We shall explore in Section 0.02.06 how well this prototype of subcritical behavior matches experimental information on Poiseuille flows with unavoidably finite spans and axial lengths.

In systems with rudimentary supercritical bifurcations, Sk0.02.04b, all perturbations decay for $T < T_{cr}$ and evolve toward the new stable flow configuration for $T > T_{cr}$. Weakly nonlinear approximations (among other methods) indicate that the Couette flow with infinite span, driven by rotation of the inner cylinder, bifurcates supercritically. This agrees quite well with the previously described experiments with large spans. Except for some unsteadiness and spanwise nonuniformity, Taylor vortices appear near the T_{cr} value computed for infinite axial length when the speed of rotation is increased very gradually. (For further qualifications see next section.) As indicated in Sk 0.02.04b, the Couette supercritical system experiences another bifurcation from the new equilibrium, always for T values to the right of T_{cr}. In the laboratory it leads to periodic wavy vortices; see Fig 0-23b here and Fig. 128 in Van Dyke's Album.

More generally, bifurcation theory studies the qualitative character of the nonlinear solutions as the system parameter is made to approach and pass a bifurcation in the solutions. While the critical value of the parameter may be determined from local linearization, the qualitative changes in the solutions at that bifurcation depend on the nonlinear structure of the equations near Re_{cr}. The approach through weakly nonlinear ordinary differential equations for the amplitude is only one of the simpler techniques of bifurcation theory; see pp 370-379 and 402-420 of Drazin and Reid (1981) for a broad heuristic introduction to the subject and its nomenclature. The richness and diversity of solutions of nonlinear equations generally call for powerful and often very abstract techniques. It is therefore not surprising that there

exist more complex configurations of equilibria at a bifurcation. Here we are concerned primarily with acquiring concepts, such as that of the threshold amplitude and saturation, which could help us interpret puzzling experimental behavior in flows of <u>Fig 0-1</u>. Because experiments are always performed in confined spaces we first need to inquire what modifications in the bifurcation behavior, say that of <u>Sk 0.02.04b</u>, take place when finite lengths are introduced in the theory.

0.02.05   Imperfect bifurcations; circular Couette flow

As mentioned in Section 0.02.02, the solutions of the base Couette flow with finite spans acquire z dependence, which can be considered as "an imperfection" in the idealized uniform flow <u>(0-01)</u>* in Section 0.02.01. Generally, for large span-to-gap ratios, the z dependence can be replaced by a new small parameter ε, a suitably weighted measure of the departure from uniformity. The theory of <u>imperfect bifurcations</u> then suggests that for small ε the locus of the stable solutions in <u>Sk 0.01.02b</u> should shift from the solid curves to the neighboring dotted curves, labeled pr and sec. The small nonzero amplitude A at moderate Taylor numbers along pr characterizes the fact that weak vorticity structures, "shadows", are built up even at slow rotations by the boundary conditions at the end faces. There is a rapid but continuous change in amplitude in the proximity of T_{cr} as T increases gradually; this corresponds to the previously described observation of the changeover to the developed Taylor cells over a narrow band around the critical value of the parameter.

Near T_{cr}, linearized NS equations for the infinite span yield a specific wavelength λ_{cr}. What happens when the finite span S does not match $n\lambda_{cr}$, the closest integral multiple of the ideal wavelength? As T increases gradually at subcritical values, the forced viscous effects of each end plate spread toward the middle on the diffusive time scale, $S/(\nu t)^{\frac{1}{2}}$. For large span-to-gap ratios, the widths of the two end cells generally accommodate most of the difference $S - n\lambda_{cr}$ as T slowly passes T_{cr}. However, for a given S, this gradually evolved

vortex pattern, called _primary_, is not a unique steady solution of the NS equations with no-slip boundary conditions. For instance, at a Reynolds number of 359 and a moderate span-to-gap ratio of 12.61, photographs in Figure 1 of Benjamin and Mullin (1982) demonstrate _fourteen additional stable vortex arrays_. The number of vortex cells ranged from 8 to 18! In 9 of the vortex arrays one or both end cells rotated in an _anomalous_ fashion, the particles in the boundary layers of the rotating end walls spiraling outward rather than inward. Ten of the NS solutions were obtained by modifying the time history of the boundary motions, i.e. through fast programmed starts. The other four states were established at an aspect ratio different from 12.61 and then compressed or stretched by careful adjustment of the span. The authors believe that there are at least 39 solutions satisfying the same boundary conditions when unstable equilibria are included.

All such postcritical Taylor-Couette flows cannot fit the dotted imperfect bifurcation loci in Sk 0.02.04b. It can be reasonably argued that the continuous dotted curve starting at T = 0+ should correspond to the primary flow which evolves during gradual changes in T. However, Benjamin and Mullin caution against the automatic asumption that "the experiment simplifies progressively as the span-to-gap ratio is made larger, leaving only a residual perturbation from behavior according to the infinite model," and supply a number of reasons for caution.

At the level of sophistication of this chapter, the B & M experiment teaches us that even at the first bifurcation the multiplicity of the solutions may lead beyond the dimensionality of rudimentary bifurcations portrayed in Sk 0.02.04b. The _secondary_ imperfect solution labeled "sec" in Sk 0.02.04b, though correctly inaccessible through slow variation of T, cannot correspond to all the other 14 stable solutions. By itself, the physical demonstration of 15 stable solutions should alert our intuition concerning possible happenings in problems governed by _nonlinear_ NS equations. One virtue of the purified problems is that some properties can be proven and physically observed, where they probably remain camouflaged by the variation in the governing parameter in nonpurified systems.

0.02.06   Interpretations of experiments on Poiseuille flow

If the introduction of a finite length into a stably evolving supercritical system can lead to the diversity of Benjamin and Mullin (1982), what can we expect when finite span S is introduced in the subcritical two-dimensional duct problem, idealized in Sk 0.02.04a? Since along $Re_{cr}B$ the equilibria are unstable, multiplicities of solutions may be altogether unobservable if the instabilities develop rapidly. The a priori hope would be that the essence of the threshold behavior, associated with $Re_{cr}B$, would remain as a diagnostically recognizable feature. The customary interpretation of the experimental evidence on Poiseuille flow has been that, in all the more careful pre-1975 experiments, the disturbances still surpassed the then ill-defined threshold $Re_{cr}B$. According to Herbert (1981, Fig. 3), if the most dangerous disturbances remained two-dimensional and characterizable by a single amplitude, the flow would evolve to a stable equilibrium corresponding to a point on BC in Sk 0.02.04a. In all the pre-1975 experiments (described in the introduction of Carlson, Widnall, and Peeters, 1982) there was inadequate identification of the disturbances and the nature of the instabilities. The fluctuations, however, were clearly three-dimensional and irregular, so the experimental loss of laminarity was construed as a necessary consequence of the inverted bifurcation. Most theoreticians believed that the unavoidably nonvanishing disturbances in real duct flows would always cause the system to cross the dashed threshold line in Sk 0.02.04a and "snap through" to a "turbulent equilibrium" before the Reynolds number could become supercritical.

Is it possible to amend these views to explain the ability of Nishioka, Iida, and Ichikawa (1975) and Kozlov and Ramasanov (1980) to reach supercritical laminar flow in channels with low but finite free-stream disturbances? A tentative reconciliation is presented below, with the aid of results of both numerical experiments and weakly non-linear theories of special secondary instabilities by Herbert (1981a) and Orszag and Patera (1981a). Herbert's remarkable analysis rather

convincingly interlaces past and current information, including addi-
tional experiments on details of induced subcritical instabilities by
Nishioka, Iida, and Kanbayashi (1978) and Nishioka, Asai, and Iida
(1980) and (1981). Here we focus on three specific issues crucial to
our understanding of Sk 0.02.04a and initiation of turbulence: (a)
Nishioka's laminarity at Re of 8000 (occasionally up to 9000);
(b) the likely nature of evolution of fluctuations above the curve
$Re_{cr}B$; and (c) the possible theoretical explanations of existence of
turbulence at Re below Re_{min2D} observed in noisier experiments.

(a) Absence of turbulence for Re > Re$_{cr}$. As Fig 0-1b informs us,
except for possible pressure disturbances propagating upstream from the
exit, the external disturbances arrive from the blow-down region of the
Poiseuille facility strongly reduced by honeycombs, screens, and con-
traction. In large-aspect ratio ducts, the boundary layers in the
accelerated entrance region are more stable than the fully developed
Poiseuille flow. Small vortical disturbances, such as those measured by
Nishioka & II (1975), with streamwise r.m.s. fluctuation u' on the
order of $U_c/10,000$ near x_{FD}, may then grow spatially up to the end of
the channel, x_E. Thus the explanation hinges first on the magnitude of
the spatial growth rates of disturbances at Re of 8000, induced by
external disturbances near x_{FD}; see Section 0.02.03, including *Note 1.

According to Itoh's 1974 theory of spatial linear instability, the
growth rates in the narrow amplified spectrum at Re of 8000 are rather
low. It is reasonable to assume that the initial amplitude of the
induced disturbances in the most amplified frequency band does not
exceed u'/100. A total amplification factor of 10,000 would be required
to generate a fluctuation on the order of $U_c/100$, empirically the
earliest likely level for the onset of nonlinear effects. The hot-wire
evidence of Nishioka & II and Itoh's theoretical results indicate that
the channel indeed ended before instabilities could build up into turbu-
lence. At Re of 9000 the amplified band is broader and its amplifica-
tion rates higher; accordingly, the runs remained laminar only spora-
dically, when the environment in the through-flow system was especially
quiescent.

As with the "spontaneous Re_{cr}" in Section 0.02.03, experimental observables depend on the spectral composition and level of disturbances in the environment, as well as on the receptivity of the shear layer to these disturbances. Had Nishioka designed a considerably longer channel, Re_{cr} still may have been surpassed, but only if the mix of the forcing external disturbances were such as not to induce any homogeneous solutions in the narrow band of amplified frequencies. For the purified problem with infinite channel length, minutest disturbances initiated at the molecular level - Brownian motion, thermal fluctuations - would presumably always be sufficient to initiate the amplified homogeneous solutions and preclude a supercritical laminar flow; see Jhaveri and Homsy (1980) for related excitation by Brownian motion of convective instabilities in fluid layers heated from below. In systems of technological interest, macroscopic environmental disturbances, <u>Fig 0-1a,b</u>, invariably induce the instabilities.

(b) <u>Three-dimensional instabilities with threshold behavior</u>. For $Re < Re_{cr}$ the locus $Re_{cr}B$ in <u>Sk 0.02.04a</u> corresponds to neutral two-dimensional, periodic, progressive wave solutions of the homogeneous NS equations with finite amplitudes $A_n(Re)$. If we could artificially induce this mode of motion with an amplitude A+, infinitesimally larger than A_n (with <u>no</u> other disturbances present), the motion would evolve, at first very slowly, toward a two-dimensional stable periodic equilibrium motion characterized by A_2 on the locus BC. In other words, the artificially excited solution would transcend the threshold of $Re_{cr}B$ and saturate on BC.

A thin ribbon, say 0.05mm thick and 40mm wide, stretched across the flow span at some height y and vibrating with the most dangerous frequency at the given Re, would elicit a forced response similar to that caused by the vibrations of the cylinder in Section 0.02.03. Again, the response associated with the particular solution would be expected to decay relative to the response associated with the dangerous homogeneous solution. A hot-wire probe, situated at a downstream position x_p, would then sense the characteristics of the homogeneous solutions and could document the possible threshold nature near $Re_{cr}B$ as

the amplitude of the vibrating ribbon is increased. This technique was originally devised by Schubauer and Skramstad (1944) for their epoch-making studies in boundary layers. It was applied successfully by Nishioka and his coworkers, 1975-1981, to explore extensively the linear and nonlinear, subcritical and supercritical behavior of the progressive wave solutions, and to demonstrate their threshold character at Re = 5,000.

In the thought experiment above, the disturbance from A_n to $A+$ was strictly two-dimensional. It was also two-dimensional in the corresponding weakly nonlinear spatial theory of Itoh (1974a) with which Nishioka & II compared their results. However, despite utmost care in the design of their facility and vibrating ribbon, Nishioka and II found small but increasing three-dimensionality of the mean flow for Re in excess of about 3000 (their Fig. 2). Consequently the unsteady distur- bances driven by the ribbon were also slightly three-dimensional. In view of the slowness in the early evolution of the two-dimensional solution away from the unstable equilibrium $Re_{cr}B$, Herbert (1981) investigated whether some three-dimensional perturbations might not grow more rapidly and make the subsequent development intrinsically three-dimensional.

In accordance with Section 0.02.01, the present base flow must consist of the sum of the parabolic Poiseuille velocity field and the neutral progressive-wave solution, characterized by the finite A_n along $Re_{cr}B$. A vanishingly small progressive wave solution of the same fre- quency, but with wavefronts skewed at an angle $\tan^{-1}(\beta/\alpha)$ with respect to the spanwise z direction is added as the testing perturbation. The resulting system of linearized NS equations (see *Note 1 at end of (b) and Section 0.04.03) was solved numerically to yield the dimensionless growth rates σ in the coefficient $\exp(\sigma t)$ of the perturbations.

A sample of these rates σ for the streamwise wavenumber $\alpha = 2\pi/\lambda = 1$ of the neutral progressive two-dimensional waves is shown in Fig 0-3a as function of the spanwise wavenumber β and different amplitudes $u'_m = A_n/\sqrt{2}$ (nondimensionalized with respect to U_c) along the locus of unstable equilibria $Re_{cr}B$. When Re is subcritically

close to Re_{cr}, A_n and u'_m are small. All three-dimensional pertur-
bations, irrespective of orientation are then exponentially damped. For
$u'_m > 0.94$ (i.e., for less than 1% of U_c!) an increasingly wider β
family of three-dimensional waves can grow at increasingly faster expo-
nential rates σ. It would appear that the 3D disturbances could indeed
"run away" from the slowly growing 2D disturbances if u'_m is large
enough. Furthermore, as Fig 0-3a discloses, the 3D components also
experience a threshold effect, grafted on top of the 2D threshold along
$Re_{cr}B$.

When the experiments of Nishioka, Iida, and Ichikawa were under
way, only the 2D threshold effect was theoretically anticipated. By
1980 there existed at least three independent, spectral computer codes
(e.g. Orszag and Kells, 1980) capable of credibly simulating temporal
evolution of the nonlinear NS solutions for duct flows with streamwise
and spanwise periodicity. At the suggestion of Herbert, Kleiser (1982)
used one of the codes (Kleiser and Schumann, 1979) for numerical experi-
mentation in the regime of parameters of the experiments of Nishioka & II
(1975), specifically for $\alpha = 1.12$ and Re = 5000. The computed neutral
amplitude u'_m on $Re_{cr}B$ then is approximately 2.5%. Starting with
the initial conditions: $u'_m = .0212$ for the fundamental, zero for its
second harmonic, and .0007 for the r.m.s. amplitude of the 3D distur-
bance wave with $\beta = 2.1$, Kleiser obtained the results plotted semi-
logarithmically in Fig 0-3b. Although the fundamental was displaced
from the neutral locus and it lost energy to its initially spurting
second harmonic, both fundamental and harmonic developed very gradually
thereafter. The 3D wave at first excited and interacted with an x-
independent streamwise vortex. Subsequently both these 3D modes grew
exponentially with nearly the temporal rate $\sigma = 0.0484$ predicted by
Herbert's linearized 3D theory described above.

Kleiser's nonlinear simulation indicates two more qualitative
changes of behavior, at dimensionless times t of 100 and 120. These
are interpreted in Chapter 2 of the Guide. For present purposes,
Kleiser's nonlinear NS computations, Herbert's 3D perturbation of
the 2D threshold level, and the Nishioka & II experiments all

suggest that 3D instabilities near the subcritical neutral branch are most likely, if not inevitable. According to Sections A.01 and 0.03.05, three-dimensionality at finite amplitudes brings forth a powerful vorticity generating mechanism inherent in the nonlinear term (2) $\underline{\omega} \cdot \underline{\text{grad}}(\underline{V})$, in Equation (A-4)*. Thus Herbert's instability contrasts fundamentally with two-dimensional instabilities which principally dehomogenize but conserve total vorticity. We can therefore expect further instabilities and faster approach to turbulence. In fact, this type of three-dimensional instability represents a prototype for many secondary instabilities.

Basically, the preceding account provides specific, highly probable guideposts for the road to turbulence from the neighborhood of $\text{Re}_{cr}B$ in Sk 0.02.04a. It concretizes the earlier vague expectations of "snapthrough instability," which were influenced by structural analogies. Once disturbances become finite, the lack of local constraint in cross-stream and streamwise directions makes flow fields susceptible to a variety of three-dimensional growths not generally met in other branches of continuum mechanics. It would seem that qualitative theories of instabilities and dynamical systems would have to take account of this essential propensity to three-dimensionality in fluid motion to begin to characterize the evolution of turbulence and turbulence itself. For Poiseuille flows, perhaps even more than for the Benjamin-Mullin Couette flows in Section 0.02.05, the rudimentary bifurcations simply cannot portray the multiplicity of possible outcomes.

---

*Note 1   Parametric instability. When NS equations are linearized with respect to a base flow, velocity profiles of the base flow and their derivatives generally appear as variable coefficients in the differential equations for the perturbations. The base flows in Herbert's 3D perturbations include periodic progressive waves with finite amplitudes. Hence the homogeneous system has some terms with periodic coefficients. Such systems are often described as leading to parametric instabilities or subject to parametric excitation or parametric resonance. Important prototypes of ordinary linear differential equations with periodic coefficients are the Hill equation and its special case, the Mathieu equation. In his readable exposition of the theory of Hill's equation, the Floquet theory, Stoker (1950, pp 192-213) describes

it as one of extraordinary elegance. Succinct outlines of the proper-
ties of the Mathieu equation and some of their implications for engi-
neering systems are given by McLachlan (1950, pp 113-144), and Nayfeh
and Mook (1979, pp 20-26). Additional details, graphs, and many further
references can be found in Abramowitz and Stegun (1964, pp 721-746) and
McLachlan (1947).

In its simplest realization the Mathieu equation describes a
spring with a partially periodic spring constant:

$$y'' + (a - 2q\cos 2t)y(t) = 0 \qquad\qquad (0\text{-}3)*$$

Its solutions (usually of interest for q small with respect to a)
may be stable or unstable in an infinite number of regions of the plane
of the parameters a and q. Of special significance is the existence
of subharmonic periodic solutions with frequencies $m/n\pi$, m and n
being integers with $m < n$. Thus in presence of a base-flow frequency
$1/\pi$ in (0-3)*, lower frequencies can be generated under appropriate
conditions, Stoker (1950, p 207). In slightly nonlinear springs, gener-
ation of harmonics m/π is commonplace. Here, ultraharmonic solutions
also exist, $m > n > 1$, as well as a neutral solution with $m = n = 1$.

Subharmonic frequencies appear in the nonlinear stages of insta-
bilities in many experimental shear layers, which are not purified like
the Poiseuille case. Hence, in such cases, finite-amplitude equilibria,
even unstable ones, are not strictly available for Herbert-type pertur-
bations of periodic base flows. Nevertheless, first instabilities in
many important shear layers lead to nearly periodic quasi-equilibria,
and the subsequent qualitative behavior of secondary instabilities
suggests that they are often parametric in nature. In particular, most
flow instabilities which bring forth larger scales and slower charac-
teristic times are parametric.

(c) Occurrence of turbulence for $Re < Re_{min2D}$; concept of Re_{mint}

The discussion in the preceding subsection (b) makes us expect three-
dimensionalization and rapid growth of 3D vorticity, initiated by
vanishingly small disturbances at the unstable equilibria along $Re_{cr}B$ in
Sk 0.02.04a. The computed $Re_{min\ 2D}$, corresponding to the leftmost
equilibrium solution at B, is about 2900. Yet spontaneous turbulent
patches are observed experimentally at Reynolds numbers as low as 1000-
1500, presumably where initial disturbances are finite and three-dimen-
sional.

Large 3D disturbances, in contrast to those discussed above, bring
in at the outset the nonlinear vorticity generating mechanism associated
with $\underline{\omega}\cdot\underline{grad}(\underline{V})$; see Section 0.03.05. A priori, it seems possible that

no primary or secondary instability might be needed to dehomogenize and amplify the vorticity as needed in two-dimensional base flows with small disturbances. Furthermore, the spatio-temporal irregularity in the causative environmental disturbances would generally be imprinted on this motion and amplified, so that the first syndrome of turbulence (Section 0.01.01) would also be present. If so, vigorously disturbed base flows could evolve continuously, without identifiable bifurcations or instabilities into turbulent flows. But do they so evolve? Or can we infer, in disturbed evolving flows, from theory or experiment, the presence of very rapid amplifications which could be usefully inter-preted as local, exponentially or even faster growing instabilities? In this segment we consider the available evidence from numerical experi-ments and analysis by Orszag and Patera (1981, 1983) and from low-Re visualization experiments in water flowing through a channel of high aspect ratio of 133, carried out by Carlson, Widnall, and Peters (1982).

Carlson & WP, p 498, report: "Below a Reynolds number of about 840, a (stimulated) disturbance was found to grow into a semideveloped spot and then to decay into streamwise structures that ultimately disap-peared." Fig 0-4b displays a fully developed spot of Carlson & WP, growing at Re $\sim$ 1000 from a disturbance initiated at G by sudden lateral injection of (incompressible) fluid through a sidewall port. Figure 10 of these authors shows a collection of spontaneously grown spots in "natural" transition in the duct at Re $\sim$ 1200. They comment: "The shape of the natural turbulent spot was very similar to that of the artificially generated spot." The suspension of mica platelets in the water provides approximate visual indications of instantaneous lines of principal normal stress everywhere (unlike the smoke in Fig 0-5, which remains nearly mass-attached). The profusion of resulting features gleaned from many photographs is schematized in a collective portrait in Fig 0-4a. The leading front of the spot (5) moves roughly with 2/3 of the centerline velocity, the trailing arc near (3), with half that speed, and (6) represents an extrapolated idealized focus. With the additional knowledge that the one inch units on the scale in Fig 0-4a

correspond to 4.23 channel depths, the main aspects of this energetic nonlinear entity come into perspective. For our specific objectives two aspects are of particular interest.

Fig 0-4a suggests that at least two identifiable instabilities are present, one manifested by the oblique waves (7), and the other by the fine-scale breakdown (8). Carlson & WP write of the latter: "...turbulence sprang forward in tongues of breakdown on these waves." An arc of dots from the upper numeral 8 to the lower 8 was added to the figure to mark the approximate beginning of (4), the region of small-scale turbulence. A clear example of the local breakdown is seen in their Fig. 7. Thus in this analog solution of NS equations with a large three-dimensional disturbance for initial conditions, the evolution is not smooth throughout but exhibits growth of wave-like formations and extra rapid local changes. The concept of successive instabilities evidently remains applicable and useful. An equilibrium state for the channel, however, cannot be well defined until, for the CWP realizations, the Reynolds number rises past 1500 (still much below Re_{min2D} and Re_{cr}), when spreading turbulence effectively crowds out the laminar regions.

The other important lesson is that at Re $\sim$ 840 turbulence can grow locally and then decay, with streamwise vortices (of the type also present in Kleiser's numerical experiment, (Fig 0-3b) as the lingering features. The streamwise vortices also happen to be the least stable linear modes. At Re of 1000, turbulent patches grow and, once born, don't decay. We shall see in Chapter 2 of the Guide that in circular pipes at Re $\sim$ 2300 equilibrated turbulent puffs propagate downstream without net growth or decay: as much vorticity is generated by the nonlinear production source as is annihilated by viscous diffusion. Below 2300, these puffs slowly decay; above 2300, they grow. For both confined flows, we are therefore led to the concept of Re_{mint}, below which turbulence may grow temporarily but does not form stable or growing configurations of self-sustaining turbulence in a given shear layer. Disturbances in a flow with Re < Re_{mint} decay on time scales relevant to the realization of the shear layer. For practical purposes such a flow

is _globally_ _asymptotically_ _stable_ and converges to states on the segment ORe_{mint} in _Sk 0.02.04a_. The _conditionally_ _unstable_ regime in Section 0.02.04 should then extend from Re_{mint} of 1000-1500 to Re_{cr} of 5800-6000 in large-aspect-ratio duct flows.

In sharp contrast, flat-plate boundary layers (which are also subcritically unstable!) have Re_{mint} approximately equal to Re_{cr}, with important practical consequences. This basic fact that turbulent spots in boundary layers grow and propagate into a _linearly_ _unstable_ laminar layer counsels caution with respect to analogies with the turbulent patches in duct flows. In boundary layers there is also no known split-ting of older patches as there is in channels; there at Re of 1000-1100 the fine-scale turbulence (4) in _Fig 0-4a_ commonly _relaminarizes_ into horizontal streamwise vortices, dividing the active turbulent region into two. To call attention to these differences in the Guide we shall reserve the term "spot" for boundary layers and call the CWP entities "turbulent patches."

To test inter alia the nature of NS solutions in the range of Reynolds numbers below Re_{min2D} where no equilibrium solutions are known (from which flows could bifurcate on a path to turbulence), Orszag and Patera (1981, 1983) turned to numerical experimentation. To keep close to analytical techniques, they decided on a large initial primary 2D wave (corresponding to the least stable linear mode at any Re, with rms amplitude u' of almost $0.2U_{max}$) and a very small perturbing oblique wave with $\alpha = 1.32$ and $\beta = 1.32$; see Section 0.04.03 for definitions. Direct temporal numerical simulation showed that at Re = 1500, the 2D wave almost maintained its energy while the 3D wave grew at a rapid exponen-tial rate, their 1983 Fig. 5. At Re = 500, both waves decayed.

Because of the arbitrary choice of the disturbances and their amplitudes, the "critical" Re of 1000 at which the 3D definitely grew exponentially has little general significance. What does matter is that, although the primary wave is not an equilibrium solution, the 3D disturbance undergoes a strong, definitely identifiable instability which makes the resulting flow three-dimensional and subject to addi-tional 3D instabilities. (In temporal formulation, the seeds for the

subsequent instabilities have to be included in the initial conditions; of course, they can also be injected "spontaneously" by round-off errors.)

The numerical investigation of the energetics of the solutions discloses that the 2D solution transfers very little net energy to the 3D solution but facilitates a large net transfer from the mean flow. The rapidity of the 3D growth suggests that the instability should be inviscid in nature; (see introduction to 0.03 Sections for definitions). Orszag and Patera show that <u>combined</u> vorticity stretching and tilting indeed fuels the instability; see Section 0.03.05. At Re > 2900, where 2D equilibrium flows exist, their analytical and numerical results parallel those of Herbert, including the amplitude and obliqueness threshold features; see Section 0.03.06b. In fact, the substantial cross-checks between the work of Orszag and his coworkers, on one hand, and the independent effort of Kleiser and Herbert, on the other, provides enhanced credibility. For large-scale computations as for complex and delicate experiments, some degree of independent duplication is desirable for assured progress, especially in areas of potential controversy.

0.02.07   <u>Instabilities in nonequilibrium flow?</u>

The experimental and numerical evidence presented in the preceding section and the experimental evidence in free shear layers (illustrated in *<u>Note 2</u> to Section 0.03.04) force us to a <u>working</u> <u>hypothesis</u> that rapid inviscid instabilities can occur in through-flow systems where no neighboring equilibrium exists or is identifiable. In presence of large three-dimensional disturbances and/or in highly unstable flows, new flow configurations can evidently evolve or bifurcate from non-equilibrium flows. Since bifurcation in streamwise thickening shear layers represents a type of imperfection not yet tackled theoretically, there is a need to fill the void empirically for application to diagnostics, partial control, etc. Operationally, exponentially growing instabilities can be diagnosed from the graph of the variables against x or t, e.g.

the fundamental and subharmonic instabilities in <u>Fig 0-9</u>, and the vorticity stretching and tilting instability in Fig. 5 of Orszag and Patera (1983). Should the initial instability be algebraic in nature (see discussion in Carlson & WP, 1982), operational definitions would be more difficult. Perhaps that is why they have not yet been identified in any experiments. A priori, for Poiseuille flow with large disturbances, they are as likely suspects as the highly specialized disturbances of Orszag and Patera.

If we think in terms of vorticity interactions and restructuring of vorticity distributions, the hypothesis seems physically reasonable, even for the plane Poiseuille flow. This flow, being strictly parallel, presents a more delicate situation. Yet large disturbances could modify the flow enough to make it inviscidly unstable, for a long enough time, to have the sequence of instabilities lead to local turbulence. This is the lesson of <u>Fig 0-4</u>. The issue then becomes whether the turbulent configuration is self-sustaining or whether it decays, and brings up the theoretically and practically important concept of Re_{mint}. Pipe flows at $Re \sim 2300$ challenge the experts on turbulence modeling and computing with the test case of self-preserving, neutral turbulent puffs. Ample detailed experimental data for the test case has been assembled by Wygnanski & SF (1973).

At this writing, the above working hypothesis, or equivalent, seems indispensible to a consistent conceptual framework for interpretation of all reliable experimental information on through-flow systems.

0.03   MAJOR MECHANISMS OF INSTABILITIES

In 0.02 Sections each process of transition to turbulence was seen
as a specific evolution of solutions of the governing nonlinear NS
equations which is determined by the shear layer geometry, on one hand,
and initiated and conditioned by usually poorly known environmental flow
disturbances, on the other. Generally, the evolution corresponds to
dynamic restructuring of the vorticity of the shear layer into suc-
cessive, more or less stable, increasingly less homogeneous vorticity
distributions with an increasing number of characteristic scales.
Operationally, each rapid restructuring is generally identifiable with
an instability that has an essentially exponential growth in some
observables in the emerging characteristic wave numbers or frequencies--
i.e., an instability of locally linearizable systems. The nature of
these instabilities can, therefore, be studied through the simpler
equations linearized around the base flow undergoing the restructuring;
see Section 0.02.02. In contrast, characterization of the intervening
equilibria (when they exist) requires demanding nonlinear techniques, at
times purely numerical. In 0.3 Sections we discuss dominant shear-layer
instability mechanisms as gleaned from linearized theory, numerical
computations, and experiments.

Shear layers, by definition, correspond to boundary-layer-like
solutions of the NS equations, characterized by narrow convected layers
of diffusing distribution vorticity bounded by walls and/or regions of
essentially irrotational flow. Viscous diffusion smoothes vorticity
distributions, i.e. opposes the dehomogenizing restructuring of the
layer during instabilities, and is generally stabilizing. To understand
the essence of an instability mechanism we can therefore further sim-
plify the linearized arguments by "turning off viscosity" just before
applying our disturbance test of Section 0.02.02, while keeping the same
velocity profile and vorticity distribution. (That distribution, of
course, grew through viscous diffusion and therefore retains dependence
on Reynolds number in any scaling.) We shall discuss five inviscid

prototype mechanisms which cause vorticity restructuring in techno-
logically important shear layers: inflectional instability, centrifugal
instability, subharmonic vortex amalgamation, instability through vor-
ticity stretching and tilting, and cross-flow instability. However, we
shall commence with the one instability which is made possible by
viscosity itself.

0.03.01   Viscosity-conditioned instability

When the viscosity is turned off for the Poiseuille parabolic pro-
file (0-02)*, which in Section 0.02.02 was seen to be unstable for
Re > 5772, the instability mechanism vanishes! The vorticity distribu-
tion, $+2yU_c/h^2$, lacks a true maximum within the flow field, $-h < y < h$,
a necessary condition for Rayleigh's inviscid inflectional instability.
Tollmien has shown that viscosity is essential in two layers: (a) the
critical layer at which the speed of propagation of the instability
waves and the mean flow velocity $U(y_{cr})$ are equal, and (b) the layer
near the wall, which has the characteristics of a diffusive oscillatory
Stokes vorticity layer; see Batchelor (1967, p 354). When the inviscid
wall boundary condition $v = 0$ is augmented by the viscous no-slip
conditions $u = 0$ and $w = 0$, the momentum equation in the x-direction
yields a relationship between the local instantaneous pressure gradient
and the diffusive flux of vorticity $(\zeta = \partial v/\partial x - \partial u/\partial y)$ out of the wall,
i.e. $-\nu \text{grad} \zeta$ evaluated at the wall:

$$-\nu \frac{\partial \zeta}{\partial y} = \nu \frac{\partial^2 u}{\partial y^2} = \frac{1}{\rho} \frac{\partial p}{\partial x} \quad , \qquad y = 0 \qquad\qquad (0\text{-}4)*$$

Here ν is the dynamic viscosity and ρ the density. In other words, an
oscillatory pressure gradient reaching a wall can be interpreted as gen-
erating oscillatory wall vorticity sources of strength given by (0-4)*.

Following up on a remark of Lighthill (1963, p 93), Section A.06 of
the Guide documents the plausibility of the following self-excitation
hypothesis: the instability amplification is maximal when an effective
tuned resonant loop across y_{cr} exists between the ζ , v, and p
oscillatory fields. As the oscillatory vorticity, generated according

to (0-4)*, diffuses outward from the wall, it decays, but its residue reinforces the vorticity transfer from the mean flow just above y_{cr}. Also above y_{cr}, its component, $\frac{\partial v}{\partial x}$, growing in y , brings about the largest sources of oscillatory pressure in the boundary layer in accordance with the linearized pressure equation:

$$\nabla^2 p = -2\rho \frac{dU}{dy} \cdot \frac{\partial v}{\partial x}$$ (0-5)*

The resulting pressure reaches the wall instantaneously and closes the reinforcing feedback loop if the pressure gradient is in phase with the original vorticity flux, (0-4)*. As one follows the phase changes in the ζ - v - p chain, Tollmien's classical result that ζ changes phase by π across the viscous layer near y_{cr} is a factor in establishing the conditions for positive feedback.

The net phase variation around the loop depends most sensitively on the thickness, δ_s , of the wall Stokes layer, which scales as $(2\nu/\omega)^{\frac{1}{2}}$, where ω is the circular frequency, i.e. quite differently from y_{cr}. To maintain optimal feedback, δ_s should then maintain a constant "tuned" ratio with respect to y_{cr} , as the Reynolds number changes.
Figure 0-14 displays the dimensionless amplification rate c_i in the temporal growth factor, $\exp(c_i tU\infty/\delta^*)$, for the Blasius layer as computed by Wazzan & OS (1969). The ratio δ_s/y_{cr} , computed from the data of Fig 0-14, varies monotonically by a mere 4 percent along the ridge of maximal amplification from $Re_\delta*$ of 600 to 50,000, which covers much more than the practical range of interest for transition. (The range based on x is $122,000 < Re_x < 844,000,000$, over which the characteristic frequency and wave number change by factors of 929 and 4.3, respectively.) This invariance evidently supports the resonant-loop hypothesis and the vorticity-based mechanism.

---

*Note 1   Receptivity to sound in wall layers. There are probably many ways irrotational pressure waves can be converted to unstable vorticity waves in a wall layer. The most effective one discovered thus far was documented experimentally by Nishioka and Morkovin (1983). As sound of frequency f impinges on a wall and reflects from it, the no-

slip condition (0-4)* generates a thin oscillatory Stokes layer at the wall. If the amplitude A of the sound pressure gradient varies with x on scales comparable to the wavelengths of the amplified waves within the area c_i > 0 in Fig 0-14 for the given frequency, the self-excited mechanism just described takes over and makes the unstable wave grow from the seeded Stokes layer at the wall. As in the discussion of Fig 0-2 in Section 0.02.03, this is a forced solution response where the amplified homogeneous part of the solution dwarfs the rest of the local response. The growing unstable field propagating downstream satisfies the homogeneous equations but is in no sense free or arbitrary; when the sound excitation doubles, the amplitude of the unstable wave also doubles. The main features of the self-excited waves may be developed in one or two wavelengths from the start of the gradient variation A(x).

In Fig 0-5 of Kegelman (1982), the axisymmetric body in the inset was irradiated by sound from a loudspeaker upstream of the open-throat wind tunnel at levels of 105-115dB. The smoke from an upstream source impinging symmetrically on the sharp nose made the spatial growth of the "forced unstable waves" visible some distance past the shoulder; there the disturbances became sufficiently large and possibly nonlinear for visual resolution. Diagnostics with a hot-wire anemometer showed that the self-excited wave pattern began building up from the Stokes layer just upstream of the ogive-cylinder junction, as one would expect from the preceding model. At the juncture (Kegelman 1982, Fig. 38), there is a pronounced local peak in static pressure associated with the flow around the shoulder. To the first order, the diffraction around the shoulder of sound with wavelengths more than four times the body diameter causes a similar pronounced peak in the amplitude, A(x). Fourier transforms of peaked shapes yield broad bands of wavenumbers. From the evident receptivity to excitations at 551 and 785Hz, the wavenumber band covers the amplified wavelengths of the boundary layer.

*Note 2   The TS abbreviation for the wall waves. The viscosity-conditioned wall waves will be referred to as TS waves. Prandtl (1952, p 117) called them Tollmien oscillations. Theodorsen (1955) proposed that they be called after Tollmien, who developed sophisticated mathematical techniques for their calculation, and for Schubauer, who with Skramstad, documented them experimentally. More frequently the letter S has been associated with Schlichting, who carried out the detailed computations with which Schubauer and Skramstad compared their results. A brief historical account of the early research on these waves and of Tollmien's role therein is given by Schlichting (1979, pp 465-67). One should perhaps add to Schlichting's account reference to Taylor's 1915 reflections on possible destabilization by viscosity.

0.03.02   Rayleigh's inflectional instability

This is the dominant first instability in the vast majority of two-dimensional and axisymmetric free shear layers. They all have maxima in their initial vorticity distributions, $\Omega(y)$, (at the inflection points of the U(y) profiles) as required by the generalized Rayleigh theorem, Section 0.03.01. With the viscosity turned off, the constant-density fluid cannot exert any torque on the fluid elements; the total vorticity, $\Omega + \zeta$, of each element is therefore preserved along its path and its material derivative vanishes:

$$\frac{D}{Dt}\{\ \Omega(y) + \zeta(x,y,t)\}= 0; \quad \zeta(x,y,0) \text{ small} \tag{0-6}*$$

In the linearized form of (0-6)*, the products of perturbation terms $u\frac{\partial u}{\partial x}$ and $v\frac{\partial u}{\partial y}$ are dropped and we obtain

$$D_B(\zeta) = -v\Omega' = +vU''; \quad \text{with } \frac{d(U)}{dy} = U' \tag{0-7}*$$

The operator $D_B(\ ) = (\partial/\partial t + U(y)\partial/\partial x)$ is the material derivative associated with the base flow. While the full equation (0-6)* tells us that the net vorticity of any element is conserved, equation (0-7)* states that the unsteady perturbation vorticity ζ changes along the mean flow as a result of a source of vorticity per unit area equal to vU". This term, therefore, represents the transfer rate from the originally steady vorticity $\Omega = -U'$ to the unsteady perturbation vorticity. This captures the essence of our description of instabilities as dehomo-genizing: inviscidly the total vorticity is preserved, but the fluid elements with high vorticity rotate and slide along the increasingly wavy streamlines to cluster near foci in each wavelength of the most unstable instability mode; see Fig 0-6 and Fig 0-7.

The linearized equation (0-7)* can characterize only the initial linear mode of the motion, but its solutions give a remarkably good account of the true growth rates, the preferred frequency, and the y distribution of the velocity perturbations (the eigenfunctions).
Figure 0-6, for a simple mixing layer, portrays the extrapolation of the inviscid linear trends of vorticity restructuring to higher amplitudes

by Michalke (1965). Numerical computations by R. Metcalfe and J. Riley, Fig 0-7 (unpublished), show how viscosity smoothes out the lines of constant vorticity by the end of the first rapid restructuring of the mixing layer (growing in t rather than x). At any time, vorticity diffuses perpendicularly to the isolines; this is the basis of Michalke's suggested smoothing of profiles in Fig 0-6, a model of entrainment in mixing layers.

Description of this powerful instability as a self-reorganization of the vorticity field through mutual interaction via the Biot-Savart law appeals to engineers. Gill (1965) provides an appealing, essentially kinematic account of the mechanism. As the Reynolds number $\Delta U \cdot \delta / \nu$ increases, the evolution grows more powerful and rapid, as comparisons of instabilities in Section 0.04.05 show. For a given fluid, it is of course only the product in the numerator of the mean velocity increment across the shear layer times its thickness δ which grows. $\Delta U \cdot \delta$ measures the circulation per unit streamwise length of the layer--i.e., the total layer vorticity per unit length, the inviscid agent in the instability. For practical purposes the linear amplification rates reach their inviscid asymptote in mixing layers for Re $\sim$ 100 when they are nondimensionalized with respect to ΔU and δ.

---

*Note 1   On nonlinear level and empirical mode selection. In contrast to acoustic resonances, shear-flow instabilities take place over continuous spectral bands of frequencies and wavenumbers. It is usually assumed that when environmental disturbances are painstakingly minimized, the spectral mode f_m with maximal amplification rate over the band is the one that first grows to nonlinear levels. From widely scattered experimental and theoretical information, nonlinear interaction may begin when the cross-stream maximum rms streamwise u'_{max} fluctuation reaches 0.004 to 0.010 of the driving mean velocity ΔU or U_∞. For instance, in some of the experiments of Kegelman (1982) associated with Fig 0-5, nonlinearly-conditioned secondary three-dimensional instability appeared visually complete when u'_{max} was 0.012 U_∞ and must have commenced at much lower levels. See also the discussion of thresholds in connection with Fig 0-3a in Section 0.02.06b. While nonlinearity of the fundamental mode f_m can facilitate such secondary instabilities (especially of the parametric type), it is believed to inhibit the growth of its competitors in the amplifiable band of the primary instability. Similarly, when amplitudes of the 551Hz and 785Hz modes in Fig 0-5 are given a small head start through the acoustic stimulation (discussed in *Note 1 to Section 0.03.01), they reach nonlinear levels first and definitely preempt any palpable growth of the maximally amplified f_m, the presumed winner in "neutral environments."

Because of the paucity of rigorous data on the diverse "natural" environments" in laboratories and in technological applications, the general view on mode selection within the available spectrum, described above, represents only a working hypothesis which may need revision and certainly sharpening. For instance, the scenario is apparently not valid for axisymmetric jets for which the actually observed "natural" frequency f is commonly just below $0.8f_m$; see Hussain and Zaman (1978) and Drubka (1982). The judgment depends on how reliable is the result $f_m = 0.017$ /U obtained on the basis of linear inviscid spatial theory for a free mixing layer with a <u>constant</u> momentum thickness θ, the strictly parallel hypothesis of Michalke (1971) and Monkewitz and Huerre (1981). In axisymmetric and planar free mixing layers, the puzzling spontaneous selection of the observed f may also possibly be influenced by feedback from the more violent higher-order instabilities with which we are familiar under the label of jet noise. This feedback is discussed in more detail in *<u>Note 1</u> to Section 0.03.04.

*<u>Note 2</u>   <u>On free-stream disturbances and turbulence onset criteria</u>. It is appropriate, therefore, to look at three concrete examples of spectral content of u' within the thin <u>laminar</u> shearing layer on the outside of the axisymmetric jet with diameter of 5.14 cm in which Drubka (1982) observed the f-selection anomaly; see <u>Fig 0-8</u> (with a logarithmic ordinate). The reader may be shocked by the dominance of the continuous ("stochastic") spectrum at the start of the inflectional instability at x/D = 0.1 in <u>Fig 0-8</u> as well as at x/D = 0.35 and 0.55, in inset of <u>Fig 0-9</u>, the respective ends of the primary and secondary instabilities. Real-life instabilities in through-flow systems grow from disturbances vastly different from disturbances exactly proportional to the eigenfunctions, allowed in most theories. For instance, the amplitude A in <u>Sk 0.02.04</u> characterizes such restricted disturbances. The contrast becomes even more impressive when one finds that Case 1L of <u>Fig 0-8</u> and <u>Fig 0-9</u> represents the nondimensionally least disturbed jet conditions on record. The full rms u' across 80% of the jet was 0.0006 times the jet velocity U_j, and reached maximal values three to five times as high in the thin outer shear layer (such as represented by the integral of the spectrum in <u>Fig 0-8</u>). In that figure, the amplitude of f, visible as a hump near 720Hz, has already risen by a factor of 5 due to the inflectional instability. The reasons for the higher hump near f/2 are examined in Section 0.03.04. (Drubka placed grids upstream of the nozzle to generate different conditions 2L, 3L, and 1T for comparative studies of jet instabilities for three initially laminar and one initially turbulent boundary layer separating at the nozzle lip; hence the other more disturbed 2L and 3L spectra in <u>Fig 0-8</u>.)

Except for people who have carefully watched signals from hot wires immersed in laminar boundary layers or free shear layers at higher Reynolds numbers and used diverse visualization techniques, most students of fluid mechanics would classify the flows at x/D = 0.1, 0.35, and 0.55 in <u>Fig 0-8</u> and <u>Fig 0-9</u> as turbulent because the spectra are not dominated by discrete frequencies. Yet, no sudden occurrences of high, nonmolecular small-scale diffusion, the third syndrome of active turbulence, Section 0.01.01, take place upstream of x/D = 1 for conditions 1L at $Re_D = 40,000$!

*Note 3   Buffeted laminar layers. Such hybrid regions with substan-
tial "stochastic" energy contributions (the continuous part of the
spectrum) occur rather commonly and deserve a special classification
such as "buffeted" or "stirred" laminar layers. In the present case,
the difference has little practical implication (except perhaps in jet-
noise experiments) because the layer soon becomes truly turbulent any-
way. However, boundary layers on blunt-body noses in streams with
higher turbulence are frequently but incorrectly assumed to be turbu-
lent. In most cases the oncoming turbulence, amplified by vorticity
stretching in the flow around the nose, merely buffets the laminar layer
without making the transport processes in the layer turbulent. Substan-
tial errors in assessment of heat transfer can thus be incurred. Stir-
ring a cup of cream with random motion does not necessarily provide the
energy and the range of scales to give the induced motion intrinsic
turbulent dynamics. A more theoretical view of buffeted layers is found
in Section A.16 of the Guide.

In the case 1L of Fig 0-8, most of the buffeting came from down-
stream activity, either directly or through conversion of the unsteady
pressure gradients at the lip. We recall that such gradients diffract
around the nozzle lip and generate vorticity fields, which in turn are
amplified, wide-band, by the mixing layer; see *Note 1 of Section
0.03.04. In that sense any separated layer is an amplifier of envi-
ronmental disturbances, a fact to remember when trying to reduce them in
an experimental facility. In cases 2L and 3L of Fig 0-8, an increasing
share of the stirring and buffeting comes from the upstream grids.

*Note 4   Desirable information on free-stream disturbances and some
consequences. In closed wind tunnels, a judicious mix of optimal honey-
combs, screens in the settling chamber, and a moderate contraction ratio
to the test section (see, for instance, Nagib, 1984) can bring the
single (inadequate) measure of the disturbances u'/U down to 0.01 to
.02 percent, still far in excess of macroscopic manifestations of molec-
ular stochastics. In the lower range of frequencies the most offending
disturbances are again of the buffeting type, propagating upstream from
the common offenders, the diffusor and the first tunnel bend. Inter-
action between residual turbulence and the driving fan, secondary flows
from tunnel bends bringing boundary layer fluid into the free stream,
interactions with and wakes from corner veins designed to counteract the
secondary flows, etc..--all contribute to the free-stream disturbances.

The above characterization of the sole u'/U measure as inadequate
refers to the fact that different important consequences ensue depending
on the mix of its ingredients: true vortical turbulence, true acoustic
waves with short wavelengths, and hybrid irrotational lower-frequency
pressure fluctuations within one or two wavelengths from their sources,
such as those in the diffusor. Spectral information from at least two
instruments with varying lateral and streamwise displacements is needed
for adequate decomposition of u' into these constituents over the
frequency range. The usually dominant random low frequency content may
come primarily from large-scale pressure fluctuations but can also be
generated by convected meandering streamwise vorticity. The low-fre-
quency pressure fluctuations modulate randomly all aspects of the flow,

even the thickness of boundary layers and free shear layers; this magnifies considerably the scatter in instability measurements, especially in wall layers where the self-excitation is sharply tuned. Convected streamwise vorticity induces streamwise vortices in boundary layers, which are the least stable modes in the stable regions. If the streamwise vortices should reach nonlinear levels (say, through stretching in the contraction shown in Fig 0-1b to form narrow duct flow), associated algebraic instabilities, e.g. Hultgren and Gustavsson (1981), could be responsible for starting the instability chain to turbulence. In the case of the anomalous Poiseuille Re_{tr} on the order of 1000-2000, which do not fit current bifurcation concepts, such a dominant role evidently has to be assigned to environmental disturbances as the most likely rational explanation; see Section 0.02.06.

The reader should be cautious in accepting the u'/U measure cited in many papers on stability experiments and check to what extent its spectrum extends toward zero. Until about 1970 the commercially available instruments cut off at 20Hz or higher. Consequently some of the classical reports understate by as much as 50% the level of disturbances (which makes some of the published correlations based on the over-all u' hot-wire measurements even more dubious).

*Note 5   Conceptual implications of disturbance environments. This series of Notes should be of interest to all fluid dynamicists without substantial experience with instability experimentation. Its net message: environmental disturbances in through-flow and technological systems tend to be omnipresent, their origins very complex and poorly controllable, and their theoretical and practical consequences nonnegligible. As initiators of the chain of instabilities they influence the specific paths to transition and can advance the onset of turbulence catastrophically for sensitive designs. Without deeper understanding of receptivities to the constituent disturbances and better diagnostics for the environment in each design system, their cumulative, interactive, and stochastic nature will make progress in rational design of transition-conditioned systems extremely difficult.

On the purely theoretical side, historically the observed causative presence of macroscopic stochastic disturbances at the birth of the sequence of flow instabilities in through-flow systems made the randomness in the final product seem more natural than surprising. Such observations do not detract from the more recent fundamental findings of "chaotic motion" in autonomous nonlinear deterministic systems associated with the concept of strange attractors. Both trends to irregular aperiodic behavior undoubtedly stem from the most extreme sensitivity of the solutions of the nonlinear equations to initial conditions. In through-flow systems the trend is compounded by the role of nonnegligible causative stochastic disturbances.

While the concept of strange attractors brings transition to turbulence rather comfortingly into the broader panorama of nonlinear phenomena, its direct applicability to NS equations is not on the horizon.

The essential character of spatial three-dimensionality in the distur-
bances and in the higher-order "inviscid" instabilities is unlikely to
be captured by the theoretical tools in the hands of searchers for
strange attractor secrets. Any promising technique would have to be
able first to discern fundamental differences between real-life three-
dimensional turbulence and nonlinear chaotic motions, restricted to two
dimensions.

0.03.03   Centrifugal instability

Although centrifugal instability can be more powerful than inflec-
tional instability in underexpanded supersonic jets, it is of primary
importance for steady wall flows with concave curvature at the boundary,
and of course in our prototype, the Couette-Taylor annulus with the
inner cylinder rotating, Sections 0.02.01 - 0.02.05. To reveal the
essence of the mechanism we shall again resort to our thought experiment
of turning viscosity off after the base flow is established. We use
polar coordinates based on the local radius of curvature R. According
to a variant of Rayleigh's criterion, any inviscid two-dimensional
curved flow for which the local vorticity $\omega_z = \dfrac{\partial V_\rho}{\partial r} + \dfrac{V_\theta}{r} - \dfrac{1}{r}\dfrac{\partial V_r}{\partial \theta}$
and the local angular velocity about the center of curvature $W = V_\theta \dfrac{1}{R}$
have opposite signs, $W\omega_z < 0$, is locally unstable. Under such condi-
tions the radial pressure gradient cannot equilibrate the centrifugal
forces, as we shall indicate heuristically below. When the flow is
viscous this inviscid imbalance still tends to drive secondary flows but
is fully impeded by friction below some geometry-dependent critical
dimensionless Taylor or Görtler number of the form $Re_\mathcal{C}(\delta/R)^{\frac{1}{2}}$, where $Re_\mathcal{C}$
is the Reynolds number based on the driving tangential velocity, and δ
its thickness in concave boundary layers (or the gap between axisym-
metric cylinders).

The nonlinearly saturated secondary flows which result from the
initial linear instability take the form of rows of steady streamwise
counter-rotating pairs of vortices (scaling with δ); these fill the
available spanwise (axial) space. The centrifugal instability thus

dehomogenizes the vorticity in the spanwise direction and creates a field of + and - tangentially oriented vorticity, where the original flow exhibited only a smooth distribution of spanwise vorticity ω_z . In contrast with previous cases, three-dimensionality of vorticity is generated here by the very first instability and is clearly abetted by different regions of the three-dimensional spectrum of environmental disturbances, namely steady or slowly meandering streamwise vorticity. On the other hand, the vortex array in the new equilibrium is steady; the second instability should therefore differ in character from the parametric instabilities in jets and wall layers for which the new quasi-equilibria are periodic in t and x and two-dimensional; see *Note 1, Section 0.02.06.

To get a feel for the mechanism of the instability, we consider a steady circular velocity field (0, V(r), 0) in cylindrical coordinates, r, θ, z. The equation for the radial component of momentum (whether viscous or inviscid) states that the centrifugal force per unit mass must be exactly balanced by the pressure gradient $\partial P/\partial r$. As usual, to test for instability we perturb the flow and check whether there is a restoring tendency. Von Karman in 1934 envisaged an infinitesimally thin doughnut of fluid at r_0 with speed V_0 displaced to a neigh-boring r_1 orbit ($r_1 = r_0 + dr > r_0$) at some axial position z. To conserve mass, this outward motion v_r must be compensated for by inward ring motions at other z stations and accommodated further by axial motions $v_z(r,z)$ of the displaced rings. The constraint due to the continuity equation $\partial(rv_r)/\partial r + \partial(rv_z)/\partial z = 0$ couples naturally the cross-stream perturbations v_r and v_z and generates the streamwise perturbation vorticity $\omega_\theta = \partial v_r/\partial z - \partial v_z/\partial r$.

Under what conditions is the difference between the ambient pres-sure gradient at r_1 , namely $\rho V_1^2/r_1$, and the centrifugal force of the displaced ring $\rho(V_0 + v_\theta^2)/r_1$ larger than zero and the disturbance counteracted? In an inviscid fluid the displaced ring must conserve its circulation, i.e. $2\pi r_0 V_0 = 2\pi r_1(V_0 + v_\theta)$. This evaluates the pertur-bation v_θ in the tangential velocity in the displaced ring relative

to the ambient fluid: $V_0 + v_\theta = r_0 V_0/r_1$. Simple algebra then reduces the inequality needed for stability to $(r_1 V_1)^2 - (r_0 V_0)^2 \sim d(rV)^2/dr, dr > 0$. Thus another formulation of the Rayleigh stability requirement is that the square of the circulation of the undisturbed flow increase outward from the center of curvature; it is numerically equivalent to $\omega_z W > 0$, which is often easier to apply.

Obviously potential vortex flows are neutrally stable, and any local rigid-body rotation is stable. The latter fact clarifies why the cores of vortices trailing behind airplanes relaminarize some distance downstream. The inviscid criterion applies locally to curved nonaxisymmetric flows. The presence of viscosity, even in the simpler linearized equations for the first instability, brings about serious analytical (asymptotics) and computational difficulties. Sufficiently reliable detail results for the Görtler instability in boundary layers along bodies with concave curvature appeared only in 1981 (see Fig 0-22, and even then some of their aspects were questioned in 1982. On the other hand, the formation of Taylor vortices in the constant annular gap between concentric cylinders when the rotation of the inner cylinder drives the flow has been a triumph of the instability theory since 1923. When the outer cylinder drives the flow, a concave boundary layer is formed at the start and the flow generally succumbs to Görtler and secondary instabilities before a fully developed laminar flow can be established across the gap. Since technologically important flows invariably possess locally curved streamlines, an engineer should be aware of the consequent possible local stabilizing or destabilizing tendencies.

As an example, let us apply the criterion to the stagnation flow in Fig 0-1a. Accordingly, the irrotational flow along streamlines approaching the airfoil just above the stagnation point has anticlockwise rotation but remains neutrally stable until the streamlines enter the boundary layer. There the vorticity ω_z becomes non-zero and clockwise, and the flow is inviscidly unstable. After exploring at length the delicate eigenvalue problem for the viscous two-dimensional stagnation region, Wilson and Gladwell (1978) concluded that no centrifugal

instability develops inside the boundary layer; presumably effects of viscosity, high acceleration, and wall proximity counteract fully the mild tendencies to centrifugal instability indicated on the inviscid basis. Apparently we should ascribe the substantially enhanced stream-wise vorticity observed growing in stagnation regions, such as in Fig 0-1a, not to centrifugal instability but to vorticity stretching of Section 0.03.05. (The theoretical and physical issues for this anomalous boundary-value problem, which include direct convection of free-stream disturbances into the region, are analyzed at some length by Morkovin (1979) and are by no means settled.) The presence of Görtler instability is often suspected but seldom documented in laminar flows, mostly because of the difficulty of measuring steady streamwise vorticity. On the basis of disconnected and partial evidence, we may conjecture that Görtler instability does start the road to transition in many practical cases of concave walls, from airfoils to windtunnel contractions. The inviscid destabilizing mechanism remains present, even accentuated by the velocity gradient, after turbulence is established everywhere in the boundary layer. Once again, it should not be surprising that more or less regular streamwise Görtler vortices have been identified in turbulent boundary layers; see Tani (1962) and Bradshaw (1973, pp 40-42). They change transport properties across the layer significantly.

0.03.04   Subharmonic vortex amalgamation

The NS numerically computed vorticity configuations in Fig 0-7 near the end of the first inflectional instability is of necessity highly idealized. It corresponds to a strictly discrete spectrum with no spectral content below the fundamental frequency f. Our glimpses of real-life spectra in Fig 0-8 and in the top insert of Fig 0-9 make us aware of the fact that there invariably exists a large reservoir of energy below the first-mode frequency f. Most of these disturbances are internalized in the real-life vorticity distributions in contrast to conditions in Fig 0-7. As such, these internal disturbances become the possible seeds for the next restructuring of the vorticity distribution; they are equivalent to a pre-stimulation of the secondary instability.

An inviscid stability analysis by Pierrehumbert and Widnall (1982) of a row of finite-area vortices, and much computing, identified two types of disturbance-conditioned secondary instabilities. The three-dimensional type will be examined in Section 0.03.05. For two-dimensional infinitesimal stimulation, the most amplified motion corresponds to a frequency-halving mode in which successive vortices rotate around each other and amalgamate, two at a time. In numerous smoke visualizations the merged pairs give impressions of smooth single vortices, whereas numerical NS experiments of Metcalfe and Riley (1981) show incompletely merged vorticity configurations such as those in Fig 0-10. At any distance from the vortices, sufficiently large with respect to the distance between them, induction by Biot-Savart law would be practically that due to a single circular vortex. While viscosity has yet to smooth the "valley" between the vortices in Fig 0-10b, the total strength of these co-rotating vortices remains constant -- that of the sum.

Vortex and vortex-loop pairing, discovered in the Fifties, has slowly become accepted as the most common of secondary instabilities in mixing layers and circular jets. As with other dominantly inviscid mechanisms, it remains operative (in a less clear cut manner) when smaller scale turbulence is present. The original inflectional roll-up and repeated subsequent pairings, in fact, have been proposed as a

model for the thickening and entrainment in mixing layers, laminar or turbulent, e.g. Ho (1982).

If the aforementioned modulation of f in Fig 0-10 contained f/3 contributions sufficiently larger than those in f/2, the one-third subharmonic would win the competition and three vortices would merge into one, as is occasionally observed in noisy mixing layers. In fact, any number of vortices can merge, as Ho and Nossier (1980) discovered through visualization when lower-frequency feedback from an impinging jet to its nozzle lip caused the modulation at the lip. Such subharmonic amalgamations are related through the theory of parametric instability sketched in *Note 1 of Section 0.02.06. The fact that the base flow is not primarily a function of the cross variable y and is nearly periodic in the direction of the flow at moderate Reynolds numbers sets up a linearized equation for the secondary instability with periodic, rather than constant or near-constant, coefficients.

---

*Note 1   Upstream influence and feedback in free shear layers. Sections A.09 and A.10 of the Guide distinguish between four types of upstream influence relevant to interpretation of instability experiments. The fourth type corresponds to the impingement feedback of Ho and Nossier (1980), above, and Rockwell and Schachenmann (1982) in Section 0.02.0 . The third type, the upstream feedback from secondary and higher downstream instabilities, does not exist in parallel-flow temporally growing instabilities such as those in the numerical experiments leading to Fig 0-7 and Fig 0-10. In temporal analysis, the flow is strictly periodic in x and the motions at all x positions continuously interact since the NS equations, linearized or not, are elliptic in nature.

In spatially growing mixing layers at low and moderate Reynolds numbers, the periodicity in x is only approximate during the first instability and ends abruptly with the pairing. The equations remain elliptic in x for pressure (finiteness of the speed of sound is immaterial to the instability at low Mach numbers), but vorticity is convected parabolically with the flow. An event such as the abrupt pairing pictured in Fig 0-___ generates a substantial pressure disturbance according to (0-5)* in Section 0.03.01 augmented by nonlinear pressure sources $-\rho \partial^2 u_m u_n/\partial x_m \partial x_n$, summed over m and n from 1 to 3. No such events are encompassed by the equations for the primary spatially growing instability downstream of the lip. The consequences of the event are therefore superposed on the primary field. The event influences the primary instability dominantly through the upstream boundary conditions at the lip. As the pressure field diffracts around the lip it generates vorticity at the lip, according to the no-slip condition (0-4)*, which is immediately convected into the separating shear layer and amplified

inflectionally. The receptivity to unsteady pressure fields in attached boundary layers requires spatial variation of amplitude $A(x)$ on the scale of amplifiable Tollmien-Schlichting wavelengths λ_{TS}. In contrast, the free shear layer through inflectional instability amplifies a far broader band of disturbances, with a λ cut-off on the order of δ , and does so much more powerfully. (Put another way, the $A(x)$ variation here corresponds to a Dirac's delta function $\delta(0+)$ whose Fourier transform has a white spectrum, stimulating all wavelengths.)

Drubka's Fig. 61 displays a spectrum of pressure fluctuations (measured on a flange attached to the nozzle lip) which contains four peaks subharmonic to f. All four peaks were identified with flow interactions occurring downstream of the first roll-up and thus testify to the upstream self-modulation of jets, at least at higher Reynolds numbers. This upstream effect, first stressed by Dimotakis and Brown (1976), is a fundamental fact for mixing layers and jets. Some of its implications were discussed in the Notes in Section 0.03.02.

*Note 2   Disappearance of intermediate equilibria in mixing-layer instabilities at higher Reynolds numbers. In Drubka's experiment 1L, the most energetic of the discrete velocity fluctuations, seeded by the pressure gradient at the lip, turned out to be that at f/2. According to Fig 0-9 , this subharmonic is more than ten times stronger than the primary fluctuation f (which, as discussed in *Note 1 of Section 0.03.02, is less than the theoretically most amplified frequency f_m). Evidently in cleaner environments the more orderly pairing can give rise to sharper, less smeared pressure gradients with longer upstream influence. Evidently the upstream self-influence of the f mode, intrinsic to the self-excited amplification process itself, is weaker. Nevertheless, the process is effective indeed: a growth factor in excess of 1000 in less than three wavelengths, λ being 0.13D long.

Both f and f/2 modes have essentially exponential growths for $x < 3D$. In accordance with linear theory they grow, at first competitively, at different rates and travel with different phase speeds. Near $x = 3D$, their phases lock nonlinearly. Traveling now at the speed of f, the less amplified subharmonic mode can receive energy from the f mode. The invigorated subharmonic then grows faster, but again at an essentially exponential rate. In the idealized theoretical case this would be the linearized rate for the growth of a perturbation of an f quasi-equilibrium consisting of at least two rolled-up vortices.

Clearly, the f mode is far short of such an equilibrium at $x = 3D$. The f mode actually completes its first roll-up while the secondary instability of amalgamation is going on! We can venture a general hypothesis: when mean vorticity is more concentrated, as at higher Reynolds numbers, the vorticity restructuring can commence on a new scale before the preceding reorganization is complete. Phrased in terms of vorticity interactions, the hypothesis seems reasonable and not a radical challenge to the hypothesis of successive equilibria. In Section 0.02.06 we found it impossible to account for the anomalously low transition Reynolds numbers in duct flows without allowing instabilities to develop from large disturbances without passing through a

flow equilibrium. Similarly, conceptual description of observed developments in higher-Re axisymmetric jets does not appear possible without allowing for simultaneous progression of instability-like restructuring on several scales from δ to D without intermediate equilibria. Drubka's 1982 detailed documentation simply provided convincing concrete illustrations. There are many other examples of overlapping instability development involving different geometries of secondary instability. One of these, the classical 1962 observations of Klebanoff et al of increasing spanwise corrugation of barely nonlinear, still growing TS waves in boundary layers is discussed in *Note 1 of the next section.

0.03.05   Instability through vorticity stretching and tilting

In two-dimensional flows the single component of vorticity satisfies the same differential equations as the specific heat $c_p T$. Total vorticity, like total heat, is conserved when the vorticity flux across the boundaries, expressed in terms of the presure gradient, is taken into account, as previously indicated. In three-dimensional flows, however, there is an additional intrinsic vorticity source rate per unit volume, $\underline{\omega} \cdot \text{grad}(\underline{V})$. One of its constituent terms is the vorticity stretching term $\omega_x \partial U / \partial x$, $\partial U / \partial x$ being the strain rate in the ω_x direction. Thus when vorticity is stretched, the positive rate of change of the vorticity is proportional to the vorticity itself, a condition for rapid growth. When the stretching is abetted by the other two contributors to the x component of $\underline{\omega} \cdot \text{grad} \ \underline{V}$, $\omega_y \partial U / \partial y$ and $\omega_z \partial U / \partial z$, an inviscid, essentially exponential growth commonly ensues. These sources represent the rate of transfer to ω_x from tilting of vortex lines into the x direction by the flow deformation. The stretching-tilting effect is a consequence of conservations of mass and inviscid angular momentum familiar from experiments on gyroscopes. On short time scales in real flows this inviscid instability overwhelms the viscous diffusion effects except at the smallest spatial scales. The effect is quintessential to the dynamics of three-dimensional turbulence.

In the sequence of instabilities the stretching-tilting effect fuels primarily the secondary and higher-order instabilities. When it does enter, it is likely to be powerful and therefore must be allowed

for in diagnostics. In most shear layers the original vorticity distri-
bution consists solely of diffused $\omega_z(y)$ layers. In the first pertur-
bation of this equilibrium, the tilting-stretching terms are given by
products of infinitesimals and therefore do not play any role during
most initial instabilities. After the buildup of vorticity concentra-
tions to nonlinear levels through the first instability, the tilting-
stretching terms become of the first order. They can then participate
in secondary instabilities in response to internalized three-dimensional
disturbances.

The theoretical and numerical investigations in two-dimensional
ducts of Herbert (1981) and Orszag and Patera (1981) discussed in
Section 0.02.06 are of this type. In Section 0.03.04 we referred to a
second family of the instabilities of the period row of finite-vorticity
cores analyzed by Pierrehumbert and Widnall (1982). This instability,
dubbed "translative" by the authors, involves stretching and tilting.
It appears most dangerous for disturbances with spanwise wavelengths
about 2/3 of the streamwise separation between vortex cores. Streamwise
vorticity, evident in the plan view of the mixing layer in Fig. 176 of
Van Dyke's 1982 Album, is believed to be associated with the translative
instability. Growth of azimuthal corrugations is clearly visible in
Figures 118, 120, and 167 of axisymmetric jets of Van Dyke. These
photographs show that the growth can be very rapid and can be proceeding
simultaneously with the secondary instability of pairing. Simultaneity
of pairing and three-dimensionalization are confirmed in probing numeri-
cal experiments with NS equations described in a 1983 manuscript by
Corcos and Lin.

In view of the intrinsic three-dimensionality of the final product
of the instabilities -- turbulence -- the participation of the stretch-
ing-tilting mechanism in secondary and tertiary instabilities could be
anticipated. It is the increased emphasis on visualization, on one
hand, and the rapid progress in computing, on the other, that is now
making possible more specific statements concerning the instability.
The evident simultaneity of many secondary instabilities at higher

Reynolds numbers again seems reasonable when seen as self-interaction of vorticity distribution evolving at different scales which include the spanwise direction. This increasing number of possible motions illustrates the notion of the trend to larger number of degrees of freedom with Reynolds number in fluid systems, as mention in Section 0.01.01.

---

*Note 1   Higher instabilities and breakdown in boundary layers. The smoke-indicated two-dimensional TS wave configurations in Fig 0-5 change rather suddenly into triangular or truss-like patterns, before becoming more irregular and turbulent farther downstream. Two types of such truss formations were observed as early as 1967 but remained not understood until 1981. In one, corresponding to higher excitation levels, the trusses formed an "in line" pattern: >>> , thus preserving the streamwise wavelength λ_{TS}. The second type of truss formation was labeled "staggered": the triangular pattern formed checkerboard fashion, so that the streamwise distance between successive trusses changed to two λ_{TS}. The 1981 Fig 0-11 by Saric displays three smoke-wire views of TS waves generated by a vibrating ribbon at three successively higher excitation amplitudes in a flat-plate boundary layer. The reader can thus compare the "linear," the staggered, and the in-line wave formations directly under otherwise identical conditions in the same environment.

It is now clear that the onset of the in-line pattern corresponds to the rapid three-dimensionalization into streamwise "valleys" and "peaks" of TS waves when they grow nonlinearly past a threshold of about $0.01U^\infty$, as classically documented with hot wires by Klebanoff et al (1962). As the growth of the TS component continues during this three-dimensionalization, the instantaneous velocity profiles at the peak spanwise locations become inflected over an increasing fraction of the TS period. A short distance downstream this is followed by periodic groups of very regular higher-frequency signals appearing over (riding on) a part of the TS wavelength. Klebanoff et al painstakingly identified the signals as coming from an instability resulting in a series of fine-scale hairpin-shaped eddies at the peak locations. Formation of local patches of turbulence at the spanwise peak locations presumably follows the hairpin eddies in two to three wavelengths. All elements of the preceding "Klebanoff breakdown" were confirmed and developed further in the case of the breakdown of ribbon-excited TS waves in Poiseuille flow in a series of experiments by Nishioka and coworkers 1975 - 1980.

The above development is fully consistent with the bottom pattern in Fig 0-11, except that the formation of the hairpin eddies has not yet been observed in smoke visualizations. The visible smoke accumulations occur in the so-called "cat's eye" region in the boundary layer which reaches slightly above y_{cr}. The local inflections and high frequency signals occur higher in the boundary layer, where no smoke is present. A separate smoke wire placed at a height of about 0.6δ should make the hairpin formation visible.

The feature of the staggered pattern not recognized in 1967 was

its subharmonic character and its implication of the parametric nature
of the secondary instability. The swift three-dimensionalization
doubles the wavelength and causes rapid rise of fluctuation energy near
f/2 in the hot-wire spectrum. Three sets of experimenters more or less
simultaneously provided complementary descriptions of this new break-
down: Kachanov and Levchenko (1982), Saric and coworkers, and A. Thomas
and coworkers. The nonlinear three-dimensionalizing effect usually sets
in at lower thresholds, on the order of $0.003 - 0.005U_\infty$. Smoke visual-
ization reveals that the instability can be switched to the "in-line"
form by additional stimulation to about $0.01U_\infty$ level. There is as yet
no information on possible higher instabilities, equivalent to Kleba-
noff's hairpin eddy formation. Both types of breakdowns have been
observed with and without artificial stimulation on bodies similar to
that in Fig 0-5. There is yet no information on the relative frequency
of occurrence of the two paths to transition outside the laboratory.

Since 1962 numerous theories claimed to "explain" the Klebanoff
breakdown, with various types of ad hoc assumptions. It is probably
safe to say that none can claim sufficient experimental evidence for its
validity, an issue of considerable delicacy. Not until the recent work
of Herbert (1981) was a rational criterion advanced for the spanwise
wavelength in the rapid three-dimensionalization process. Based on our
general discussion of secondary instabilities, a revision of the num-
bering in the literature seems desirable. Specifically, the hairpin-
eddy instability called secondary by Klebanoff should probably be
called tertiary. The earlier rapid three-dimensionalization processes
almost surely represent genuine secondary instabilities with nonlinear
thresholds in both types of breakdown. They both appear to be para-
metric, because of the periodicity of the TS waves, and involve vorti-
city stretching and tilting in the development of the three-dimensional
vorticity formations. More definitive statements concerning matching of
theory and observation must await further work.

Kachanov and Levchenko (1982) repeatedly observed artifically
unstimulated subharmonics at 0.3f and 0.7f, which call for theoretical
explanations. They believe that when a parametric instability of a
periodic system with frequency f develops to nonlinear levels and
approaches saturation, it may allow co-existent solutions with af and
bf , where a and b are proper fractions with a sum equal to unity.
They document experimentally that small artificial excitations at either
frequency af or bf indeed cause growth of spectral humps at both
frequencies. A general theoretical demonstration of such an effect in
parametric systems is desirable. Inter alia, it would strengthen diag-
nostics in nonlinear phenomena in other fields as well.

For the sake of completeness of our present picture of transition
initiated by TS instability, the experiments of Arnal and Juillen
(1978) deserve a reference. In presence of a non-separating adverse
pressure gradient, the three dimensionalizations of Fig 0-11 appear
absent. A genuine nonlinear, essentially two-dimensional, roll-up
evidently takes place near the inflection point of the velocity profile.

We thus have a third topography of boundary layer breakdown, although details of higher instabilities remain unexplored.

0.03.06   Cross-flow instability

Cross-flow instability refers to the initial instability of a boundary layer for which the streamline direction at its outer edge and the shear stress at the wall are not contained in the same plane through the local normal to the body; see Fig 0-12. In this figure local orthogonal coordinates are chosen with y in the direction of the normal to the body, x tangent to the body and parallel to the outer streamline, and z tangent to the body and perpendicular to the xy plane. At a given x,z position the boundary layer velocity vector twists from the shear stress direction at the wall to the potential streamline direction at $y = \delta$, tracing out the surface marked in gray in Fig 0-12. The negative gradient of the tangential component U(y) in the xy plane gives the $\omega_z(y)$ vorticity distribution (which alone characterized the shear layers studied thus far). The gradient of the local cross-flow velocity component W(y) in the yz plane yields the new feature of the unperturbed layer: a streamwise $\omega_x(y)$ vorticity distribution (positive and negative).

Such boundary layers are encountered on sweptback wings, yawed by cylinders, and other three-dimensional surfaces. Poll's 1980 photograph of the oil flow visualization of the front part of a circular cylinder yawed at 55°, Fig 0-13, tells us that the dominant instability of this more general vorticity distribution brings about a roll-up into curved one-sided quasi-stationary nonlinear vortices on the scale of δ . The pattern has been observed widely and with other means, including traversing hot-wire anemometers. The anemometers also show some unsteady signals, possibly directionally amplified waves in secondary instabilities of the new base flow. The serious gap in our knowledge concerning secondary instabilities and onset of transition to turbulence in cross-flow geometries is covered in practice by rather crude empirical correlations.

When a disk like a circular buzz saw rotates in free air, a three-dimensional boundary layer builds up at the disk and is cast off at its edge; see Fig. 5.12 of Schlichting, 1979 ed. Again, similar curved quasi-stationary vortices form and rotate with the disk. Since in the disk case the boundary layer is flat and of constant thickness, both theory and experiment are simpler, though very demanding. Much of our still meager understanding has been built up on the disk prototype.

Early theory established that the instability is inviscid; the effect exists when viscosity in the instability equations is set to zero. Heuristic arguments centered on the analogy with two-dimensional inflectional instability. In Fig 0-12 there is an inflection point I of the W velocity projection, which corresponds to a local maximum of the vorticity component ω_x. In a projection plane through the y axis rotated somewhat beyond 90° from the xy plane, the inflection point falls near where the projected velocity profile becomes negative. We now know that for such an orientation, periodic vortical disturbances locally perpendicular to the plane can have near maximal amplification along their axis and yet remain stationary with respect to the wall; see Tani (1981). On sweptback cylinders and wings the orientation of the growing vortices is close to the local freestream direction, Fig 0-13.

We note that once again the first instability results in a periodic dehomogenization of the vorticity distribution. This distribution, however, is stationary with respect to the wall and thus differs significantly from the inflectional instabilities already discussed. Because of their convected periodic patterns, they led to parametric secondary instabilities. No perturbation study of steady streamwise vorticity distribution in boundary layers in either the cross-flow or the Görtler instabilities has yet been reported; the breakdown pattern is probably different. Furthermore, in two-dimensional inflectional instability, the total vorticity is conserved in the dehomogenization process. Here, the initialpresence of the finite additional vorticity component ω_x in Fig 0-12 and the finite strain rate $\partial U/\partial x$ around the cylinder makes some of the vorticity stretching terms of first order, even in the initial instability. Thus the vortex stretching mechanism, also invis-

cid, may possibly contribute a net source of vorticity in the cross-flow instability.

Subsequent secondary and tertiary instabilities in cross flows remain uncharted. They tend to cause transition in boundary layers of yawed cylinders at Reynolds for which the boundary layers on unyawed cylinders remain laminar. Similarly, on airplane wings swept back in excess of about 20° this road to transition is believed to be shorter than that initiated by the competing TS mechanism. It seems reasonable that three-dimensional boundary layers (with more than one component of vorticity) should reach the intrinsically three-dimensional state of turbulence more rapidly. However, hard documentation for these observations is missing. Indeed, much basic research remains to be done on cross-flow and subsequent instabilities.

0.03.07   On some missing links

The six preceding 0.03 Sections cover the most important identified instability mechanisms in mechanically driven nonstratified shear layers. All but the fourth and fifth do commonly initiate the different types of sequences of instabilities discussed in the 0.02 Sections. However, these mechanisms can also apply in secondary and higher-order instabilities. Thus the Klebanoff breakdown in boundary layers commences with the viscosity-conditioned TS mechanism of Section 0.03.01, proceeds with the parametric form of the vorticity stretching and tilting instability of Section 0.03.05, and is followed by a somewhat three-dimensional version of inflectional instability of Section 0.03.02.

In many real-life paths to transition the whole sequence or some of the mechanisms in the sequence remain unidentified. One important case concerns the path to turbulence in wall layers with distributed roughness, of obvious interest in applications. Recent theories proposing that the effects of distributed roughness make mean velocity profiles inflectional and thus more susceptible to TS waves have been disproved

experimentally by Reshotko and Leventhal (1981). The perspective on the roughness problem thus remains as outlined by Morkovin in 1978, pp 17-20 -- namely, poor.

It is instructive to consider the example of the transition process downstream of an isolated three-dimensional roughness of height k on the order of 0.2δ or less. It is known that when its Reynolds number Re_k (i.e., ku_k/ν with u_k representing the velocity at height k in the layer with the roughness absent) approaches 600, the periodic vortex loops growing inflectionally on its near wake are becoming sufficiently strong to court further instabilities. Moderate acoustic stimulation of the proper frequency can make the turbulence onset jump from very far downstream to within $30\delta - 60\delta$ of the protuberance, a curious incubation distance. The mechanism of this rather spectacular turbulence-triggering instability is not known. Hence, in this sequence, our understanding remains limited to the first of the instabilities. Even though the equations describing the base flow in the vicinity of the obstacle and its perturbations would have to be solved on a very advanced computer to provide enough spatial resolution, we can safely classify it as inflectional and understood. All features of the amplification process, including its sensitivity to sound, follow the charted behavior of its prototype, the separating mixing layer.

If it now could be proved that transition in presence of sandpaper is similarly controlled by Re_k at the small number of the highest protuberances in the probability distribution of the grains, we would achieve a quantum jump in our understanding. Problems with spatial resolution, the masking effects of free-stream disturbances, and the length of the incubation process have all conspired against conclusive tests of the above hypothesis.

When the missing link in our understanding of observed transition is that of the primary instability, the transition category is called a bypass. In other words, bypasses are those roads to transition which cannot be identified as starting from a known linear instability. The very term "bypass" is a reaffirmation of the fact that judiciously utilized linear theories -- generalized Tollmien-Schlichting waves,

Görtler theory, etc. -- provide us with the basic framework within which some organization of our multifarious observations can be rationally effected (e.g., Reshotko's 1969 analysis of contradictions among super-sonic facilities). Thus transition due to distributed roughness repre-sents a bypass today. Another bypass, as little understood in detail now as in 1943 when Charters first described it, is the phenomenon of transverse or lateral contamination. We still cannot rationally predict the spreading angle of the turbulent front (wedge), nor why it drops to roughly a half at supersonic speeds.

Insufficient attention to the possibility of bypasses in new designs involving uncharted ranges of governing parameters cost tens of millions of dollars in the ill-fated 1956-58 designs of heat-sink noses of re-entry vehicles; see Murphy and Rubesin (1966). Referring to that inci-dent, C. duP. Donaldson wrote in 1970, "...the nature of transition on blunt bodies at very high Reynolds numbers has been a source of embarrass-ment to aeronautical engineers". Since we still do not understand the mechanisms in the smooth-wall transition, even when compressibility effects are absent, the case remains an embarrassment. An up-to-date critical review of the sole available tool, that of correlation of transition Reynolds numbers in different environments, is found on pp 17 and 18 of Batt and Legner (1983).

0.04   TOOLS AVAILABLE FOR DIAGNOSTICS AND ESTIMATES

0.04.01   Varied applicability of linearized theories

How can the broad-brush information in the preceding sections be
utilized in the field or laboratory? What available detailed informa-
tion can be especially useful? Let us first concretize the judgment
problem by considering the following historical experimental paradox.
A simple mixing layer which is unstable at practically all Reynolds
numbers is significantly stabilized by one-sided constraint of a wall.
However, constraining the resulting boundary layer by adjoining a
second parallel wall to form a duct flow has the opposite effect and
brings the commonly observed Reynolds number of transition Re_{tr} down
by large factors.

Clearly only a broad conceptual framework can encompass such
diverse facts. In fluid mechanics we are blessed with the framework of
the Navier-Stokes equations as a basis. The NS system offers a most
reliable set of constitutive equations, but they are nonlinear. It is
the multiplicity of solutions of these nonlinear equations (see Section
0.02.05) which is at the heart of the problem of instability. Computer
solutions of specific nonlinear problems are currently limited to con-
ceptually critical, simple prototype geometries. We are therefore
effectively restricted to linearized stability codes buttressed by
theoretico-empirical qualitative understanding. The qualitative under-
standing itself is based on the mathematical structure of each problem
and on associated detailed experimental information, the subject matter
of the Guide. One of the purposes of the 0.04 Sections is to illustrate
the character of the available linearized information and its judicial
application.

Returning to the comparison between the free layer, the boundary
layer, and the Poiseuille duct flow, we observe first that the trend in
the quantitative measure of linear stability, Re_{cr}, is correct in the

first step but contradictory in the second. For Blasius boundary layer Re_{cr} based on δ is approximately 1500 ($Re_\delta{}^* \sim 510$), while in the Poiseuille flow Re_{cr} based on the comparable thickness, half of the duct height, is 5772. Both the wall-layer instabilities are of the weaker, viscosity-conditioned type, and both are classified as having the fickle subcritical or inverted bifurcation. However, since even the Poiseuille Re_{min2D} of 2900 (see Sk 0.02.04b) exceeds the observed Re_{tr} of 1000-2000 in noisier facilities, we are led to environmental disturbances and early nonlinearity as the most likely suspects. The combined consequences of Nishioka et al (1975), Orszag & Patera (1981), and Carlson & WP (1982), discussed in Sections 0.02.06b and c, have now solidified the suspicions into a most probable explanation for the paradox.

Another part of the explanation probably stems from the fact that the slow streamwise shifting of the intrinsic scale, $\delta(x)$, in boundary layers is assumed away through the quasi-parallel hypothesis. With this assumption, the linear mathematics and the charts versus Re for the Blasius and Poiseuille cases may look alike, but we must reintroduce the variability of δ in our physical interpretation. In Fig 0-14, as we follow the streamwise developments in the boundary layer, the abscissa changes and with it the amplification rates. Thus the disturbance growing at the most amplified rate becomes "detuned" along the layer and would eventually be damped if nonlinearity and secondary instability did not interfere. See top of Fig 0-11. There is no detuning in the Poiseuille case; see related discussion in Section 0.02.06a.

The main conclusion of the comparison, however, is the recognition that we cannot rely on theory, linear or nonlinear, for help in specific assessments of confined open-system flows, typified in Fig 0-1c. For duct and pipe flows, we must resort to organized accounts of experimental information, with qualitative appreciation of the behavior of turbulent spots, puffs, and slugs, and of the enhanced upstream pressure influence in confined flows. The 0.04 Sections therefore concentrate on the linear properties of free shear layers and boundary layers and on the broader qualitative aids in their interpretation.

0.04.02   On relations between temporal T and spatial S
characteristics of instability theory

In linear problems, complex notation permits simultaneous efficient accounting of the amplitude and phase in oscillatory solutions of equations. The relation between any physical property of the periodic solution, $v(x,y,t)$, such as velocity components, vorticity, pressure, etc., and its complex T or S formulation is given in the first line of Table I, borrowed from Obremski et al (1969). In the temporal formulation, initial data would be prescribed along the x axis, $v(x,y,0)$, and the x variation represented spectrally in terms of the real wave number $\alpha = \alpha_r = 2\pi/\lambda$. For a representative Fourier wavenumber the parameters of the problem would then be α_r, v_r, ω_i, and Re_δ^*, as defined in Table I. In the S formulation, the solution would proceed in time from the initial distribution $v(x,y,0)$, with spatial initial data $v(0,y,t)$ being supplied continuously for the fluid convected into the open domain; see Section A.09 of the Guide. It is efficient to furnish the information $v(0, y, t)$ in a Fourier representation in terms of the real circular frequency $\omega = \omega_r = 2\pi f$. For a representative Fourier frequency the corresponding parameters would again be four in number: ω_r, α_r, α_i, and Re_δ^*.

The reader can verify that $c_r = \omega_r/\alpha_r$ is the speed at which the physical periodic pattern moves in the streamwise direction. The amplification rates are defined as the coefficients in the exponent, i.e. the slopes in semilogarithmic plots of any physical variable against t or x. When in the quasiparallel approximation the amplification eigenvalues ω_i or α_i vary slowly with t or x, the total amplification of the wave involves t or x integration along the path, as indicated in Table I. When the T formulation is applied to boundary layers growing in x, the x integrand is given by the Gaster transformation (rather than by $\omega_i/c_r = \alpha_r c_i/c_r$ as used by Schubauer and Skramstad in the report on their classic 1943 experiment). We recall that the group velocity, defined in Table I, is the speed of propagation of wave energy.

The complex cross-flow distribution $v_1(y)$ on the first line of Table I represents the computer eigen or characteristic solution, i.e. the first nonzero solution of the homogeneous set of linear perturbation equations about the base flow $U\{y; \delta^*(x)\}$. It is a solution only when special eigenvalue relations hold between the four parameters of the T or S problem. An arbitrary choice of two parameters (commonly α_r, Re_δ^* or ω_r, Re_δ^*) determines the other two. To obtain a feeling for the physical problem the reader is strongly advised to study the graphically presented behavior of the S eigenfunctions $u_1(y)$, $v_1(y)$, $p_1(y)$, and $\zeta_1(y)$ (and some of their physically relevant products) for five Reynolds numbers in a flat-plate boundary layer and their interpretation by Hama, Williams, and Fasel (1980). (One word of caution: the printed Fig. 14 is in error.) An interesting sample of inviscid eigenfunctions for the velocity components of a family of mixing layers is easily accessible as Fig. 8 of Monkewitz and Huerre (1982).

Most computer codes do not provide the eigenfunctions routinely; they stop with a tabular or graphical representation of the eigen relations -- the essential performance parameters of the instability. T maps of the eigenvalue relations for the Blasius layer, $U =$ const for the accelerated stagnation flow, $U = a_1 x$, and the retarded boundary layers in special adverse pressure gradients $U = a_1 x^{-.0476}$, with an inflection point at $y/\delta = 0.24$, are displayed in Fig 0-14, Fig 0-15, and Fig 0-16. The velocity profiles of the base flows for these cases are all members of the Falkner-Skan similarity solutions of boundary layer equations, with parameter $\beta = 0, 1, -0.1$, respectively; see Schlichting (1979, p 164). No comparably detailed plots are available for the S formulation.

We can use these T maps in spatially amplifying boundary layers because the amplification rates are small. Gaster (1962) proved that the T and S systems are equivalent to second order in the maximum T amplification rate, ω_{imax}; the correspondence is shown at the bottom of Table I. We note that the Gaster relation is less useful for free layers because the amplification rates are rather large.

Currently, even mathematical journals accept papers on stability problems in the S formulation. When Gaster first submitted a manuscript with the S formalism, it was sidetracked for several years as not correctly posed mathematically. At this writing, emotional preferences with respect to the two formulations have not fully subsided. The problems, especially beyond the linear stage, appear sufficiently difficult to make us value contributions to insight from either formulation, keeping in mind the limitations of each approach.

In through-flow systems, illustrated in Figs 0-la,b,c, the distances grow spatially. Except for fully developed confined flows, the base flows also thicken in x. By assuming quasi-parallel flow, the S approach suppresses the dependence on x of the base flow $U\{y; \delta^*(x)\}$, a constraint for which we must mentally correct in our interpretations. At this level of approximation the S and T results are equivalent within the approximation of Gaster's transformation. In particular, they agree that all variables propagate at the same phase speed and amplify equally at all heights of the layer because the eigenfunctions $v_1(y)$ also have their slow x-dependence suppressed. First-order corrections for nonparallelism have now been computed in several ways, e.g. Gaster (1974) and Saric and Nayfeh (1977). In non-parallel base flow the characteristic functions v_1 become x-dependent and the physical variables no longer grow together proportionately. With minor exceptions, the changes have more theoretical than practical significance for boundary layers. Hence the working hypothesis of equivalence of the T and S formulations at the level of Gaster's transformation is both tenable and practical.

At the level of secondary instabilities, where the mathematical and computational difficulties are severe, much of the insight cited in 0.02 and 0.03 Sections has been achieved through the T formulation with the x-independence replaced by periodicity in x. That insight is not contradicted by experimental results when in our interpretation we allow for the growth of the layer in x (if present) and for the possible presence of significant upstream influence; see *Note 1 of Section 0.03.04.

0.04.03   On the role of oblique waves and Squire's theorem

The wave fronts of the T and S waves in Table I are obtained by setting the exponent constant, i.e. $\alpha_r x - \omega_r t = $ const, in both cases. Oblique waves generated by oblique vibrating ribbons have verified the expected fact that they too represent bona fide solutions of the linearized equations. For an oblique wave with its normal inclined at an angle $\tan^{-1}\beta/\alpha_r$ to the x axis, the exponent in the first line of Table I becomes $i(\alpha_r x + \beta z - \omega_r t)$. For incompressible flows, the T linearized equations for the oblique waves turn out to be identical to those of a two-dimensional wave with wave number α_{2D} and Reynolds number Re_{2D}, which are related to the parameters of the oblique wave by the Squire transformation

$$\alpha^2 + \beta^2 = \alpha_{2D}^2 \ , \quad \alpha\cdot Re = \alpha_{2D}\cdot Re_{2D} \qquad (\underline{0\text{-}8})*$$

Thus we can use two-dimensional maps such as in Fig $\underline{0\text{-}14}$ to infer the eigennumbers for the oblique case.

Consider the critical two-dimensional case for which Re_{2D} is minimum and the amplification rate, c_i , is zero. From the first relation in $(\underline{0\text{-}8})*$ we infer that α for $c_i = 0$ is less than α_{2D}, and from the second that Re must be more than Re_{2D}. Therefore Squire's theorem follows, namely: the oblique waves become critical at higher Reynolds number higher than the two-dimensional TS waves. For spatially nonneutral waves, α_i differs from zero and Re_{2D} becomes complex. That destroys the usefulness of $(\underline{0\text{-}8})*$ for comparison of physical flows but not its computational advantages. It was, for instance, found effective by Gaster (1975) in the wave-packet paper discussed below. For compressible flows the equations are still more complicated, and at low supersonic Mach numbers the most amplified waves are actually inclined at approximately 55°. Like sweepback, obliqueness maintains upstream influence, here needed for self-excitation of the wave.)

Even at incompressible speeds where $(\underline{0\text{-}8})*$ is valid, there are regions of parameters where oblique waves are more amplified than the

two-dimensional ones. This is most easily seen from computations with various constant β values. The amplified areas within the $\beta = 0.1$, 0.2, and 0.3 neutral curves in <u>Fig O-18</u> (courtesy of T. Herbert) extend below the lower critical loop of the two-dimensional waves, $\beta = 0$. Thus at a given Reynolds number oblique disturbances with long wavelengths can be more amplified than the two-dimensional wave with the same α . The three Re_{cr} conditions, each marked with a dot in <u>Fig O-18</u>, follow the Squire theorem; at the points of vertical tangency, the local obliqueness angles are 20°, 38.3°, and 60°, as β rises from 0.1 to 0.2 and 0.3. Thus, unless oblique waves are stimulated by some three-dimensionalizing agent, the two-dimensional waves have a head start in amplification and tend to dominate, especially at lower Reynolds numbers.

Because of linearity we are free to superpose oblique waves; we can Fourier-synthesize them over both α and β to fit whatever geometry of stimulation there may be. An impulsive puff from a wall hole under a boundary layer initially stimulates waves in all directions, creating a spreading and TS amplifying kidney-shaped wave packet in the laminar layer. Its properties were investigated in a classic experiment by Gaster and Grant (1975). Gaster (1975) also computed the evolution of this laminar spot from the S linearized equation by assuming that the spectra were initially flat in α and β , as well as in ω , as befits a Dirac delta function event. With allowance for a slight phase shift within the distribution, the agreement between the measured and predicted fluctuations was most gratifying before nonlinear growth interfered.

A two-dimensional TS wave traveling in the x direction in a Blasius layer has no component of velocity u_s in the direction s of its wave front. An oblique wave, however, does. In the momentum equation for that direction, the vertical component of the fluctuation, v, multiplied by $dU/dy \cdot \cos(x,s)$ creates a forcing source term for u_s, even though the fluctuating pressure gradient, $\partial p/\partial s$, is zero. The gradient $\partial u_s/\partial y$ yields vorticity normal to the front while the rest of

the fluctuating motion generates vorticity parallel to the crest, as in the two-dimensional wave. Two waves of equal strength but of opposite obliquity produce a spanwise corrugated pattern in the form of line 1 of Table I multiplied by $2\cos/\beta z$. According to Herbert (1981, 1982), this composite wave, which has streamwise vorticity, is the perturbation, which in the secondary instability grows exponentially when it interacts with a two-dimensional TS wave grown beyond a nonlinear threshold. Among these spanwise corrugated waves, the one with maximum amplification presumably determines the spontaneously selected spanwise scale β observed in Poiseuille secondary instability (Section 0.02.06b) and in Fig 0-11 for boundary layers.

An alternate explanation for the staggered pattern in Fig 0-11 is possible in terms of resonant triads of waves proposed by Craik (1971). According to a weakly nonlinear interaction involving quadratic terms alone, the superposed pair of waves above can grow rapidly in conjunction with a two-dimensional wave with $\alpha_{2D} = 2\alpha_{obl}$, all traveling at the same speed c_r. At this writing, experiments capable of discriminating between the alternate explanations have not yet been performed. A reader interested in graphical information concerning oblique wave eigenvalues beyond Fig 0-18 will benefit from examining c_r and c_i plots versus β at a fixed Re, such as in Fig. 2 of Craik (1971); the second plot is known as a kidney plot. Gaster (1977) in a paper describing his techniques for obtaining the oblique spectra in the puff-wave-packet problem, includes detailed kidney maps for Re_{δ}^* of 1000, 2000, and 3000.

0.04.04 Comparing TS instability of boundary layers

Knowing how to read maps may seem mundane, but it is valuable not only for applications but also for forming a concrete picture of the terrain--the specific trends in the major instability characteristics. Before focusing on these trends, let us illustrate the elementary process of extracting detail information from the maps at hand. The first facts to ascertain for any map are the time and length scales used in nondimensionalization. The T maps of <u>Fig 0-14</u> to <u>Fig 0-17</u> are all based on $\delta^*(x)$, the local displacement thickness, $U_e(x)$, the local potential velocity at the edge of the boundary layer, and the derived time scale, δ^*/U_e.

Any physical condition of a boundary layer is specified by the dimensional triad of δ^*, U_e, and ν, and hence by Re_δ^*. Suppose we wished to find from the T map in <u>Fig 0-14</u> for the Blasius layer the locally most amplified dimensional frequency and its <u>spatial</u> dimensional amplification rate of $Re_\delta^* = 1000$. One major characteristic of the layer, the crest along ridge of maximum amplification, is the locus connecting smoothly the points of tangency between the curves c_i=const and the vertical lines of constant Re_δ^*. The point $Re_\delta^* = 1000$, $\alpha_r = 0.25$ and $c_i = 0.01$ is one such point of tangency and maximum amplification. To get its circular frequency $\omega_r = \alpha_r c_r$, we interpolate between the neighboring curves of c_r=const and obtain $\sim 0.25.0.351$; the dimensional frequency is then $0.0878 U_e/\delta^*$ radians per unit time.

To get the spatial amplification rate we utilize Gaster's transformation and the definition of the group velocity:

$$-\alpha_i = \alpha_r c_i/c_g \; ; \qquad c_g = c_r + \alpha_r (\partial c_r/\partial \alpha_r)_{Re} \qquad \underline{(0\text{-}9)}^*$$

The partial derivative in $\underline{(0\text{-}9)}^*$ is found from the intercepts of the

neighboring c_r curves on the vertical line: $\Delta c_r = 0.02$, $\Delta \alpha_r = 0.29 - 0.22$, yielding approximately 0.42 for c_g. The dimensional amplification rate $-\alpha_i/\delta^*$ then comes out $\sim 0.006/\delta^*$ per unit length. The corresponding temporal amplification is $\alpha_r c_i U_e/\delta^* \sim 0.0025 U_e/\delta^*$ per unit time.

This little exercise brings out the fact that the <u>dimensionless spatial rate</u> has a clear physical meaning: in a downstream distance corresponding to one displacement thickness, the traveling disturbance at the given frequency grows by a factor $\exp(-\alpha_i) \sim 1 - \alpha_i$. (The temporal rate has no such comparable simple meaning; see <u>Table I</u>.) Since the displacement thickness is an intrinsic local property of a layer, comparison of amplifications of two different layers on a "per δ^* basis" should be generally meaningful.

The information provided by the shape and height of the ridge of maximal amplification offers a more global measure for comparison. A sea of stability surrounds the amplified range along the zero level curve $\alpha_i = o$ or $c_i = 0$, variously called neutral, or critical, or of marginal stability. (By definition in Table I, the T and S formulations give the same neutral loop.) The easiest way to comprehend the differences between boundary layers with and without pressure gradients is to contrast the neutral curves of the Falkner-Skan family as was done in <u>Fig O-17</u>. The accelerating boundary layers in plane stagnation regions, $\beta = 1$, are clearly most resistant to TS instability, having $\mathrm{Re}\,\delta^*_{cr}$ in excess of 10,000 and a very narrow spectral band of excitability. Since they approximate conditions on a circular cylinder past 30°, a full page is given to the detailed amplification map in <u>Fig O-15</u>. Back in <u>Fig O-17</u> we recognize a progressive destabilization of the accelerated layers, as β along with the favorable press`e gradients decrease toward zero, the flat-plate case.

This classical boundary layer also deserves a full page map, <u>Fig O-14</u>, to allow more accurate interpolations. In this diagram,

moving leftward from far right--i.e., from nearly inviscid conditions at very high Reynolds numbers--corresponds to a thought experiment in which viscosity steadily increases. The upper branch II of the neutral curve and the lower branch I meet asymptotically at Re of infinity. The Blasius boundary layer is thus unstable at infinity only to an infini- tesimally narrow wave band--i.e., it is inviscidly neutrally stable. Moving left with increasing viscosity, we observe the amplification to increase toward the ridge of maximum amplification with a narrow crest of c_i = 1.96 near Re_δ^* of 7000. This corresponds to the destabiliza- tion due to viscosity which puzzled the early researchers. We recall from Section 0.03.01 that, along this ridge of optimal tuning of TS waves, the ratio of the Stokes-layer thickness δ_s to the critical height y_{cr} remains essentially invariant. As we move leftward past the ridge, the layer stabilizes; the intuitively normal trend of stabi- lization with increasing viscosity now obtains.

The full-page map Fig 0-16 for a typical adverse pressure gradient illustrates the effect of an inflection point in the boundary layer profile. The broad opening of the neutral curve at far right signifies that the layer is inviscidly unstable for waves of wavelengths from $\lambda = 2\pi\delta^*/0.523$ to ∞ at high Reynolds numbers. The presence of the wall inhibits but does not prevent the inflectional instability. Moving to the left with increasing viscosity, the layer destabilizes beyond the inflectional rates! The ridge of the viscously tuned TS mechanism still yields the highest amplification rates, despite the inflection in the velocity profile. Hot-wire measurements reveal two maxima in u' corres- ponding to a double maximum in the computed eigenfunctions. Here the TS and the inflectional mechanisms compete, with TS winning the race. To the left of the ridge, viscosity again stabilizes the flow. We can continue to follow the effects of increasing adverse pressure gradients in Fig 0-17. The spectral band of inviscidly unstable waves broadens continuously up to β = -0.1988, the boundary layer on the verge of separation (with $\partial U(y)/\partial y$ = 0 at y=0). The surprising destabilization

due to viscosity still takes place for the highly retarded boundary
layer with $\beta = -0.14$, but disappears for the separating layer.

In view of this disappearance we might ask whether the inviscidly
unstable separating layer is as unstable as the fully separated mixing
layer in Fig 0-19. The ultimate answer is no; the boundary conditions
$v=0$ and $\partial v / \partial y = 0$ at the wall still partially inhibit the full dynamics
and kinematics portrayed in Fig 0-6. Comparing quantitatively the
instability of shear layers from different families of profiles requires
care for a number of reasons, some of which will surface in our dis-
cussion of mixing layers in the next section.

---

*Note 1   Limitations on usage of linear solutions. An important
concrete example of limitations on linear concepts is illustrated in
Fig 0-11 due to Saric (1981). A traveling disturbance amplifies inside
the neutral loop until it reaches branch II appropriate to its frequency
and Re_δ; it decays thereafter, unless it has grown to nonlinear levels.
For the frequency of these experiments with plane wave stimulation,
branch II was reached at the 170 cm station from the leading edge of the
plate in all three cases. From the measured y-maximum fluctuations u'_m
in percent of $U = 6.6$ m/s at branch II, as indicated under each photo-
graph, and from the smoke evidence, we conclude that when u'_m was
raised to the $0.003U$ level, the disturbances passed out of the linear
regime. The nonlinear developments in the two lower photographs were
already discussed in *Note 1 of Section 0.03.05. For the upper picture
hot-wire   measurements confirmed that the fluctuations indeed attenu-
ated and behaved linearly. The smoke distribution that, together with
the vorticity in the neighborhood of y_{cr}, had been gradually dehomoge-
nized and concentrated in the so-called "cat's eye" regions up to branch
II, starts spreading away from the concentrations. Besides molecular
diffusion, modification of streaklines near y_{cr} as the cat's eye regions
contract with decaying fluctuations is probably responsible. The experi-
ments underscore the importance of simultaneous global visualization
techniques and quantitative point measurements (with due concern for
interference and contamination). In connection with the issue of visual
evidence, it is desirable to comment on the change in sharpness of the
visual smoke-line definition downstream of station 205 in the lowest
picture. Most experienced smoke interpreters would judge that fuzzi-
ness, associated with small-scale turbulent motion, starts appearing
above the centerline near station 210 and that at 220 most of the smoke
near the centerline is engulfed by new turbulence. This is an example
of the type of diffusive change mentioned in Section 0.01.01 in connec-
tion with definable onset of turbulence.

0.04.05   Mixing layers

Wakes, jets, and mixing layers are all inviscidly unstable so that important viscous effects are not commonly encountered in technology. We have already discussed some of the viscous low-Re issues in connection with the cylinder wake in Sections 0.02.02 and 0.02.03. The Re-development of wakes and jets is complicated by the fact that their natural scale, the width or diameter, D, gets augmented at higher Reynolds number by a second, natural scale, the decreasing thickness δ of the boundary layer, which separates from the parent body of the wake, or from the parent-nozzle of the jet; see Fig 0-1c. Since these separating layers are de facto mixing layers, it is desirable to understand well the behavior of such layers first.

As in the wake case in Section 0.02.02, there are problems in defining Re_{cr} theoretically and experimentally. A convincing demonstration that Re_{cr} is not zero for practical purposes is still missing. The easily accessible Fig. 13.2 of Betchov and Criminale (1967) presents a linear viscous T map for the profile $U = a\tanh(y/L)$ together with the limiting inviscid eigenvalues corresponding to infinite Re_L. While the low-Re_L features may be debatable, the important message is that viscous effects beyond Re_L of about a hundred do not play a significant role in linear theory.

Because of the high amplification rates, the Gaster transformation ceases to be a useful bridge between the T and S formulations of stability as in Table I. The two formulations now differ, for instance in their predictions for the tanhy profile as demonstrated by Michalke (1964, 1965). In the important mid-range of frequencies Freymuth's 1966 experimental results agreed more with the T predictions than with the S analysis shown by the solid line in Fig 0-19. Historically, this discrepancy delayed the general acceptance of the spatial theory for almost a decade, even though the S eigenfunctions and phase speeds fit Freymuth's experiments significantly better. As we see from Fig 0-19, the 1981 spatial theory of Monkewitz and Huerre resolved most of the confusion.

The irony of the situation is that when one uses the tanhy profile one violates the definition of inviscid theory as enunciated in the introduction to the 0.03 Sections. Mentally, we should turn off the viscosity only for the fast processes of the instability, not for the slow development of the base flow. The Blasius profile referred to in the legend of Fig 0-19 represents a viscous similarity solution to the same equation that gave us the Blasius boundary layer. The difference lies in the boundary conditions: the no-slip wall conditions are replaced by the requirement of zero disturbances at negative infinity after the wall terminates at the lip. It appears that when the quasi-parallel spatial theory deals with a realistic initial distribution of vorticity, it agrees with instability experiments rather well, considering that mixing layers are generally much less parallel than boundary layers.

The boundary layer thickness used in the defining parameters of Fig 0-19 is the momentum thickness, θ . The map for the Falkner-Skan separating boundary layer in the preceding section uses δ^* in its nondimensionalization. For a given set of profiles the ratio δ^*/θ defines the well-known form parameter, H, for which the Falkner-Skan family varies from 2.216 for the stagnation flows to 4.029 for the separating profile (Table III of Obremski & ML, 1969). Because of this gradual shift the quantitative comparison between the profiles in Fig 0-17 would differ if θ had been used as the scale length. And obviously, the quantitative comparison between a profile of one family expressed in terms of δ^* and another with θ as variable, could lead to erroneous conclusions. That is a general problem in comparing instabilities, illustrated in the preceding section when we proposed to compare the map of the separating boundary layer with the inviscid map of the mixing layer in Fig 0-19.

A more basic question arises in this respect: does one thickness characterization have an edge over another as being more intrinsic to the instability process? For example, is θ or δ^* preferable for

correlating transition characteristics on a sphere in presence of distributed roughness? (An historical, unanswered question.) To correlate Re_{cr} across the full Falkner-Skan set of families requires both characterizations, or more exactly δ^* and the shape factor; see Section 3.4 of Obremski & OM (1969). There is yet another mostly untested candidate, the vorticity thickness defined by the ratio of the mean velocity change across a layer to its maximum slope (or vorticity), $\delta_\omega = \Delta U/U'_{max}$, which for the tanhy profile is equal to 4θ .

The paper of Monkewitz and Huerre (1981) bears indirectly on these issues. The authors provide and compare the inviscid maps for two families of the technologically important mixing layers between streams with finite mean velocities U_2 and U_1. One family, nondimensionalized with respect to δ_ω and $(U_1 + U_2)/2$, is $U = 1 + \lambda\tanh(y/2)$, with $\lambda = 2(U_2 - U_1)/(U_2 + U_1)$ varying from zero to unity. The other family of the base flows again represents solutions of the Blasius equations for the diffusion layers between the U_2 and U_1 streams. The corresponding length scale is the classical Blasius thickness, based on U_2, $\delta_B = (\nu x/U_2)^{\frac{1}{2}}$, and the velocity scale is the upper, higher speed, U_2 . Readers are invited to give themselves an instability-comparing tour through their S maps as we did in the preceding section, and to ponder on what aspects of the profiles may cause the observed differences.

---

*Note 1   What accuracy in U profiles for reliable predictions? One would think that the 20% discrepancy in the maximum amplification rate seen in Fig 0-19 would have called the suitability of the tanhy profile into question earlier, at least if there had not been the T versus S distraction. There are, however, associated issues of biases and smearing in measurements of profiles in thin layers with nominally zero velocity at one edge and of the criteria for best fit with theory. Different individual decisions in these issues modify the adopted measure of thickness and the effective U"(y) distribution and, through them, the amplification rate. Monkewitz and Huerre in their Fig. 1d show the relative fit between a recent experiment and the two profiles used in the theory. Insistence on best fit for the maximum vorticity definitely favors the Blasius layer.

Discussion of the role of profile curvature U"(y) in Section 3.1 of Obremski & ML(1969) demonstrated that it constitutes the single most important determinant of the TS layer instability. We can see the main

reason from Eq(0-7)*; U"(y) sets the strength of the rate of vorticity transfer from the steady mean flow to the unsteady fluctuations. (When U" is zero, as in plane Couette flow, the flow is altogether stable to linearizable perturbations!) Generally, therefore, a seemingly satisfactory match between a profile used for the base flow and the real profile in the laboratory or in a future flight of a new design may hide nonnegligible differences in the second derivative.

*Note 2   On design risks. Consider the implications of the sensitivity of instability calculations for an engineer who contemplates a design in which a boundary layer is pushed beyond its Re_{cr}. His problem is not unlike that of a drunk who ventures onto a busy street trusting that he will not fall down before he gets to the other side. If the boundary layer remains laminar, who cares about what happens on the other side, namely in the wake? The drunk's risk rises with blustery weather and slippery streets--i.e., with environmental disturbances. So does the designer's risk. The simile points up the issue of judgment of risk in potentially unstable situations--or persons. If onset of turbulence meant a mere 20% degradation of performance 3% of the time, engineers and their financial backers might be willing to cross the street. But how does one measure the risk if there is no stochastic information on transition (for the specific design) which could be converted into quantitative probability statements?

Since capability for such probability assessments is not on the horizon, engineers must temper their innate optimism and try to understand the capricious nature of the boundary layer. In view of the sensitivity to U", discussed above, it would be wise to insist on having their judgment supported by the best computer codes. That is not a minor matter. They first need a reliable code for prediction of the potential flow for their three-dimensional shape. The next step requires accurate computations of three-dimensional boundary layers (with a weary eye on the danger of laminar separation). This capability remains an art, still in development stages. Having obtained their U"(y) and W"(y) distributions (see Fig 0-12, which follows Fig 0-2), they will need a reliable specialist in three-dimensional linearized stability computations. Such computations are not yet as "standard" as for two-dimensional or axisymmetric flows. Nor do they have precomputed maps for profiles like that in Fig 0-12 on which to train their engineering intuition.

Only then can they be ready to face the decision of how far beyond Re_{cr} and Re_{mint} (if there is information on Re_{mint} for that geometry) they dare to push the boundary layer in their design. In their deliberations they must not forget the danger of the missing links of Section 0.03.07. Distributed roughness and unexpected isolated roughnesses have historically prevented the laminar-flow airfoils of World War II to achieve more than some 30% of the laminarity designed for. The third law of aerodynamics (and airline ground crews) states that surfaces in flight service become fouled. In the low-level part of flights a pilot, like the vacation driver, has to worry about insect impactions and must

be concerned with even small protuberances near the leading edges of the wings and on the nose of the fuselage rather than with the windshield; see Coleman's 1961 research on insect impaction. In matters of design, transition is easier to control than to postpone, or to predict.

0.04.06   Basic compressibility effects on stability

Ironically, Michalke's student Gropengiesser completed a dissertation in 1968 dealing with spatial inviscid stability of compressible mixing layers, based on the generalized Blasius solutions rather than on the hapless tanhy profiles. Inset to Fig 0-20 summarizes the geometry and the boundary conditions, which include the possibility of static temperature differences between the upper and lower regions; note that subscript 2 now refers to the lower stream. With this interchange of subscripts, Gropengiesser's scales are identical to the M & H scales of δ_B and U_2 above. Many of his stability maps extend to Mach number 5 and, of course, include M = 0. No comparisons between Gropengiesser's incompressible results and the experiments of Freymuth (1966) seemed to have been made at the time, comparisons which could have clarified the T vs. S confusion early. The dissertation, which is in German, has not attracted enough attention even though it is available from DFVLR. It is not referenced by Monkewitz and Huerre.

Compressibility introduces variable density ρ and the coupling of viscous dissipation into the dynamics of the system. For instance, Fig 0-20b illustrates the effect of having the lower fluid at a static temperature T_2 below that of the static temperature T_1 of the upper stream. From the inset of Fig 0-20 we see that because of the dissipative heating (at constant pressure) the maximum static temperature in the mixing layer exceeds both T_2 and T_1 . The layers become hotter and thicker as Mach number increases. This affects directly the baseflow vorticity and other relevant distributions as reported in Figs 4-7 of the dissertation.

These mechanically driven temperature and density effects on stability of compressible flows are interpreted at length in Sections A.08 and A.11-A.15 of the Guide. The interpretations are based mostly on the comprehensive pioneering studies of Mack (1969) and the earlier work of Lees. Two general trends are worth mentioning here. The first stems from the fact that the source $vU"$ of unsteady vorticity in Equation (0-7)* is essentially replaced by

$$v \cdot \{\rho_B U'\}'/\rho_B \ , \qquad \rho_B(y) = \text{ base flow density.} \qquad (0\text{-}10)*$$

Thus most of the earlier statements concerning the incompressible distribution $U"(y)$ and the consequences of its vanishing in the boundary layer can be rephrased in terms of the coefficient of v in (0-10)*. In particular, an effective generalized inflection point is now found where this coefficient goes to zero. For Gropengiesser's mixing layers the y distributions of the coefficient of v in (0-10)* for different Mach numbers and T_2/T_1 ratios are exhibited in Fig. 7 of the dissertation. Since the layers are inflectionally unstable in the first place, the additional effects are gradual. Boundary layer flows at walls impermeable to heat, which have no inflections in their velocity profiles, become slightly inflectionally unstable as soon as Mach number is larger than zero. The inviscid component of the instability of compressible boundary layers increases with Mach number roughly in proportion to the distance from the wall of the generalized inflection point. The trend toward inflectional instability parallels in all repects but one the trend in incompressible boundary layers with increasing adverse pressure gradients described in Section 0.04.04.

This exceptional development contradicts the usual expectations associated with an increase in the inflectional component of instabilities. Instead of rising, the overall instability subsides with increasing Mach number. Both the extensive computations of Mack (1969) for the flat-plate boundary layers and Gropengiesser (1969) for the

mixing layers document this fact. It is conjectured on varied circum-
stantial evidence(e.g. Fig 0-24) that decrease in upstream influence
(which is exerted at the speed of sound) may be responsible for the
observed increase in stability of both free and wall layers with M.
Upstream influence plays an essential role in the linear self-excitation
of low-speed instabilities; see Lighthill (1963, pp 91-93). Blocking of
linearizibly weak upstream-traveling pressure fields is difficult to
demonstrate. However, if we can show blockage of stronger, nonlinear
fields involved in an instability, the principle must be valid for
weaker fields as well. Figures 0-24a,b,c, due to Dyment and Gryson
(1978) document pictorially the inhibition of upstream influence as Mach
number increases in the case of a 2D wake generated by a flat plate
perpendicular to the flow. Large disturbances from the unstable motions
are prevented from reaching the origin of the two shear layers through
the outer stream when an enclave of supersonic flow is formed along the
widening wake. Disregarding the black shadow of the external support
system, the reader can trace first the Re-controlled shortening of the
distance to the first roll-up as the Mach number increases from 0.3 to
0.6 while the Reynolds number UH/ν grows from 8.2 x 10^4 to 1.35 x 10^5.
The thin shear layers leaving the sharp edges of the plate become turbu-
lent quite early. Turbulence on a scale small with respect to the
distance between the two "vortex sheets" does not hinder their strong
antisymmetric instability.

In Fig 0-24, the arrow helps the reader locate the nearly sonic
streamwise flow just outside the first bulge of the upper sheet; the
nearly sonic flow steepens the compression phase of the acoustic waves
propagating upstream from the region of sudden vortex formations and
oscillations. In shadowgraphs such weak shocklets manifest themselves
as a fan of black-white curved wavefronts.

When M rises further to 0.76 and Re to 1.55 x 10^5, the insta-
bility and the sources of the shocklets move dramatically downstream;
see Fig 0-24. Either the configuration of the two vortex sheets has
become substantially more stable, despite further rise in Re, or it is
less disturbed by the antisymmetric upstream traveling pressure waves,

or both. The most likely explanation is the second. Such delays of instabilities are rather common for non-slender wakes.

While the transonic inhibition of the upstream influence by way of the free stream appears clear in Fig 0-24, upstream signals can still propagate through the body of the wake. However, the shift of the location of the first roll-up farther downstream suggests that the partially blocked signals are less effective in stimulating the instability. In the case of wall-layer instabilities, upstream influence through the subsonic portion of the boundary layer is always possible, however ineffective it may become.

It is believed that the effect demonstrated for the nonlinear disturbances in Fig 0-24 is the main cause of the dramatic loss of effectiveness in self-excitation as M_1 increases, which is seen in the maps of linearized amplification rates $-\alpha_i$ in Fig 0-20. As mentioned in Section 0.04.03, oblique waves maintain upstream influence to higher Mach numbers and should therefore become more dangerous than their two-dimensional counterparts. This expectation is born out by Gropengiesser's plots of $-\alpha_i$ against the spanwise wavenumber β (his Fig. 32-35). At M_1 of 2, the maximum amplification occurs for wavefronts swept back about 60° for both of the conditions in Fig 0-20.

The fact that for $M_1 > 1$ pressure disturbances can travel at smaller speeds than the mean flow in parts of the shear layer and free stream has two additional consequences observable in Fig 0-20. New modes of instability (called after their discoverer, L. Mack) can arise in which vorticity disturbances traveling along streamlines and pressure disturbances propagating along local Mach lines are so tuned as to extract energy from the stream. In Fig 0-20 the crests of the inflectional, initially dominant first mode decline to zero by $M_1 = 3$, but new, weaker second-mode crests emerge just before M_1 reaches 2. In boundary layers the pressure fluctuations can be trapped against the wall and grow larger than in Fig 0-2. It is believed that at hypersonic speeds Mack's second and third modes probably cause most of the boundary layer transitions not produced by roughness.

The last additional effect is confined to the lower left regions of
Fig 0-20 and is of little practical consequence. Within the heavy lines
labeled $\overline{u}_1 - c_r = \overline{a}_1$ the infinitesimal instability waves travel super-
sonically with respect to the free stream and therefore radiate acoustic
energy outward. Historically it had been postulated that the drain of
energy from such supersonic disturbances would make positive amplifica-
tion impossible.

Clearly, there is a wealth of information in these and the thirty-
odd additional maps of Gropengiesser (1969). If his theory should work
as well as that of Monkewitz and Huerre, judged by Fig 0-19, his disser-
tation would indeed represent a treasure chest of useful tools.

0.04.07   Görtler instability in concave boundary layers

While the inviscid mechanism of centrifugal instability, outlined
in Section 0.03.03, is relatively simple, its correct mathematical
description for slowly growing boundary layers along concave walls
presents delicate questions and may still not be fully settled; see
P. Hall (1982). In contrast, all the TS maps discussed in the 0.04
Sections thus far have been agreed upon since the eigenvalue problem has
been computerized. The G maps in Fig 0-22 of Floryan and Saric (1982)
and Fig 0-25 of Ragab and Nayfeh (1981) represent the culmination of a
critical development over nearly a decade and should be preferred to the
many others in the literature.

The disturbance pattern in Görtler's instability (see Section
0.03.03) involves all three components of motion as indicated in
Fig 0-21. As hinted in that sketch, the earlier theories were temporal,
but the physical growth is steady and spatial, in the x direction. This
very steadiness makes the phenomenon less accessible to measurements and
therefore much less explored, with less accuracy especially in the
embryonic stages. DC hot-wire measurements in spanwise traverses are
far less accurate than the time-dependent measurements in TS experimen-
tation at comparable stages of development. One also loses the con-
venient and powerful spectral decomposition. The alternative technique,

visualization, calls for even greater finesse in order to achieve good resolution. The data of Tani and Sakagami (1962) referred to in Fig 0-22 were obtained with hot wires and the data of Bippes (1972) by visualization. The reader is referred to the English translation of Bippes' dissertation to develop appreciation for the nature of the problem and the required accuracy.

These and other experiments indicate that the Görtler vortices observed in a laboratory are strongly dependent on conditions in the test facility. In other words, those streamwise disturbances in the flow, which penetrate the boundary layer, initiate the motion. The instability then filters and amplifies these disturbances from within a rather broad band of wave numbers, comprising the maximum amplification line in Fig 0-22. In contrast to the conditions in the mixing layer and other experiments, no spectral information whatsoever exists comparable to that for time-periodic instabilities in Fig 0-8 and Fig 0-9 to help us better understand the mode selection process. There may well be simultaneous linear amplifications going on as in Fig 0-9, but they have remained below our resolving power thus far.

Clever techniques for stimulating discrete wavelengths were devised by Bippes and by Wortmann (1964) to gain some control over the unknown initial conditions. They also tested for neutral stability--i.e., whether such a forced disturbance decayed or grew; the issues are comparable to those discussed in connection with Re_{cr} in Section 0.02.03. The quantitative judgment is limited, however, as already discussed. An average neutral locus from these experiments is indicated by the line with heavy dots on the right of Fig 0-22, labeled $\beta_{exp} = 0$. We note that this is to the right of the theoretical neutral curve $\beta = 0$. Either theory or experiment, or both, may be responsible for this dis-crepancy.

How can these maps be used? The physical conditions are defined again by U_∞, ν, a boundary layer thickness δ_r, and in addition by the radius of curvature of the surface, denoted by R in Fig 0-22. Since we use Re for Reynolds number rather than R, we can drop the double underlining without any confusion. Although the surface is

curved, the pressure gradient is postulated to vanish. To first-order accuracy the boundary layer profile is that of Blasius. The thickness δ_r here is $(\nu x/U_\infty)^{\frac{1}{2}}$, the same as that used by Monkewitz and Huerre (1981) and Gropengiesser (1969) in the mixing layer. The thickness δ_r^* in the TS flat-plate map in Fig 0-14 is $1.72\delta_r$. Some Görtler instability maps use the momentum thickness $\theta = 0.664\delta_r$ as the scaling length. In logarithmic coordinates the conversions are simple.

To enter the map we need to know the nondimensionalizing scales, here δ_r and U_∞, and the special definitions of G, α , and β . The Görtler number G is the Reynolds number Re_{δ_r} multiplied by the small dimensionless parameter which characterizes curvature effects, $(\delta_r/R)^{\frac{1}{2}}$. The reader must be alert to the switch in the wave number definitions from all our previous usage: α is now the spanwise dimensionless wave number $2\pi\delta_r/\lambda$, and β is the streamwise dimensionless growth rate defined operationally below.

For historical reasons the expression for total spatial amplification is more complicated than that in Table I:

$$\ln(A_2/A_1) = \int_1^2 \beta' \, \delta_r \, dx'/x' \text{ (dim)} = \int_1^2 4\beta dG/3G \text{ (nondim)} \qquad (0\text{-}11)*$$

In Fig 0-22 let us follow a streamwise vortex of fixed dimensional wavelength λ . As the boundary layer thickens the abscissa of the vortex path, α , grows proportionately to δ_r , while its ordinate G varies as $\delta_r^{3/2}$. Since the map is logarithmic, the path has an upward slope of 3/2. Generally this takes us to higher and higher amplification rates β . Floryan (1980) in his Fig. 13 converted this traditional map to one with identical coordinates but with lines of constant $\hat{\beta} = \beta/G$. This greatly facilitates step by step computations of total amplification $(0\text{-}11)*$ along the path.

The experimental points for a given flow tend to follow paths with slopes of 3/2. To help identify the dimensional λ along any of the paths, the wavelength parameter Λ was devised; it is merely the

Görtler number G, referred to λ rather than δ_r. Once the Görtler vortices are large enough to be identified on the map, they are usually beyond the neutral curve and grow at constant λ. As already mentioned, conditions in the facilities generally "choose" the wavelength without much regard for the existence of a locally most amplified wave number. Nevertheless, the map does indicate the dangerous territory and represents our sole quantitative tool for Görtler instabilities.

The placement of an experimental point on the map is governed purely by G and α. When the point falls on a constant β curve it does not mean that the theoretical rate was actually observed. Because of the resolution problems, few observed vortices remain in the linear range long enough to define unambiguous exponential growths. On the other hand, there is no rapid shift to turbulence once slow saturation begins unless free-stream disturbances are high. All the points entered in Fig 0-22 are laminar, of course.

There is yet little agreement on the nature of secondary instabilities, which may well be disturbance conditioned and differ between facilities. Work is going on in a number of research organizations, and we may expect clarifications and new information soon.

From a practical viewpoint, a more serious limitation of the information is its avoidance of non-zero pressure gradients. Ragab and Nayfeh (1981) discuss the subject and provide some quantitative information, such as the neutral curves for the Falkner-Skan β profiles, in Fig 0-25. Even if some extra approximations were necessary for their computations, the trends in the figure should be trustworthy. Clearly more effort is called for, both theoretical and experimental.

---

*Note 1)   On instabilities between rotating concentric cylinders.
This note is by way of introducing two broad comments on nonlinear developments in our prototype flow in Sketch 0.02.04b (the Couette flow with inner cylinder rotating) in a chapter devoted primarily to linear tools. It is also a way of urging the reader, especially one with appreciation for "structure" in physics and mathematics, to benefit from the critical expository survey of the field by DiPrima and Swinney (1981). Not much can be added to their presentation and informative figures. In particular, their Fig. 6.6 concretizes our Sketch 0.02.04b;

their Fig. 6.1 updates Coles' 1965 classification of the stability regimes (including rotation of the outer cylinder); their Fig. 6.5 illuminates the cell selection mechanism; their Figures 6.7 and 6.8 summarize the full range of developments in spectral terms; and their Fig. 6.9 illustrates the imperfection of the first bifurcation through a series of solutions of NS equations for an annulus of finite length. And, of course, their Fig. 6.1 (converted here into Fig 0-23 and referred to in the 0.02 Sections) beautifully captures the pictorial panorama of a sample sequence of the instabilities, which has inspired and challenged students of the subject since G. I. Taylor published the equivalent of (a) in 1923.

The first comment concerns the contrast between the spatial nature of the growth in the Görtler instability and the accepted designation of the instabilities in Fig 0-23 as temporal. In the latter case, any change in local vorticity is not convected away by the stream as in the concave boundary layer. In the closed confined space, the disturbance feeds back repeatedly onto itself and viscous diffusion ultimately must even out any differences between initial developments along the span. When long settling times are allowed, initial disturbances due to a small incremental step in the rotation rate are uniform around the periphery and a "weighted spanwise averaged" amplitude A(t) can be assigned to the mode motion almost immediately (Section 0.02.05). Recent work of Park and Donnelly suggests that traveling, disorderly "dislocations" between vortex cells may be lingering beneath the w eighted average long past the diffusion time appropriate to the length of the annulus. Most instabilities are hyper-sensitive to even smallest disturbances in the proximity of a bifurcation point. Associated aperiodic behavior can be present near the very first bifurcation.

When settling times are short and the start-up rotation vigorous, or even programmed in time, the situation may be likened to the initial development in a high-Re jet in Fig 0-1c. There, too, the shear layer is born suddenly with pre-existent, possibly irregular or programmed, vorticity distributions. As we have seen, in the jet the specific p..th through the instability stages, and their competition (or connivance), is the subject of much research. In the rotating annulus, these developments are generally of little interest, and the focus of study is on the final equilibrium configuration, brought about by confinement, dissipation, and continued effects of spanwise diffusion. The fascinating multitude of final NS equilibria is described in Section 0.02.05 with the evidence of Benjamin and Mullin (1982). Similar freezing at an intermediate development stage cannot occur in the jet case, because diffusion as well as instabilities continuously change its scale in the x direction. For this system: Re $\neq$ const, but Re = f(x).

The annulus phenomena generally represent the strictly parallel, pure or purified flows. However, when the outer cylinder is given the initial impulsive start, the system acquires an Re(t) nature. In fact, it corresponds to the temporal Görtler instability grafted upon a temporally growing base-flow boundary layer. Temporal equivalent of Fig 0-22 are then in order. As noted earlier, for the Re(x) and Re(t)

MICROCOPY RESOLUTION TEST CHART

NATIONAL BUREAU OF STANDARDS-1963-A

systems, bifurcations from non-equilibrium flows may represent a neces-
sary extension of the theoretical concepts originally developed for pure
and purified flows.

A second comment stems from Batchelor's 1960 observation on a paper
of Donnelly and Simon. His point was that at higher Reynolds numbers
the steady Taylor vortices really consist of a core of solid body rota-
tion and thinner boundary layers at the walls and between the cells.
The observation surely remains valid at still higher Re after single or
double waviness sets in; see Fig 0-23b,c. Internal boundary layers are
a way of life at high Reynolds numbers; Tollmien's critical layer is
another example. It would seem that the viewpoint could provide a
bridge between the more globally oriented studies of annulus phenomena
and the aerodynamicist's outlook typified by this report.

The boundary layers between the cells really form extended narrow
jets subjected to an adverse pressure gradient as they "impinge" on the
other side of the annulus. The outward moving jet is the stronger one,
with a higher Reynolds number. Aerodynamically, the movement toward and
nearer the outer wall is then the most unstable local flow and the
likely site for genesis of turbulence. This region is the experimen-
tally crucial one. At the earliest transition, measurements elsewhere
merely probe the "buffeted", still laminar layers discussed in *Note 3
to Section 0.03.02. Strong support for this view is provided by the
visualizations of Tillmann (1961) and unpublished visual observation in
the USSR.

In a similar vein, the surprisingly regular small scale features in
the outer stagnation regions in Fig 0-23d suggest that a local instabil-
ity probably is taking place there, even though the flow is turbulent.
Turbulent flow in an annulus does not escape centrifugal instability.
The instability and the confinement combine to generate purified fixed-
scale coherent turbulent structures. As in the case of turbulent puffs
in circular pipes at Re = 2300, the structures are in equilibrium, ready
to be analyzed by specialists in turbulence simulation.

0.04.08   Looking forward and back

Throughout the 0.04 Sections, intended as an overview of our linear tools, notes and comments on secondary and higher instabilities were interwoven. They prepared the setting for further comments on what can be said rationally concerning expectations of post-primary instabilities. Basically, for the class of through-flow systems depicted in Fig 0-1b, the answer is: not much. The various reasons were described earlier, especially in Section 0.02.06. The answer for flows typified by Fig 0-1d is: quite a bit. As described in *Note 1 to the preceding section, the best guide to this information is the survey of DiPrima and Swinney (1981).

In the Introduction, the question of imprinting of turbulent shear layers by the specific sequence of instabilities leading to turbulence and the possible lingering effect of such imprinting on the turbulence characteristics was mentioned; it was aimed at the people concerned with future research in turbulence. In free shear layers (exemplified by Fig 0-1c the subsequent turbulent behavior and turbulent restructuring seems to be related to dimensional properties of the inviscid similarity solutions for these flows. In the first edition of his book on turbulent shear layers Townsend demonstrated the existence of similarity solutions for different classes of free turbulent flows without using the concept of eddy viscosity. However, arguments with eddy viscosity do not change the dimensionality of the problem. In both cases one is led to the same classification of x^n growth for the width, the center-line velocity and the Reynolds number (based on either viscosity); an easily accessible table is on p 734 of Schlichting (1979).

Two free flows are special: the axisymmetric jet and the two-dimensional wake. They exhibit a constant Reynolds number. In the axisymmetric wakes Reynolds number decays as the negative 1/3 power of x, while Re of mixing layers and two-dimensional jets grow with the first and one-half powers, respectively. Now, laminar free shear layers are equally inviscidly unstable; Townsend's dimensional arguments hold

equally well for the nonlinear stages of each laminar instability. For
the circular jet and the two-dimensional wake, in fact, similarity
solutions of the same dimensionality exist in presence of viscosity!

The full meaning of existence of a similarity solution is not
clear. Do all the nonlinear flows have to approach these solutions
asymptotically in some sense? However, what seems to be clear is that
we must expect different kinds of secondary and higher instabilities for
the axisymmetric wake and the mixing layer. The dimensionality of these
flows decrees it.

The two-dimensional far wake and the axisymmetric far jet in a
sense resemble the laminar flows for which Re = const, discussed in the
preceding *Note 1. In Section 0.02.03 we examined the 2D cylinder wake
at low Re and noted that it decayed altogether; presumably conditions
were not sufficiently inviscid. As presaged by Taneda's (1959) visual-
ization experiments, it now appears that at Re in excess of about 100,
2D wakes, laminar or turbulent, widen by entrainment in the nonlinear
stages of each instability and that their unsteady large-scale motion
detunes as the width changes. While the energy of this motion decreases
along the layer because of the detuning and viscosity, another inviscid
instability of the inflectional wider wake takes place, on new, larger
scales.

This behavior differs from that of mixing layers on at least
two important counts. The instability does not appear to be subharmonic
and tightly coupled to the preceding instability. It probably would not
be obtainable by a perturbation analysis of the type used by Pierrehum-
bert and Widnall (1982). It does not rely on amalgamation of active
nonlinear vorticity mode units, as does the mixing layer. Secondly it
develops slowly over a large number of wake diameters; that is one
reason why it has not been studied and documented earlier. The mixing
layer instabilities are rapid and vigorous, as befits a shear layer with
the fastest growing Reynolds number. For the wake of nonconstant width,
the constancy of the Reynolds number implies gradual readjustment of
length scales, coupled with proportionately gradual decrease of the
momentum defect. The gradual changes are accelerated during the active
stage of the instabilities.

This view represents the combined wisdom extracted from correlated research of Cimbala and Roshko at California Institute of Technology and Nagib, DesRuelle, Wlezian, and Way at Illinois Institute of Technology. Several manuscripts on the research are in preparation at this writing. The behavior has been observed for several turbulent wakes at moderate Reynolds numbers. It also provides a plausible explanation for the discrepancies in measured far-wake similarity scalings published in the literature, as analyzed by LaRue and Libby. At each restructuring-instability, the so-called virtual origin of the wake is changed.

The picture seems to be rather consistent for the first exceptional class, the two-dimensional wakes. For the second exceptional class, it would be desirable to analyze the few reliable cases of past experiments on axisymmetric far jets, and perhaps perform new experiments in this new light. From this viewpoint, also, dimensional considerations constrain the mixing layer to have Re $\propto$ x, and be most unstable, with increasing scales of instability. The inviscid subharmonic vortex amalgamation of Section 0.03.04 fits the requirements, for both the laminar and turbulent mixing layers.

It would appear that attention to inviscid scaling in free shear layers can help to unify the perception of flows that have been considered largely as separate special cases.

The remaining class of flows are the boundary layers, the flows which have been most investigated. In this area the strength of our linear tools is substantial, although still limited, especially for three-dimensional surfaces. For use with confidence, Görtler instability codes have to be broadened; they also require additional experimental buttressing. Figure 0-1a tells us that even two-dimensional boundary layers are subject to many special conditions, from roughness to curvature, to pressure gradients and local separation. We have accumulated a great deal of knowledge on all such problems in recent years.

For instance, most of the unifying observations concerning non-linear effects and higher instabilities, in the 0.02 Sections and in the Notes in the 0.03 Sections, and the preceding remarks on free shear layers could not have been made only three years ago. Nevertheless, in some areas our knowledge remains scant and imprecise--for instance, in the areas of (presumably linear) receptivity to turbulence, sound, vibrations, etc. Section 0.03.07 outlines areas of outright theoretical ignorance. Such gaps are covered by ad hoc empirical information without unifying concepts. Yet, considering the intrinsic difficulty in understanding non-equilibrium nonlinear phenomena, the overall progess has been impressive. To complete the picture, the reader is invited to reread the Introduction. Comments and suggestions made there should make much more sense in the light of the totality of the report.

0.04.09   Addendum for engineers

Logically, the look back at the main import of this report should end with the preceding section. However, in a research report funded by the Air Force, some comments are perhaps in order on the ever-recurring question posed by engineers: How can this knowledge be applied to technological problems? The shortest answer is: with very careful judgment. Utilization of incomplete and partially ad hoc information requires considered ad hoc judgment. The degree of care and type of judgment depend on the specific objectives of the proposed application and the background and attitudes of the engineers who use the information.

To be truly responsive to the question we should recognize three types of objectives in an engineer's involvement with the transition problem. They are not mutually exclusive. As engineers, we may wish (a) to understand transition phenomena as a background for dealing more judiciously with everyday problems involving assessment, delay, and various controls of transition; (b) to devise quantitative methods, utilizing semi-empirical theory as aids in larger design decisions before models are built for testing; (c) to predict transition on powerful computers for fundamental design decisions.

In connection with (c), E. Reshotko (1976) listed six capabilities that a method for transition prediction would have to possess before it could be called rational. It should be able to take into account on a logical quantitative basis: (1) disturbance environments (nature and spectra); (2) receptivity; (3) linear amplification (TS, Görtler, cross-flow instability); (4) 3D and nonlinear growth, secondary instabilities; (5) turbulent spot formation; and (6) completion of transition to turbulent flow. All this would be needed, plus careful attention to the missing links of Section 0.03.07. The need for two levels of computer support to provide accurate boundary layer profiles before embarking on the prediction should not be underestimated; this need was addressed in *Note 2 on design risks in Section 0.04.05.

The increased insight described in the present report makes us only more aware of the complexities in the transition processes and the multitudes of parameters that modify them. In 1983 the prospects for capabilities (4) and (5) remain dim. The implications of strange-attractor theories are truly relevant here. The sensitivity to initial conditions in NS systems is such that at stages (4) and (5) the developments are almost surely "chaotically unpredictable", though nonturbulent.

Our hope is that all the primary instabilities may prove to be invariably the slowest ones in the instability sequences. Then we might be able to rely primarily on our linear tools. If, for instance, the distance from x_{cr} to x_{nl} (the position where nonlinearity becomes operative) were invariably some 70% of the distance to x_{tr}, the details of stages (4) to (6) would not be of much consequence and could be safely covered by ad hoc empirical factors. Such a situation seems to exist for the TS instabilities in moderately benign environments. There seem to be no hard data to verify similar behavior in situations where Görtler instability or cross-flow instability are dominant.

Our weakest capability may well be associated with (1), the disturbance environment. *Notes 2, 4, and 5 in Section 0.03.02 attempt to convey some of the issues concerning definition and measurements of these disturbances. Not one laboratory team has yet achieved an evaluation of the disturbance contents in its streams in sufficient detail to be useful in receptivity research. Under the circumstances, what disturbance environment can an engineer assume for key design conditions? Even when it is given, the single u'/U_∞ specification is very inadequate for the judgment required, as illustrated in *Note 4 in Section 0.03.02.

Since Reshotko's 1976 comments, we have recognized more deeply the implications of the fact that the Navier-Stokes solutions are extremely sensitive to initial conditions. The solutions≡ the sequences of instabilities along the transition path are therefore extremely sensitive to environmental disturbances; these determine the spatial initial conditions in through-flow systems. This fact, combined with our lack of capability (1) to specify the controlling environmental disturbances

for any design conditions, make the determination of transition inaccessible to probabilistic treatment. The situation is foreign to normal design experience. Transition-conditioned design seems to require a special design philosophy.

This state of affairs renders Reshotko's requirements for a rational prediction technique virtually unattainable. The approach of type (c), namely to use computerized transition prediction for fundamental design decisions, is therefore ill-advised and dangerous. The approach (a) follows traditional paths, with the benefit of improving tools and information.

Approach (b) aims to take optimal advantage of computers; it therefore uses linear theory to clarify the features of the rate-controlling initial instability and to guide the design choices. The crucial aspects of the approach hinge on the limitations of the linear theory and the reliability of the empirical rules supplementing the theory. The streams of data and graphs pouring out of computers have a way of making them seem much more real than the many underlying assumptions warrant. They tend to induce intuitive appreciation of a computer transition behavior which is partly fictitious; they distort features governed by nonlinearity and the empirical rules.

A common version of approach (b) is a modifed e^n method, originally proposed by A. M. O. Smith for TS-initiated instabilities alone. In its prediction form, really approach (c), track is kept of the total amplification of waves of different frequencies along the surface. When one of the amplitudes has increased by a predetermined factor e^n from its value on the neutral curve, transition is said to begin; see Jaffe & OS (1970). Smith's 1956 collection of supporting data from wind tunnels and flight tests on varied shapes showed n varying from 4.2 to 20.9 at start of measured transition, depending on pressure gradients and free-stream disturbances. (Smith quotes values of n of 4.2 and 18.6 for an adverse and a favorable pressure gradient, respectively, from the same tunnel with low disturbances judged by 1943 standards!) These specific historical examples suggest that it takes an act of faith to trust some

"average" fixed n to characterize the complex processes in transition. Values of n from 9 to 11 became popular with many engineers "because we have nothing better". Very few took the time to study the detailed arguments in Smith and Gamberoni (1956).

Smith actually started with Liepmann's nonlinear criterion of maximal TS Reynolds stress growing to the level of laminar shear stress at the wall, combined with reasonable scaling laws. The Reynolds stress depends specifically on the initial value of the fluctuations induced by free-stream disturbances. He wrote in the 1956 report, "Therefore a careful evaluation...demands at least a frequency spectrum to supply data on initial values of disturbance. A mean value of u'/U is unsatisfactory...". His efforts took a tangential approach for the very reasons stressed here: the lack of knowledge of environmental disturbances and associated receptivities. Without such knowledge, linear theory can yield only dimensionless ratios.

Yet such ratios represent a cumulative measure of the strength of the instability at any pretransition $Re_\delta^*(x)$. In Section 0.04.04 we gained useful insight from comparisons of local amplification rates. A procedure that takes into account the shape of the ridge of amplification and discloses the most amplified disturbance up to any Re_δ^* station clearly provides a better measure of the character and strength of the instability.

A concrete example may be helpful. Allowing for an internalized spectrum at the neutral curve with fluctuation u'/Hz of, say, $0.00007U_\infty/Hz$, a cumulative growth factor of $e^5 \sim 150$ would place the most dangerous frequency at a stage comparable to that at station 170 in the bottom photograph of Fig 0-11. Evidence from ONERA-Toulouse, discussed in Chapter 3 of the Guide, suggests quite strongly that the disturbance spectrum within the boundary layer decays surprisingly fast in the stable regions up to the neutral curve. This implies that free-stream disturbances can be quite large and still yield the above initial level in the most dangerous frequency at the neutral position. The point of the concrete example is to convince the reader that a safe e^5

level can be chosen for numerical design experimentation. For instance, using e^5 as an allowable upper limit, together with other desiderata, an airfoil shape could be designed. Two-dimensional laminar-flow airfoils could be redesigned in this manner, if need be, and if a reliable and practical way of solving the insect and service-conditioned roughness problem were found; see *Note 2 in Section 0.04.05.

The problem is more complicated for three-dimensional boundary layers. Oblique waves, steady or oscillatory, can amplify faster than the TS waves with fronts normal to the edge velocity in Fig 0-12. Also the direction of propagation can change with x and z. Obviously the process of comparing cumulative growths up to a given x,z position for different frequencies and different wave orientations is expensive. (Remember also the need for the other two supporting computer programs before the instability code can be applied--see *Note 2 in Section 0.04.05. They would be needed with each design change of shape.) The overriding question, however, is the rationality and safety of the design procedure. For instance: Are nonlinear thresholds in two-dimensional and three-dimensional instabilities comparable? Should the same n be used?

This fictitious example illustrates both the nature and the power of the e^n method when used in approach (b). It certainly represents a valuable advance over approach (a). Used with judgment, it is rational, despite the intrinsic uncertainties in the transition processes.

This outlook cannot be found in the open literature. Over the years, the preceding ruminations have been the subject of many a philo-sophical night session among devotees of transition lore. Perhaps it is time to put the gist of them down on paper as a general message from the old guard to the neophyte transitionists.

REFERENCES

ABRAMOWITZ, M. & STEGUN, I. A. (1964): Handbook of Mathematical Functions, Nat. Bur. Standards, U. S. Gov. Printing Office.

ARNAL, D. & JUILLEN, J. C. (1979): Experimental results on the influence of the transition process on the initial structure of the turbulent boundary layer. (In French) ONERA reprint T. P. No. 1979-128.

BATCHELOR, G. K. (1960): A theoretical model of the (Taylor) flow at speeds far above the critical, pp 416-418. Appendix in R. J. Donnelly and N. J. Simon: An empirical torque relation for supercritical flow between rotating cylinders, J. Fluid Mech., v 7, 401-418.

BATCHELOR, G. K. (1967): An Introduction to Fluid Dynamics, Cambridge Univ. Press.

BATT, R. G. & LEGNER, H. H. (1983): A review of roughness-induced nosetip transition, AIAA Jour., v 21, 7-22.

BENJAMIN, T. B. & MULLIN, T. (1982): Notes on multiplicity of flows in the Taylor experiment. J. Fluid Mech., v 121, 219-230.

BIPPES, H. (1972): Experimentelle Untersuchung des Laminar-Turbulenten Umschlags an einer Parallel Angeströmten Konkaven Wand, Sitzung-berichte der Heidelberger Akad. der Wissenschaften, Math-Natur-wissenschaftliche Klasse, No. 3, Springer Verlag. Also in English: NASA-TM-72243; March 1978.

BETCHOV, R. & CRIMINALE, W. O. JR. (1967): Stability of Parallel Flows, Academic Press.

BRADSHAW, P. (1973): Effects of Streamline Curvature on Turbulent Flow. AGARDograph AG-169, 80 pages, NATO.

CARLSON, D. R., WIDNALL, S. E. & PEETERS, M. T.: A flow-visualiza - tion study of transition in plane Poiseuille flow. J. Fluid Mech., v 121, 487-505.

CHARTERS, A. (1943): Transition between laminar and turbulent flow by transverse contamination. NACA TN 891.

COLEMAN, W. S. (1961): Roughness due to insects, pp 683-747 of Vol II Boundary Layer and Flow Control, G. V. Lachman, ed., Pergamon Press.

CORCOS, G. M. & LIN, S. J. (1983): Deterministic models of the shear layer, Part II: The origin of the three-dimensional motion. MS.

DESRUELLE, D. (1983): Beyond the Karman vortex street. MS thesis. Illinois Institute of Technology, Chicago IL 60616.

DIMOTAKIS, P. E. & BROWN, G. L. (1976): The mixing layer at high Reynolds number: large-structure dynamics and entrainment. J. Fluid Mech. v. 78, 535-550.

DONALDSON, C. duP., SNEDEKKER, R. S., & YATES, J. E. (1970): Experimental study of transition induced in an accelerated boundary layer at low Reynolds numbers. Report 152, Aero Res. Assoc. Princeton Inc. AFOSR-TR-71-3106.

DRAZIN, P. G. & REID, W. H. (1981): Hydrodynamic Stability, Cambridge Univ. Press.

DRUBKA, R. C. (1982): Instabilities in near field of turbulent jets and their dependence on initial conditions and Reynolds number. PhD thesis, Illinois Institute of Technology, Chicago, IL 60616.

DYMENT, A. & GRYSON, P. (1978): Study of subsonic and supercritical turbulent flows by ultrarapid visualization. Paper No. 28 of Unsteady Aerodynamics, AGARD Conf. Proc-227.

FLORYAN, J. M. (1980): Stability of boundary-layer flows over curved walls. PhD thesis, Virginia Polytechnic Institute and State Univ., Blacksburg, VA 24061.

FLORYAN, J. M. & SARIC, W. S. (1982): Stability of Görtler vortices in boundary layers. AIAA Jour. v 20, 316-324.

FREYMUTH, P. (1966): On transition in a separated laminar boundary layer. J. Fluid Mech., v 25, 683-704.

GASTER, M. (1962): A note on the relation between temporally-increasing and spatially-increasing disturbances in hydrodynamic stability. J. Fluid Mech., v 14, 222-224.

GASTER, M. (1974): On the effects of boundary-layer growth on flow stability. J. Fluid Mech., v 66, 465-480.

GASTER, M. (1975): A theoretical model of a wave packet in the boundary layer on a flat plate. Proc. Roy. Soc., London, v 347, 271-289.

GASTER, M. (1977): Series representation of the eigenvalues of the Orr-Sommerfeld equation. Paper 2 of Laminar-turbulent transition, AGARD Conf. Proc., 224.

GASTER, M. & GRANT, I. (1975): An experimental investigation of the formation and development of a wave packet in a laminar boundary layer. Proc. Roy. Soc. London A., v 347, 253-269.

GILL, A. E. (1965): A mechanism for instability of plane Couette flow and of Poiseuille flow in a pipe. J. Fluid Mech., v 21, 503-511.

GROPENGIESSER, H. (1969): On the stability of free shear layers in compressible flows. (In German) Deutsche Luft. und Raumfahrt, FB 69-25, 123 pp. Also 1968 doctoral dissertation, Technical Univ., Berlin.

HALL, P. (1982): Taylor-Görtler vortices in fully developed or boundary-layer flows: linear theory. J. Fluid Mech., v 124, 475-494.

HAMA, F. R., WILLIAMS, D. R. & FASEL, H.: Flow field and energy balance according to the spatial linear stability theory of the Blasius boundary layer. Pages 73-85 in Laminar-Turbulent Transition, ed. R. Eppler and H. Fasel, Springer Verlag.

HERBERT, T. (1981): Stability of Poiseuille flow--theory and experiment. Proc. Fluid Dyn. Transactions, v 11, Polish Acad. Sci. Also Report VPI-E-81-35, Engr. Sci. and Mech., Virginia Polytech. Inst. and State Univ., Blacksburg, VA 24061.

HERBERT, T. (1983): Subharmonic three-dimensional disturbances in unstable plane shear flows. AIAA Paper No. 83-1759.

HO, C. M. (1982); Local and global dynamics of free shear layers, Chap. 30 of Numerical and Physical Aspects of Aerodynamic Flows, ed. T. Cebeci, Springer Verlag.

HO, C. M. & NOSSIER, N. S. (1981): Dynamics of an impinging jet. J. Fluid Mech., v 105, 119-142.

HULTGREN, L. S. & GUSTAVSSON, L. H. (1981): Algebraic growth of disturbances in a laminar boundary layer. Phys. Fluids, v 24, 1000-1004.

HUSSAIN, A.K.M.F. & ZAMAN, K.B.M.Q. (1978): Free shear layer tone phenomenon and probe interference. J. Fluid Mech., v 87, 349-383.

ITOH, N. (1974): A power series method for the numerical treatment
of the Orr-Sommerfeld equation. Trans. Jap. Soc. Aerosp. Sci.,
v 17, 65-75.

ITOH, N. (1974a): Spatial growth of finite wave disturbances in
parallel and nearly parallel flows, Part 1. Theoretical analysis
and numerical results for plane Poiseuille flow, Trans. Jap. Soc.
Aerosp. Sci., v 17, 160-174.

JAFFE, N., OKAMURA, T. T., & SMITH. A. M. O. (1970): The determination
of spatial amplification factors and their application to predicting
transition. AIAA Jour., v 8, 301-311.

JHAVERI, B. & HOMSY, G. M. (1980): Randomly forced Rayleigh-Benard
convection. J. Fluid Mech., v 98, 329-348.

KACHANOV, Yu. S. & LEVCHENKO, V. Ya. (1982): Resonant interactions
of disturbances in transition to turbulence in a boundary layer.
(In Russian) Preprint No. 10-82, Inst. Theor. Appl. Mech. USSR
Acad. Sci., Novosibirsk. English version submitted to J. Fluid
Mech., 1983.

KEGELMAN, J. T. (1982): Experimental studies of boundary-layer
transition on a spinning and non-spinning axisymmetric body.
PhD thesis, Univ. Notre Dame, Notre Dame, IN 46556.

KLEBANOFF, P. S., TIDSTROM, K. D., & SARGENT, L. M. (1962): The
three-dimensional nature of boundary-layer instability. Jour.
Fluid Mech., v 12, 1-34.

KLEISER, L. & SCHUMANN, U. (1980): Treatment of incompressibility
and boundary conditions in 3-D numerical spectral simulations of
plane channel flows. Pages 165-173 of Proc 3rd GAMM-Conference
on Numerical Methods in Fluid Mechanics, ed E. H. Hirschel ,
Vieweg, Braunschweig.

KOLMOGOROV, A. N. (1962): A refinement of previous hypotheses concerning
the local structure of turbulence in a viscous incompressible
fluid at high Reynolds numbers. J. Fluid Mech., v 13, 82-85.

KOZLOV, V. V. & RAMASANOV, M. P. (1980): Experimental investigations
of the growth process of disturbances in Poiseuille flow.
(In Russian) Preprint No. 80-21, Inst. Theor. Appl. Mech., USSR
Acad. Sci., Novosibirsk.

LIEPMANN, H. W. (1979): The rise and fall of ideas in turbulence.
Am. Scientist, v 67, 221-228.

LIGHTHILL, M. J. (1963): Introduction to boundary layer theory. Pages 46-113 of Laminar Boundary Layers, ed. L. Rosenhead, Clarendon Press, Oxford.

LUMLEY, J. L. (1981): Coherent structures in turbulence. Pages 215-242 of Transition and Turbulence, ed. R. R. Meyer, Acad. Press.

MACK, L. M. (1969): Boundary-Layer Stability Theory. Jet. Prop. Lab. Report 900-277, Pasadena, CA 91103.

McLACHLAN, N. W. (1947): Theory and Application of Mathieu Functions. Clarendon Press, Oxford.

McLACHLAN, N. W. (1950): Ordinary Nonlinear Differential Equations. Clarendon Press, Oxford.

METCALIFE, R. W. & RILEY, J. J. (1981): Unpublished numerical experiments.

MICHALKE, A. (1964): On the inviscid instability of the hyperbolic tangent velocity profile. J. Fluid Mech., v 19, 543-556.

MICHALKE, A. (1965): On spatially growing disturbances in an inviscid shear layer. J. Fluid Mech., v 23, 521-544.

MICHALKE, A. (1965a): Vortex formation in a free boundary layer according to stability theory. J. Fluid Mech., v 22, 371-383.

MICHALKE. A. (1972): The instability of free shear layers. Pages 213-329 of Progress in Aerosp. Sciences, D. Kuchemann, ed., Pergamon Press.

MONKEWITZ, P. A. & HUERRE, P. (1981): The influence of the velocity ratio on the spatial instability of mixing layers. Phys. Fluids, v. 25, 1137-1143.

MORKOVIN, M. V. (1969): Critical evaluation of transition from laminar to turbulent shear layers with emphasis on hypersonically traveling bodies. U.S. AFFDL TR-68-149.

MORKOVIN, M. V. (1978): Instability, Transition to Turbulence and Predictability. Keynote address at AGARD Copenhagen Symposium, May 1977, AGARDograph No. 236, NATO.

MORKOVIN, M. V. (1979): On the question of instabilities upstream of cylindrical bodies. NASA CR 3231.

MURPHY, J. D. & RUBESIN, M. W. (1966): A re-evaluation of heat-
transfer data obtained in flight tests of heat-sink shielded
re-entry vehicles. Jour. Spacecraft & Rockets, v 3, 53-60.

NAGIB, H. M. (1984): Management and control of turbulence for
wind-tunnel design. In v 16 of Annual Review of Fluid Mechanics.

NAKAYA, C. (1976): Instability of the near wake behind a cylinder.
J. Phys. Soc. Japan, V 41, 1087-1088.

NAYFEH, A. H. & MOOK, D. T. (1979): Nonlinear Oscillations, Wiley &
Sons.

NISHIOKA, M., ASAI, M., IIDA, S. (1979): An experimental investiga-
tion of the secondary instability. Pages 37-46 of Laminar
Turbulent Transition, ed. R. Eppler & H. Fasel, Springer Verlag.

NISHIOKA, M, IIDA, S., ICHIKAWA, Y. (1975): An experimental investiga-
tion of the stability of plane Poiseuille flow. J. Fluid Mech.
v 72, 731-751.

NISHIOKA, M. IIDA, S., KANBAYASHI, S. (1978): An experimental investi-
gation of the subcritical instability in plane Poiseuille flow.
(In Japanese). Proc. 10th Turbulence Symposium, Inst. Space Aero.
Sci., Tokyo University, pp 55-62.

NISHIOKA, M. & MORKOVIN, M. V. (1983): Experiments on a mechanism of
boundary-layer receptivity to time-periodic pressure gradients.
MS.

NISHIOKA, M. & SATO, H. (1978): Mechanism of determination of shedding
frequency of vortices behind a cylinder at low Reynolds numbers.
J. Fluid Mech., v 89, 49-60.

OBREMSKI, H. J., MORKOVIN, M. V., & LANDAHL, M. (1969): A Portfolio
of Stability Characteristics of Incompressible Boundary Layers,
with contributions from Wazzan, A. R., Okamura, T. T., and Smith,
A. M. O. AGARDograph No. 134, NATO.

ORSZAG, S. A. & KELLS, L. C. (1980): Transition to turbulence in
plane Poiseuille and plane Couette flow. J. Fluid Mech., v 96,
159-205.

ORSZAG, S. A. & PATERA, A. T. (1981): Subcritical transition to
turbulence in planar shear flows. Pages 127-146 of Transition
and Turbulence, ed. R. E. Meyer, Academic Press.

ORSZAG, S. A. & PATERA, A. T. (1983): Secondary instability of wall-
bounded shear flows. J. Fluid Mech., v 128, 347-385.

PIERREHUMBERT, R. T. & WIDNALL, S. E. (1982): The two- and three-
dimensional instabilities of a spatially period shear layer.
J. Fluid Mech., v 114, 59-82.

POLL, D. I. A. (1978): Some aspects of the flow near a swept attachment line with particular reference to boundary layer transition. Doctoral dissertation, College of Aeronautics, Cranfield Institute of Technology.

PRANDTL, L. (1952): Essentials of Fluid Dynamics. Hafner Publ. Co. New York.

RAGAB, S. A. & NAHFEH, A. H. (1981): Gortler Instability. Phys. Fluids, v. 24, 1405-1417.

RESHOTKO, E. (1969): Stability theory as a guide to the evaluation of transition data. AIAA Jour., v 7, 1086-92.

RESHOTKO, E. (1976): Boundary stability and transition. Pages 311-350 of v 8 of Annual Review of Fluid Mechanics.

RESHOTKO, E. (1976a): Where are we? Where do we go from here? Keynote address in Proc. Low-speed Boundary-Layer Transition Workshop II, ed. W. S. King & M. Yokota, RAND Corp. Rept. P-6119, 1978.

RESHOTKO, E. & LEVENTHAL, L. (1981): Preliminary experimental study of disturbances in a laminar boundary layer due to distributed surface roughness. AIAA Paper 81-1224.

ROCKWELL, D. & SCHACHENMANN, A. (1982): Self-generation of organized waves in an impinging turbulent jet at low Mach number. J. Fluid Mech. v 117, 425-441.

SARIC, W. S. (1981): private transmittal of Fig 0-11.

SARIC, W. S. and NAYFEH, A. H. (1977): Nonparallel stability of boundary ary layer flows with pressure gradients and suction. Paper 6 in Laminar-Turbulent Transition, AGARD Conf. Rept-224.

SAVAS, O. (1979): Some measurements on synthetic turbulent boundary layers. PhD thesis, Calif. Institute of Technology, CA 91225.

SCHLICHTING, H. (1979): Boundary Layer Theory, 7th ed. McGraw-Hill Co.

SCHUBAUER, G. B. & SKRAMSTAD, M. K. (1943): Laminar-boundary-layer oscillations and transition on a flat plate. NACA Adv. Conf. Rept., later Tech. Rept. No. 909.

SMITH, A. M. O. & GAMBERONI, H. (1956): Transition, pressure gradient and stability theory. Rept. ES26388, Douglas Aircraft Co.

STEWART, R. W. (1968): Turbulence, film of Nat. Com. for Fluid Mech. Films; also illustrated summary, pp 82-88 of Illustrated Experiments in Fluid Mechanics, ed. A. Shapiro, MIT Press, 1972.

105

STOKER, J. J. (1950): Nonlinear Vibrations, Interscience Publ.

STUART, J. T. (1971): Nonlinear stability theory. Annual Review of Fluid Mechanics, pp 347-370.

TANEDA, S. (1959): Downstream development of the wakes behind cylinders. J. Phys. Soc. Japan, v 14, 843-848.

TANI, I. (1962): Production of longitudinal vortices in the boundary layer along a concave wall. Jour. Geophys. Res., v 67, 3075-80.

TANI, I. (1981): Three-dimensional aspects of boundary-layer transition. Proc. Indian Acad. Sci. (Engg. Sci), v 4, 219-238.

TANI, I. & SAKAGAMI J. (1964): Boundary layer instability at subsonic speeds. Pages 391-403 of Proc. Third Congress of International Council of Aerospace Sciences, Stockholm, 1962. Spartan Books.

TAYLOR, G. I. (1915): Eddy motion in the atmosphere. Phil. Transactions A, v 215, 23-26.

TENNEKES, H. & LUMLEY, J. L. (1972): A First Course in Turbulence, MIT Press.

THEODORSEN, T. (1955): The structure of turbulence. Pages 55-62 in 50 Jahre Grenzschichtforschung, ed. H. Görtler and W. Tollmien, F. Vieweg & Sohn. (See Fig. 6)

TILLMAN, W. (1961): Turbulenzentstehung bei der Stromung zwischen rotierenden Zylindern. Z.f.angew.Phys., v 13, 468-475.

VAN DYKE, M. (1982): An Album of Fluid Motion. Parabolic Press, P. O. Box 3032, Stanford, CA 04305-0030.

WAZZAN, A. R., OKAMURA, T. T., & KELTNER, G. (1973): Spatial stability of incompressible two-dimensional Gaussian wake in steady viscous flow, Phys. Fluids, v 16, 1368-1370.

WAZZAN, A. R., OKAMURA, T. T., & SMITH, A. M. O. (1968): Spatial and temporal stability charts for the Falkner-Skan boundary layer profiles. Douglas Aircraft Co. Rept. No. DAC-67086. More easily accessible in Obremski & ML (1969).

WILSON, S. D. R. & GLADWELL, I. (1978): The stability of a two-dimensional stagnation flow to three-dimensional disturbances. J. Fluid Mech., v 84, 517-527.

WORTMANN, F. X. (1964): Experimentelle Undersuchungen laminarer Grenzschichten bei instabilier Schichtung. Pages 815-825 of Proc. XI International Congress on Applied Mechanics, Munich, ed. H. Gortler, Springer-Verlag.

WORTMANN, F. X. (1964): Experimental investigations of vortex occurrence at transition in unstable laminar boundary layers. AFOSR Rept. 64-1280, AF 61 (052)-220.
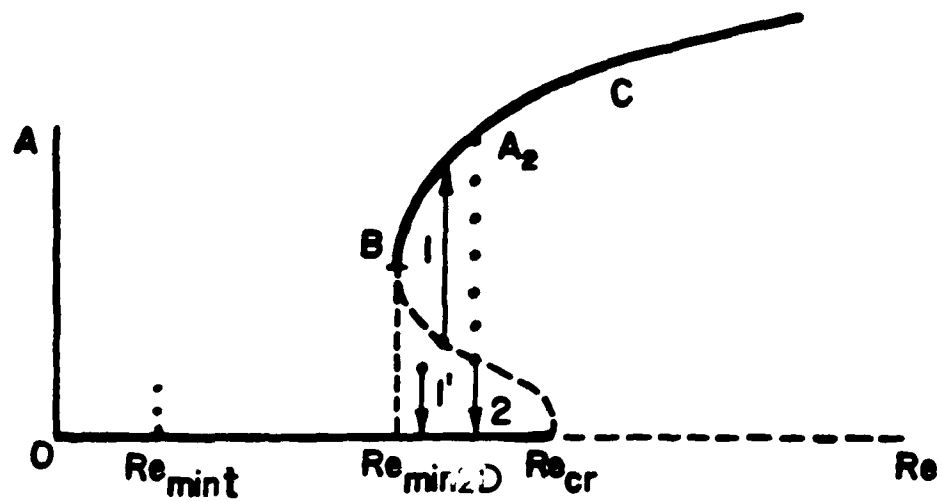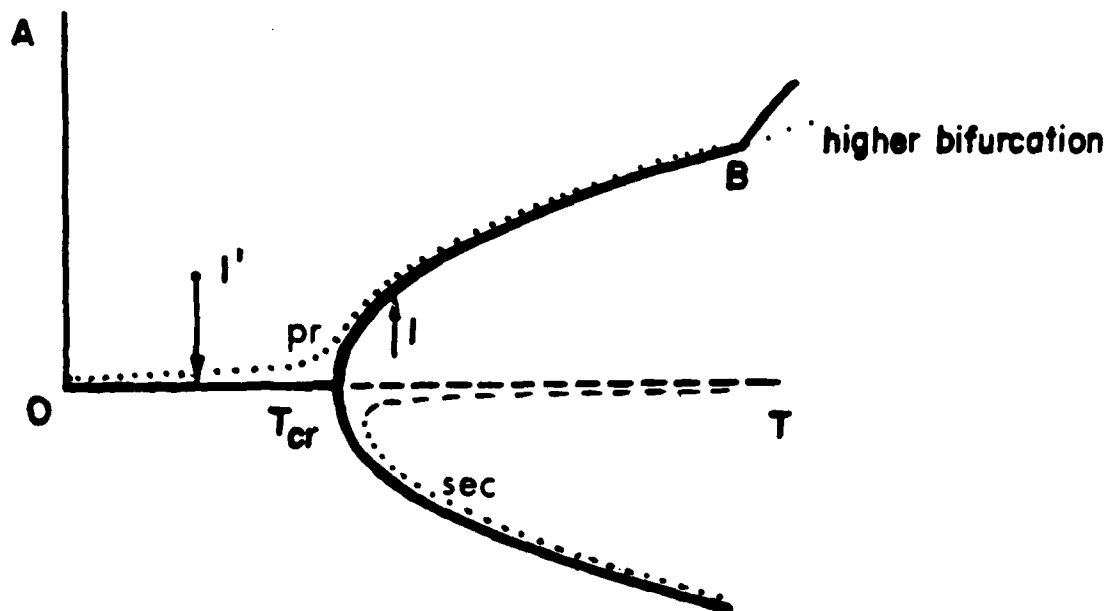
Sketch 0.02.04   Bifurcations: (a) subcritical,   (b) supercritical

TABLE I

Temporally and Spatially Varying Physical Disturbances

Temporal Wave	Spatial Wave
$v = \mathrm{Re}\left\{ v_1(y)e^{i(\alpha_r x - \omega_r t)} \, e^{\omega_i t}\right\}$	$v = \mathrm{Re}\left\{ v_1(y)e^{i(\alpha_r x - \omega_r t)} \, e^{-\alpha_i x}\right\}$
Fourier parameter $\alpha = \alpha_r$	$\omega = \omega_r$
eigenvalue $\omega(\alpha, R) = \omega_r + i\omega_i$	$\alpha(\omega, R) = \alpha_r + i\alpha_i$
phase velocity $c_r = \omega_r/\alpha_r$	$c_r = \omega_r/\alpha_r$,
group velocity $c_g = (\partial\omega_r/\partial\alpha_r)_{Re}$	$c_g = (\partial\omega_r/\partial\alpha_r)_{Re}$.
amplification rate $\omega_i = \alpha_r c_i > 0$ for instability	$-\alpha_i > 0$ for instability
total amplification $\log_e (A_2/A_1) = \displaystyle\int_{t_1}^{t_2} \omega_i \, dt$ $= \displaystyle\int_{x_1}^{x_2} \frac{\alpha_r c_i}{c_g} \, dx$ by Gaster Transformation	$\log_e (A_2/A_1) = -\displaystyle\int_{x_1}^{x_2} \alpha_i \, dx$
initial data given along x-axis	initial data given along t-axis

Gaster Transformation: $\alpha_r(T) = \alpha_r(S)$, $\omega_r(T) = \omega_r(S)$, $\dfrac{\omega_i(T)}{\alpha_i(S)} = -\left(\dfrac{\partial\omega_r}{\partial\alpha_r}\right)_{Re}$. These relations hold to order $(\omega_{i \, max}^2)$.
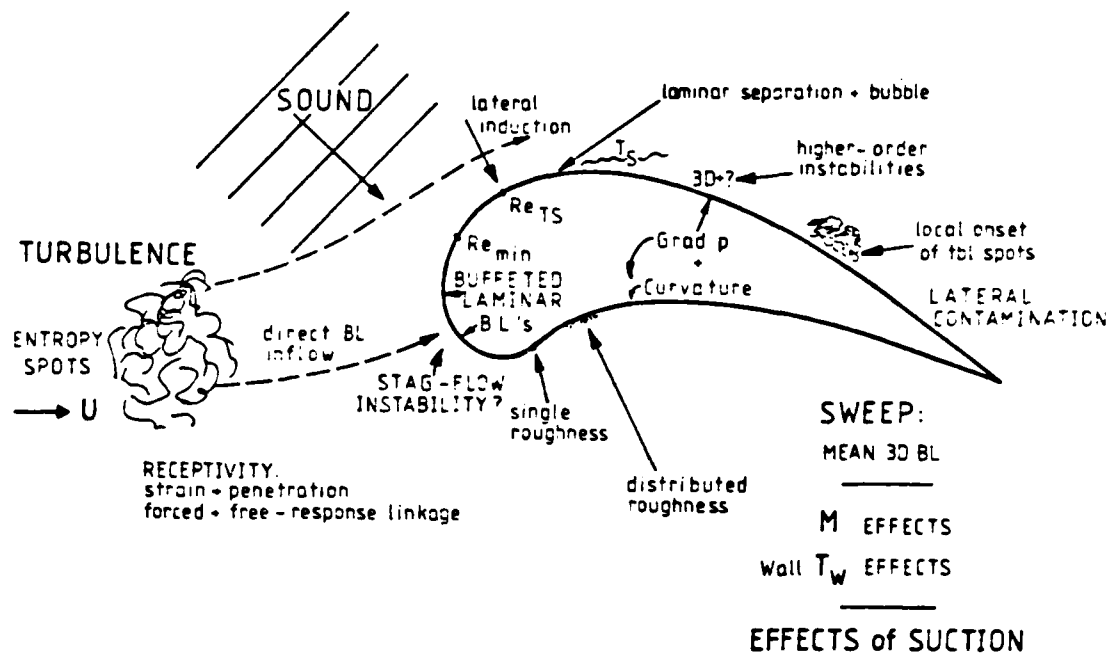
Fig 0-1a Typical transition issues in external flows
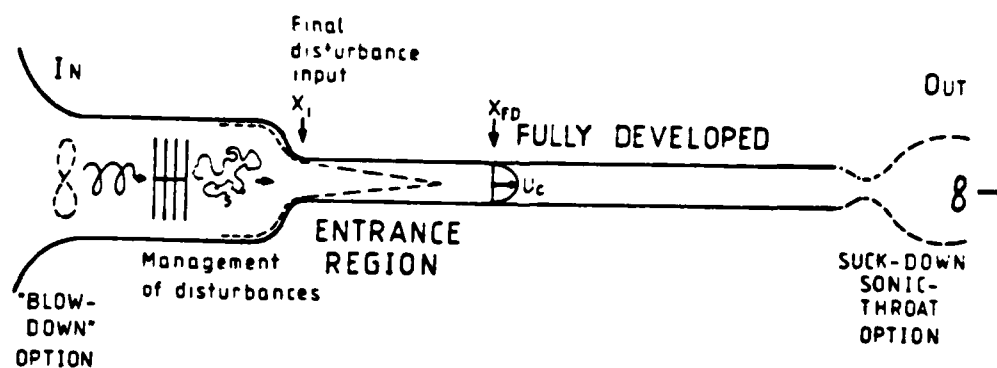
Fig.0-1b Internal flow facility

BEHAVIOR

Thin-vortex sheet   jet-scale

large - α_i
short linear
regime

$f\theta/U$ fD/U

LAMINAR
BL-θ

PAIRING

S

Turbulence
onset in strained
local field

U ⟶ "Potential core"

S

Singular-line
receptivity to
pressure fields

NONLINEAR:
MEAN-FLOW
MODIFICATION

COMPOSITE
SPECTRA:

Strongly
non ll

2 lengths
$\theta \ll D$

Symmetry vs
antisymmetry
n=0 vs n=1

KEY COUPLING
LINK IN RESONANCES
WITH FREE SHEAR LAYERS
(even turbulent ones)

Fig.0-1c Jet instabilities and transition
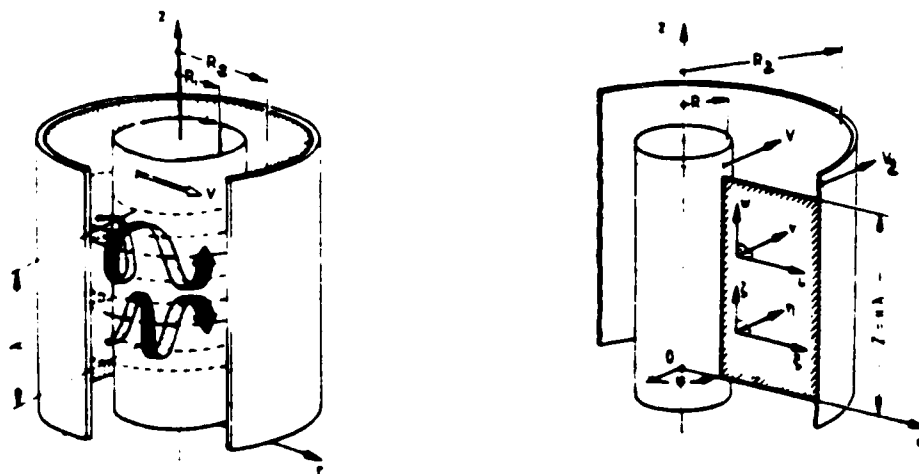
Fig. 0-1d   Couette-Taylor rotating cylinder and instability

M. Nishioka and H. Sato
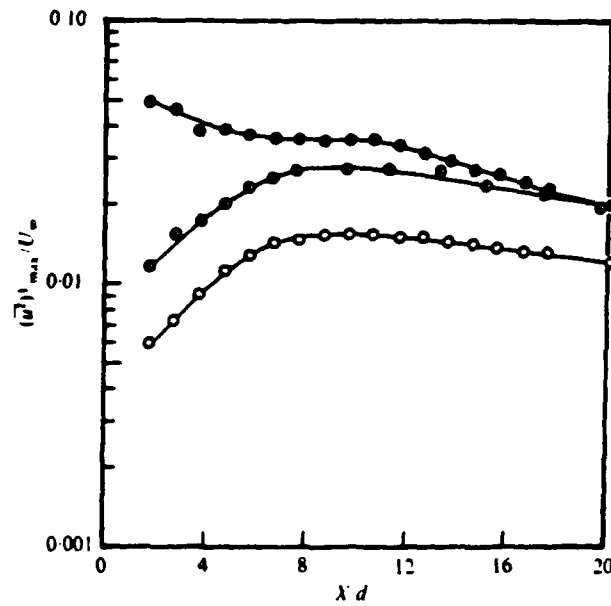
FIG. 0-2 The streamwise development of a sinusoidal fluctuation ($f = 12\ \text{Hz}, R = 30$) with various cylinder amplitudes, a/d: $\bigcirc$, $a/d = 0.04$: $\bigoplus$, $a/d = 0.08$; $\bullet$, $a/d = 0.15$.
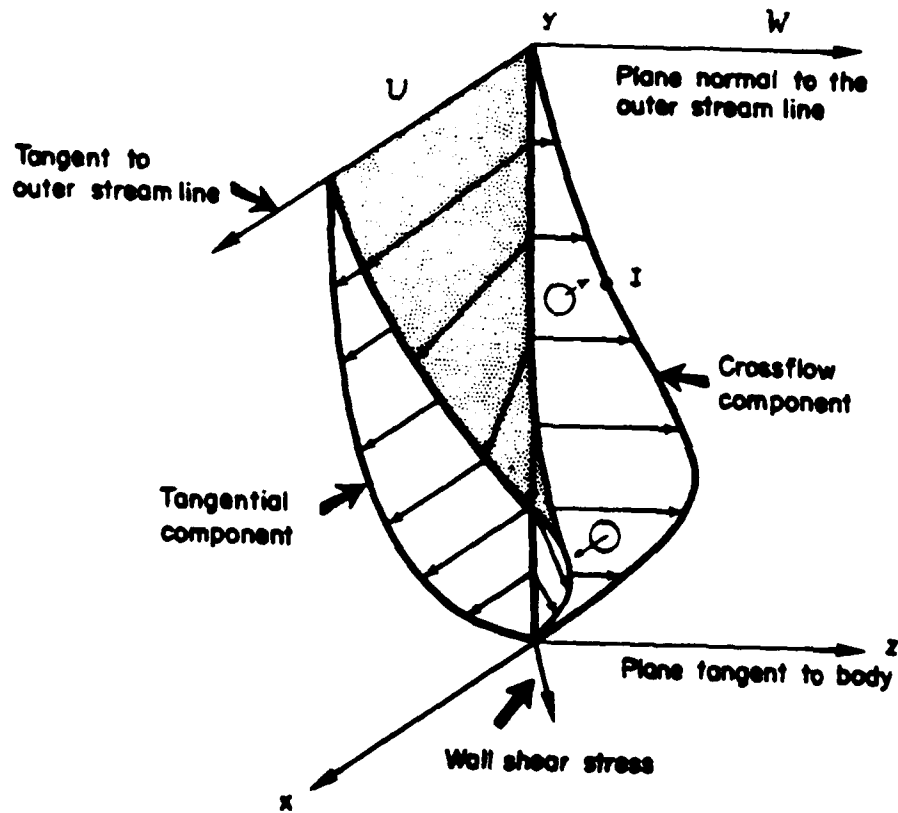
Fig.0-12 Velocity Profiles In A Three-Dimensional Boundary Layer
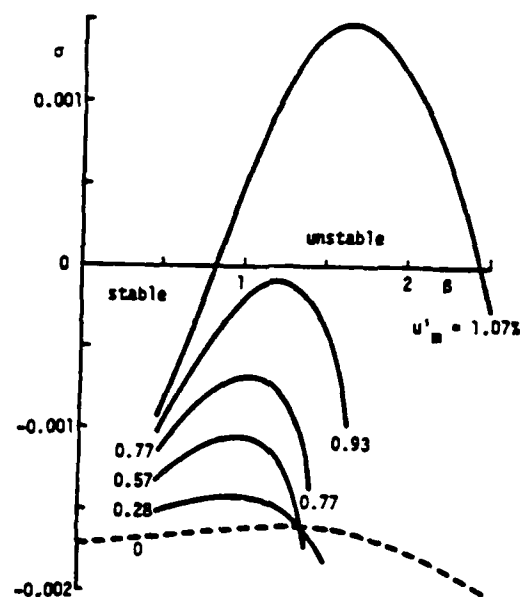
Figure O-3a Growth rate σ of 3D disturbances vs. β at α = 1 for various amplitudes u'$_m$ (%) according to linear theory (Herbert   ), showing the onset of secondary instability at u'$_m$ = 1% for β = 1.25.
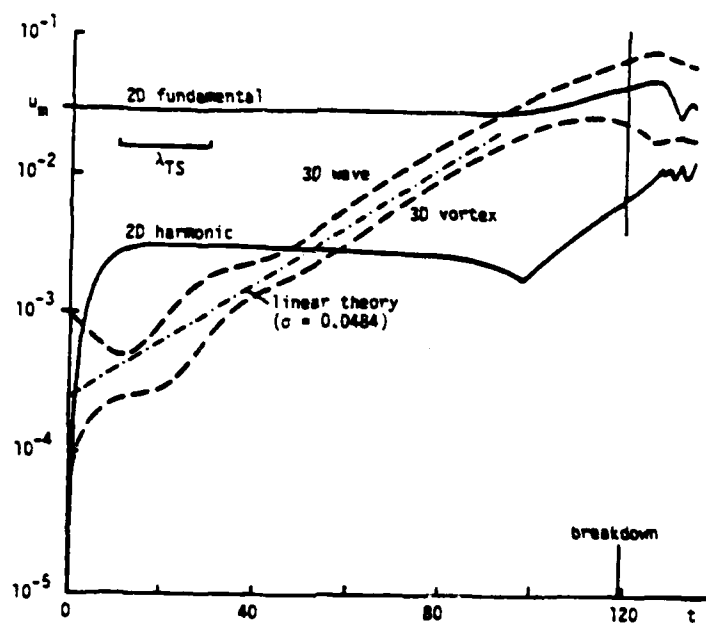
Figure O-3b Evolution of 2D and 3D components at R = 5000, α = 1.12, β = 2.1. Simulation (Kleiser 1981) and theory (Herbert   ).

D. R. Carlson, S. E. Widnall and M. F. Peeters

a

Flow direction
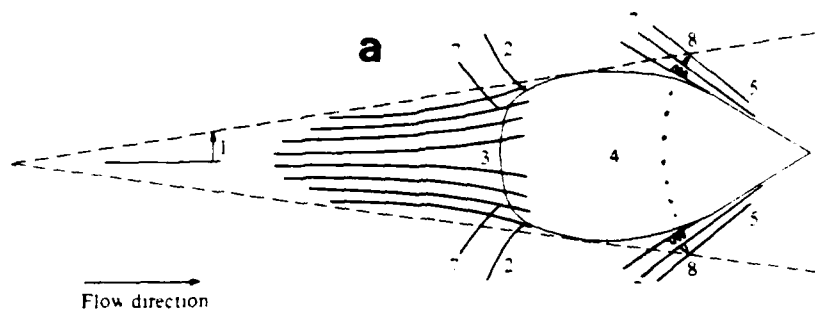
Spot nomenclature: (1) spreading half-angle; (2) spanwise tips; (3) streaks; (4) region of small-scale turbulence; (5) spot leading edge; (6) spot front; (7) oblique waves; (8) tongues of breakdown.

b
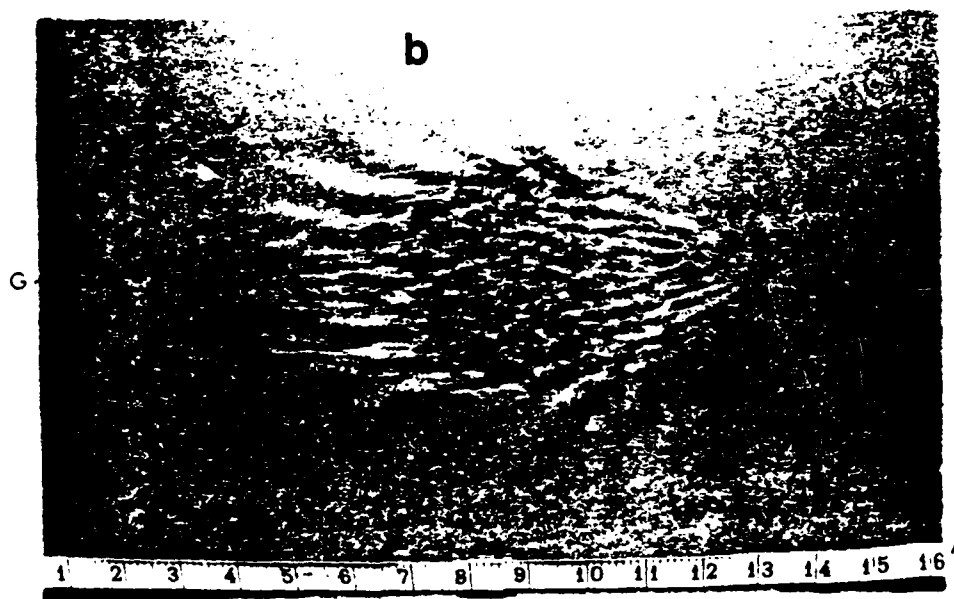
Fig 0-4   Turbulent patch, stimulated at point G

in plane Poiseuille flow at Re of 1000.
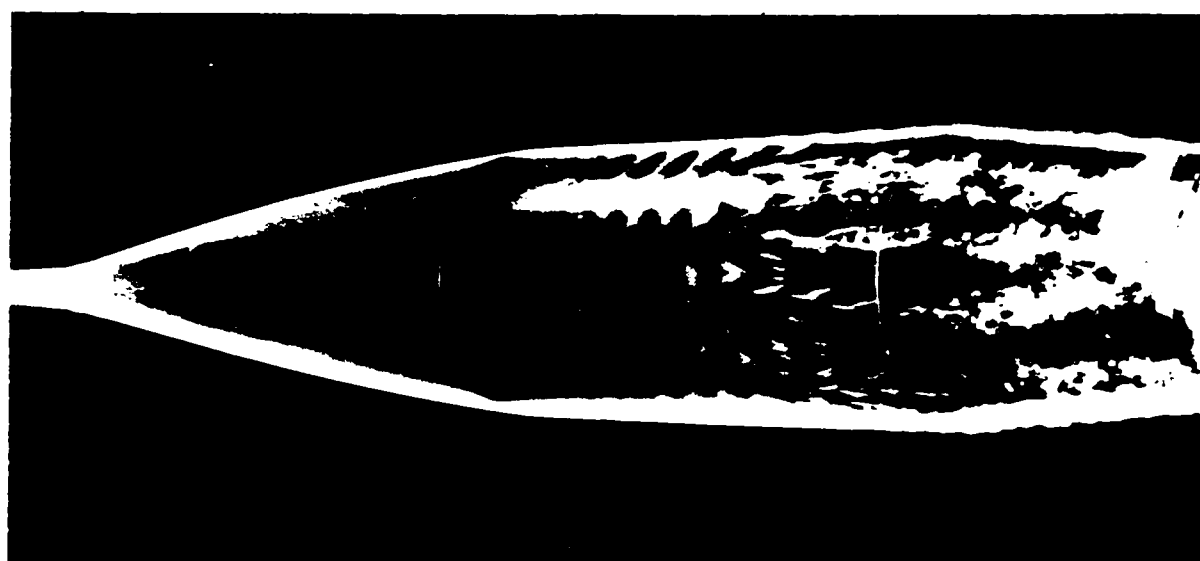
$Re_L = 814,000, \alpha = 0$ excitation at f = 551 Hz ↑   785 Hz ↓

a →

U →

sound

609 60

304 80   203 20   101 60

101 6

3 CALIBER
SECANT OGIVE NOSE

2 CALIBER
CYL BODY

7°

I CALIBER
BOATTAIL

1844.23

1901.79 RAD

463 90

DIMENSIONS IN MILLIMETERS
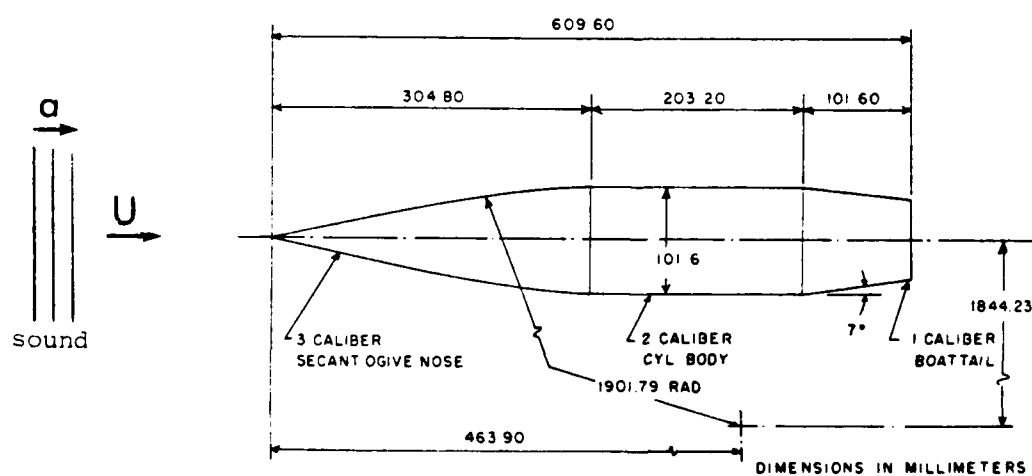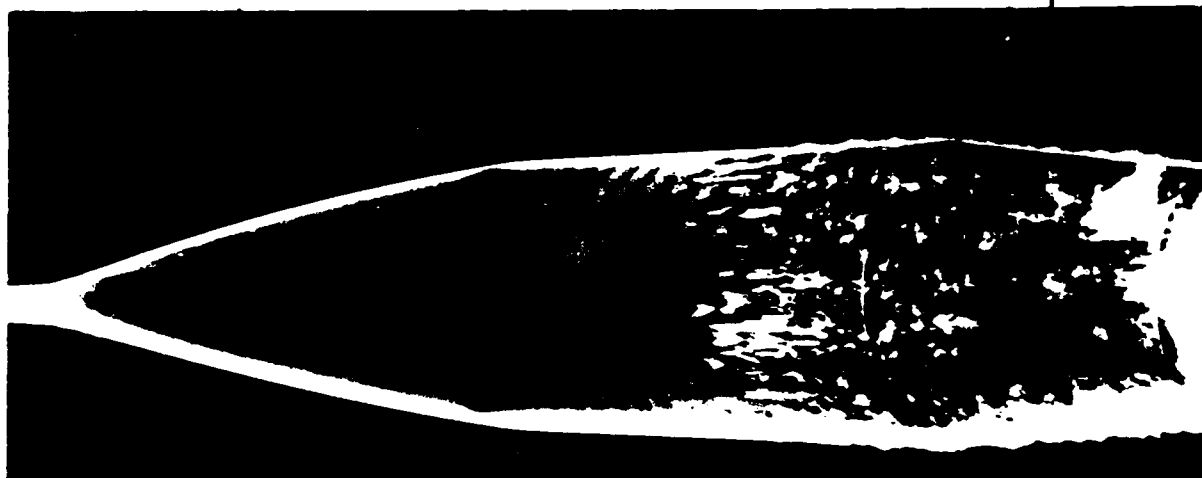
Fig 0-5   Sound induced TS waves on ogive-cylinder body at U of 21.6 m/s
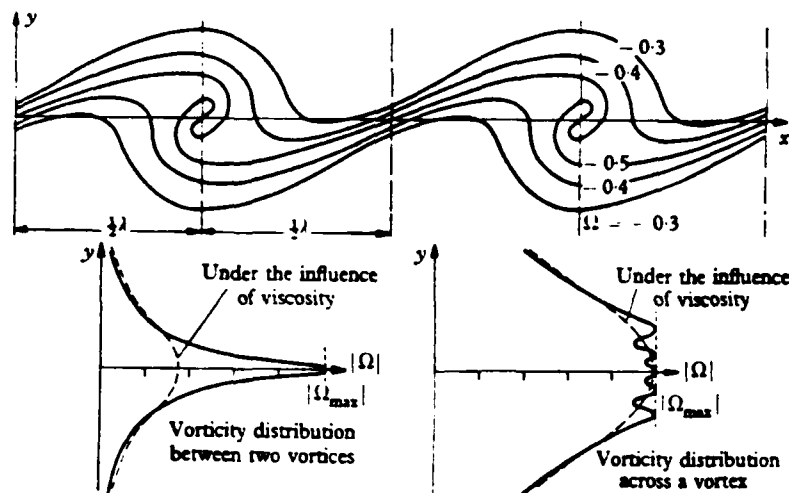
Vorticity distribution expected in a free boundary layer during rolling-up (inviscid non-linear theory).

FIG·0-6

Michalke (1965)

J.F.M. 22

CONTOUR FROM -1.1200   TO 0.   CONTOUR INTERVAL OF   .70000E-01

Total Vorticity $\Omega(y) + 3(x,y,t)$

N·S COMPUTATIONS

FIG 0-7

Metcalfe · Riley
(1981)
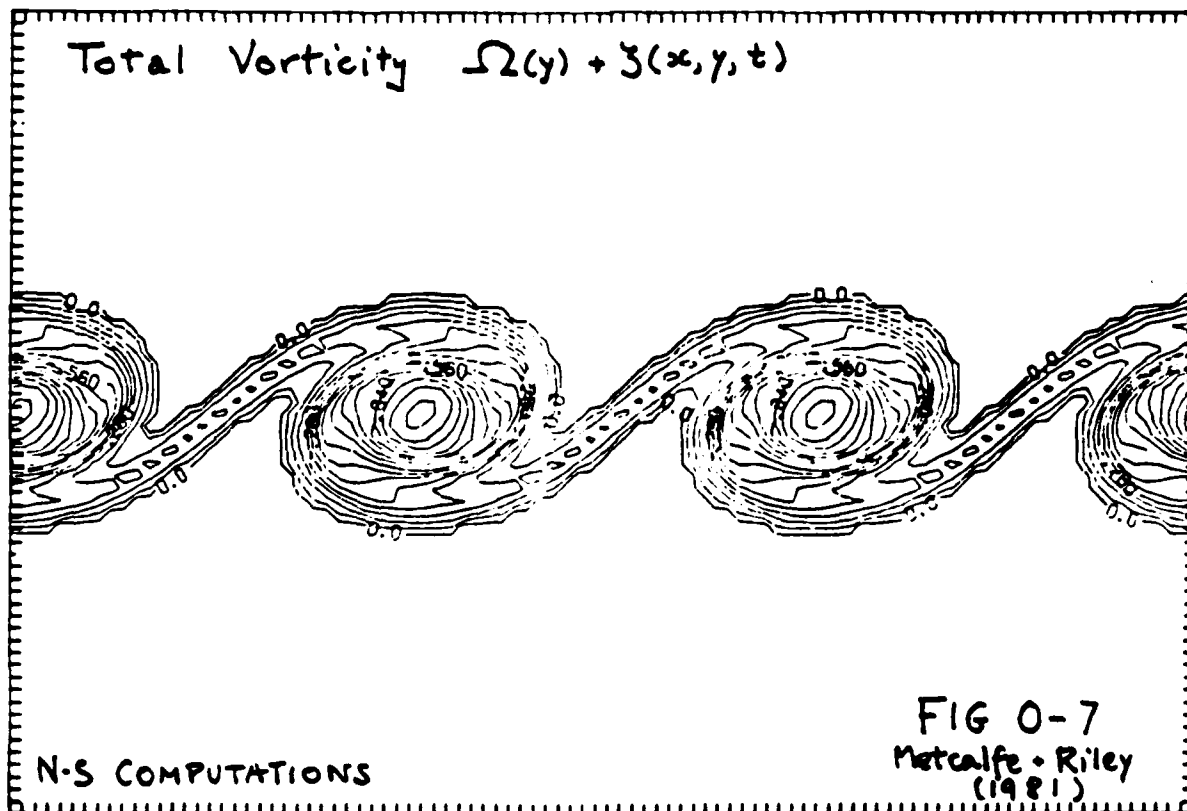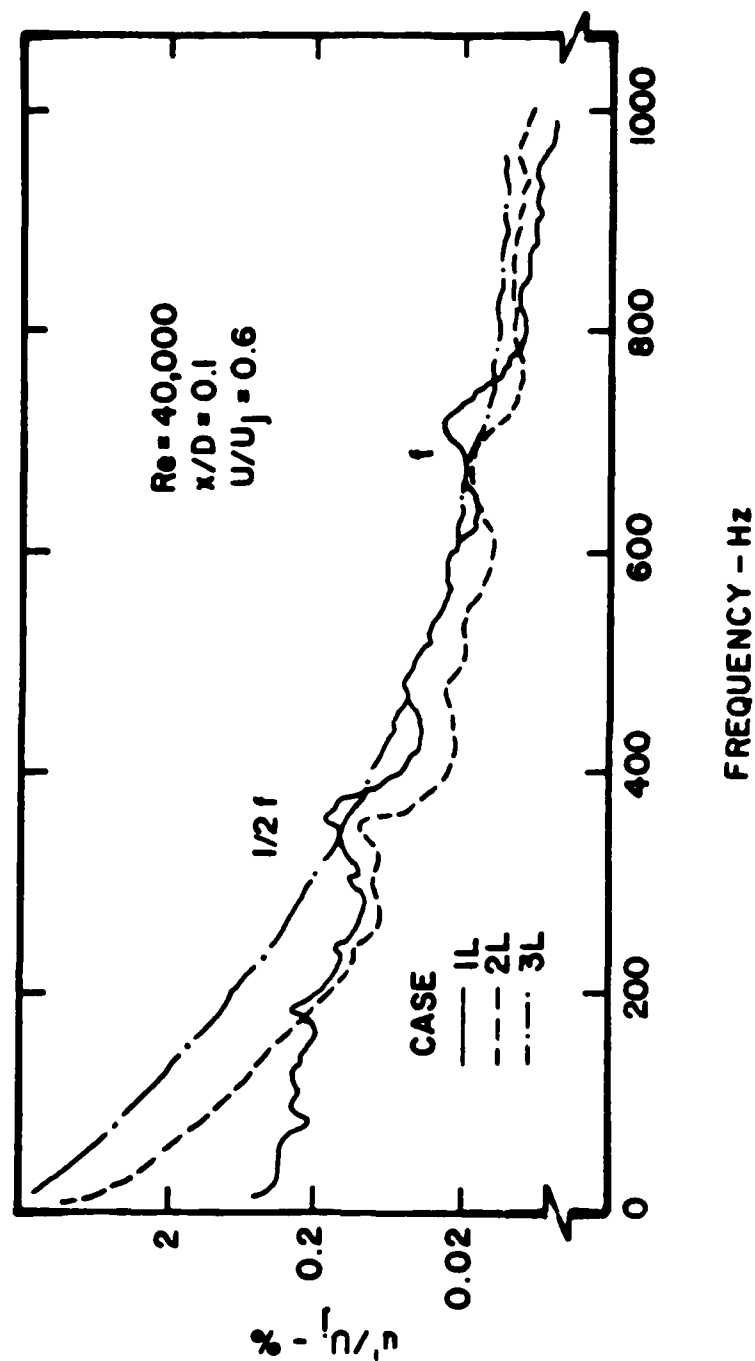
Fig 0-8   Spectral content of u' fluctuations in the thin mixing layer near the exit nozzle of a relatively quiet axisymmetric jet of diameter D = 5.14 cm.
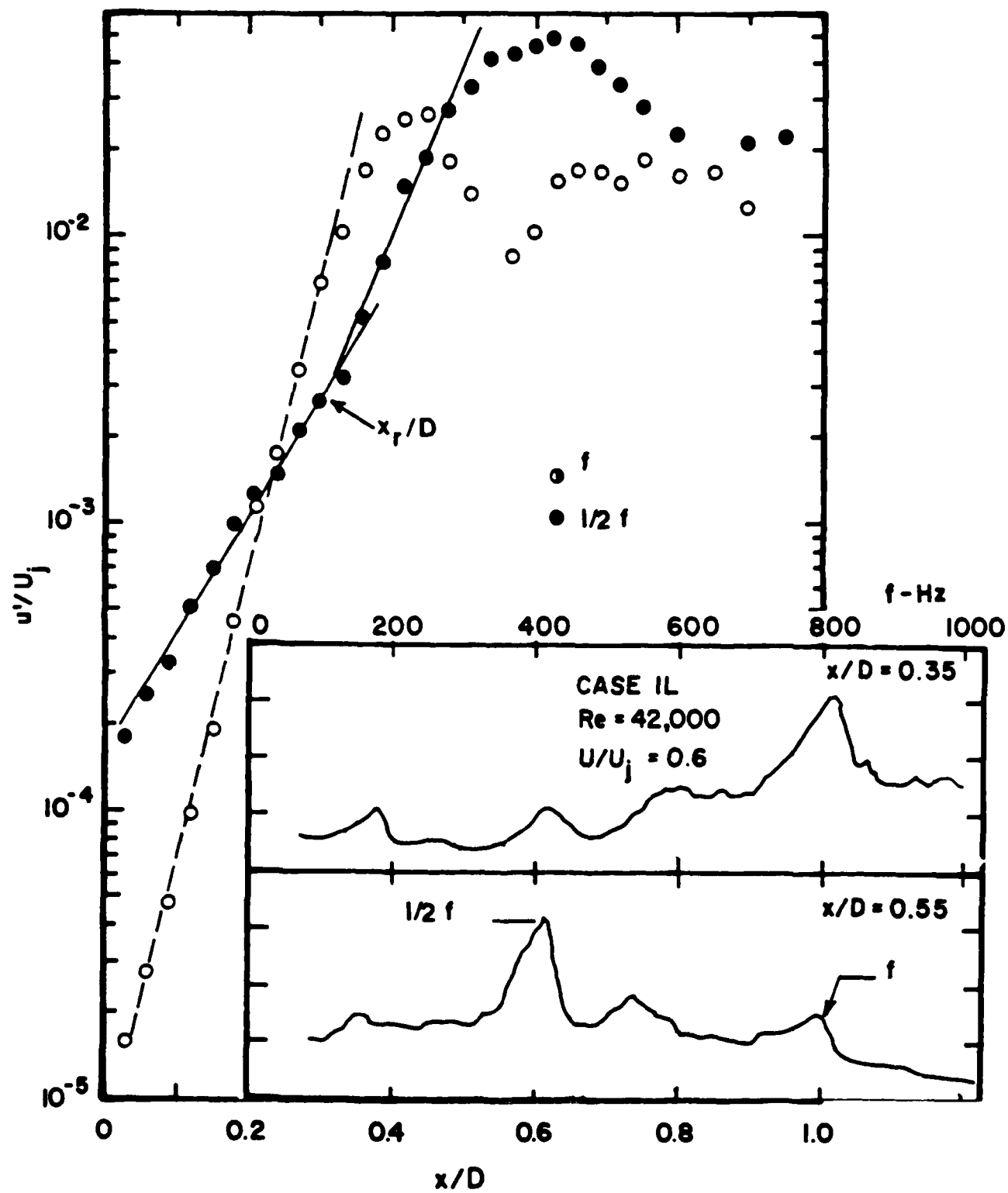
Fig 0-9   Growth of fundamental f and subharmonic f/2/ spectra near
           saturation of f and f/2 in mixing layer of Fig 0-8.

PHASE = PI/8.   C2768A
TKQ/J(F) = 2.6

PHASE = PI/8.   C2768A
TKQ/J(F) = 5.1
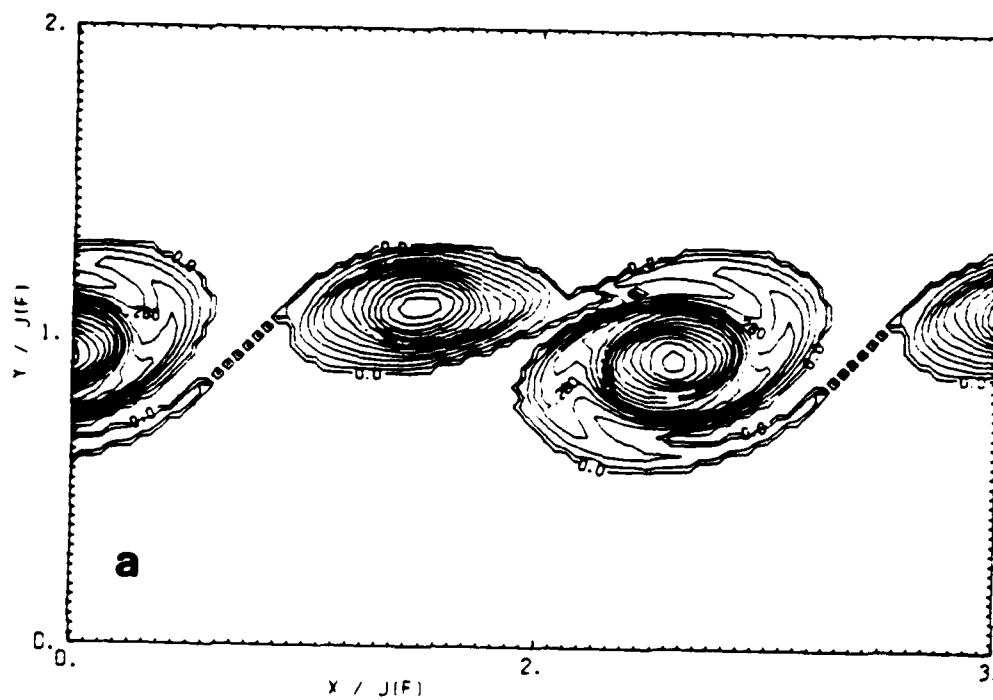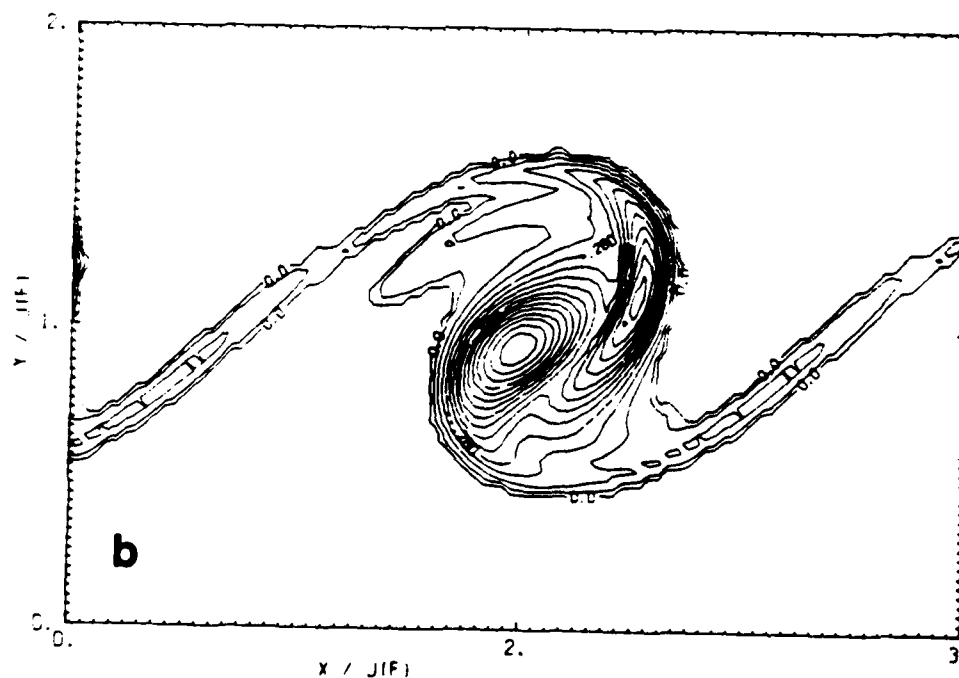
Fig O-10   Simultaneous temporal growth of fundamental f and subharmonic
           f/2, prestimulated at equal amplitudes, $\pi/8$ out of phase.
           Dimensionless time: 2.6 in (a), 5.1 in (b).   NS computations.

Branch II ↓   U = 6.6 m/s;   f = 39 Hz stimulated at x = 47 cm;   = 0.5 cm

u'_m = 0.2%   -   Detuning and decay ↑
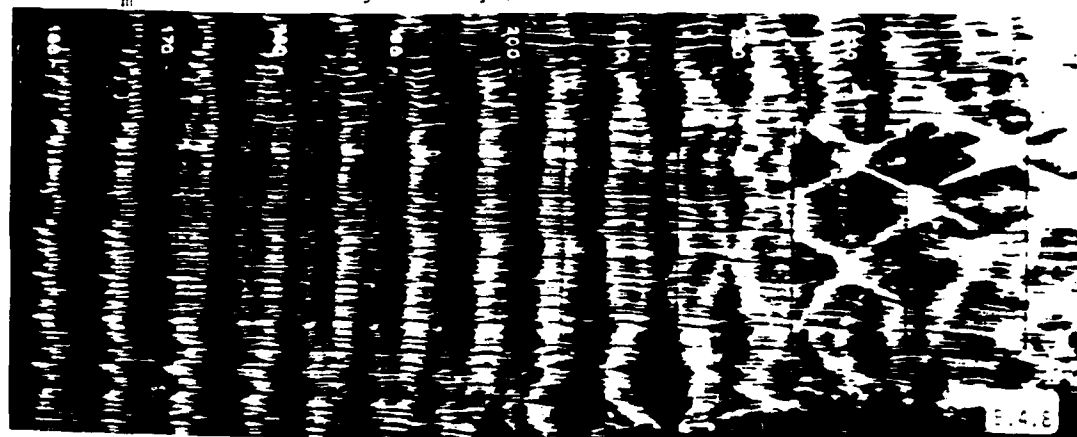
u'_m = 0.3%   -   Secondary subharmonic 3D instability ↗

u'_m = 1.0%   - ↑ Secondary 3D instability and tertiary Klebanoff breakdown

Fig 0-11   Post TS amplitude-conditioned secondary instabilities and breakdown.

Figure O-13 A surface oil flow pattern showing a transition to turbulence which is produced by 55° sweep-induced instability of the laminar boundary layer, at 33.54 m/s.

Fig 0-14 T stability map of flat plate boundary layers.
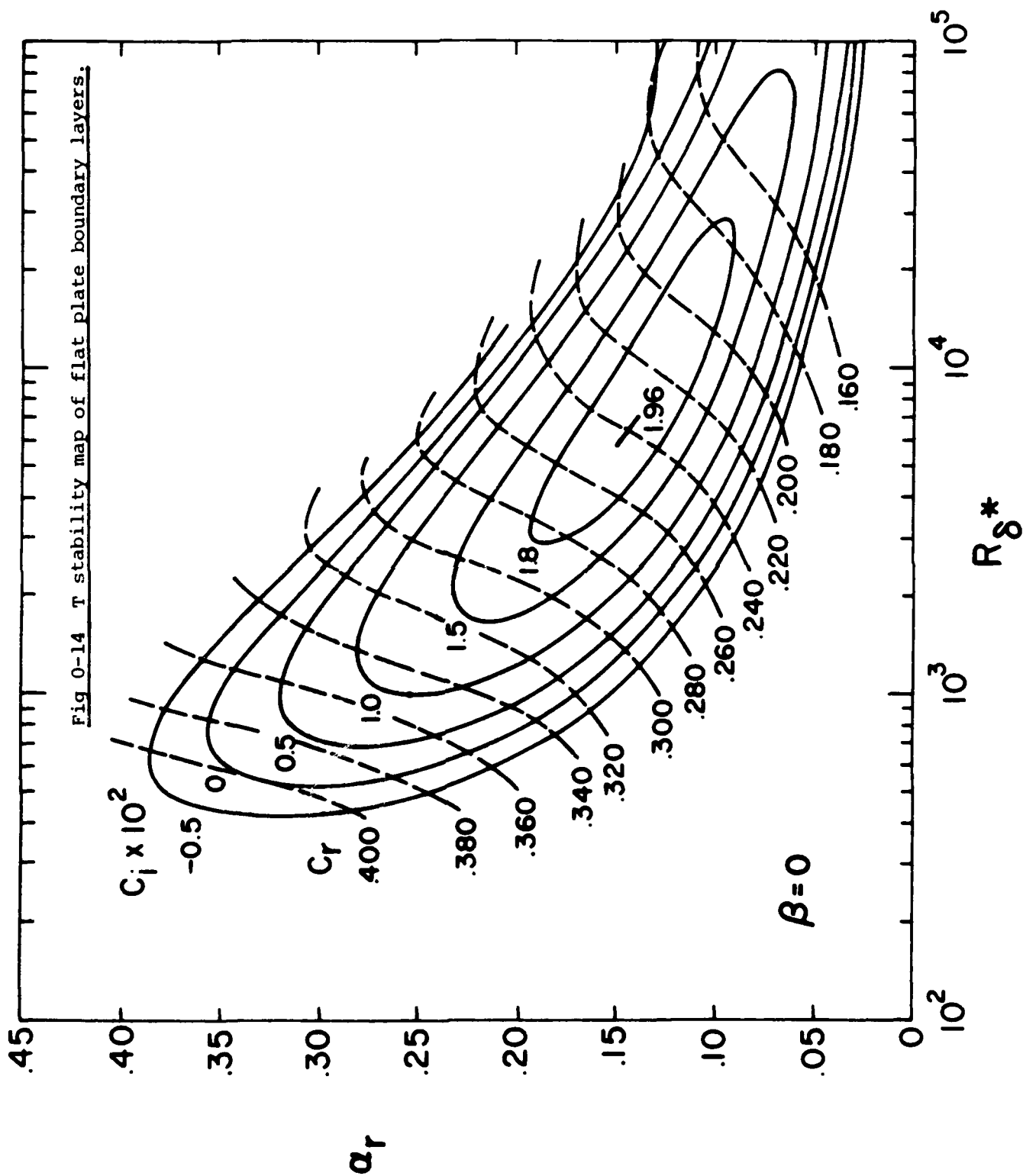
Fig 0-15 T stability map of plane stagnation boundary layers.
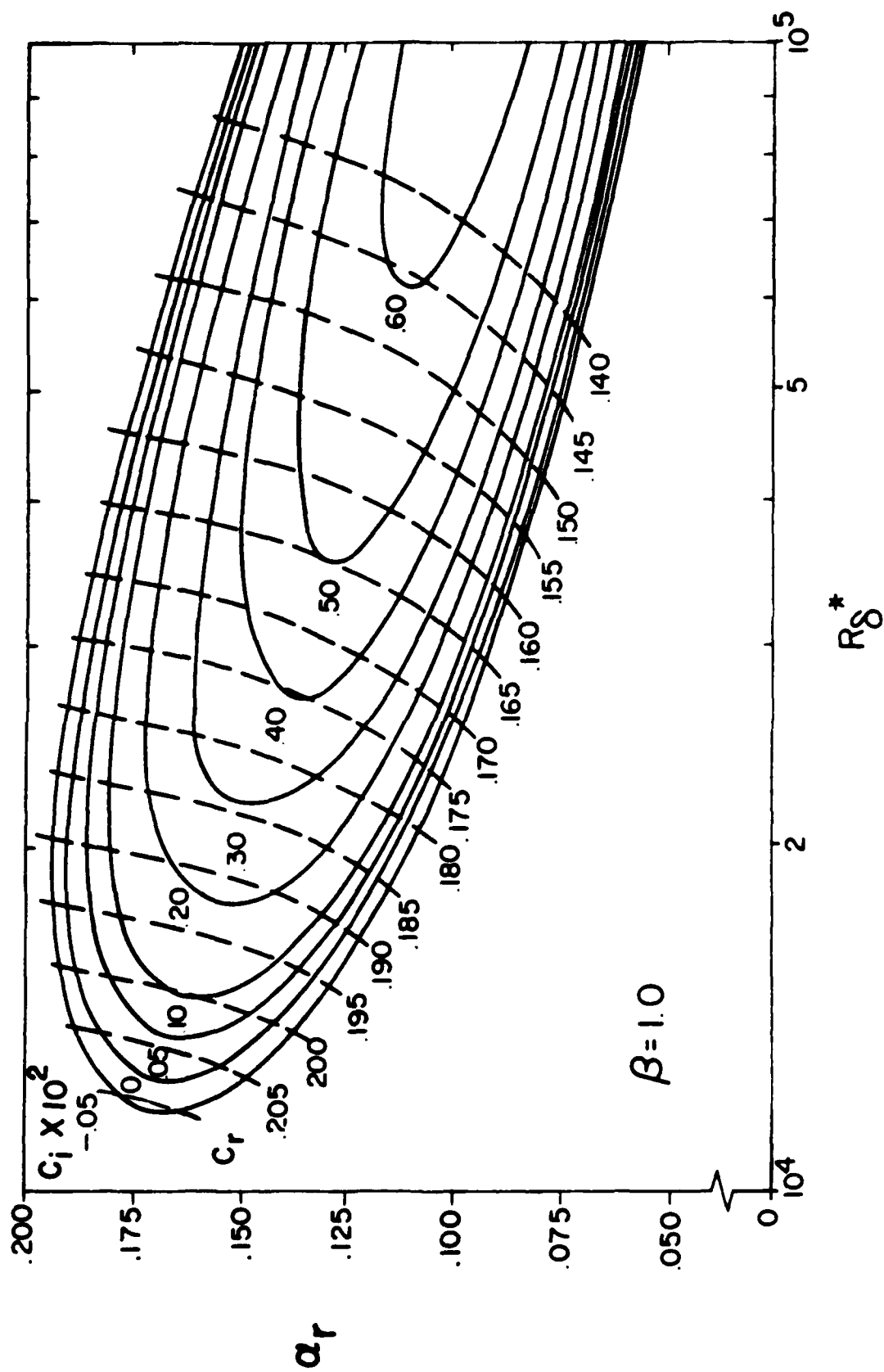
Fig 0-16   T stability map of inflected boundary layers with edge velocity $U = a_1 x^{-0.0476}$.
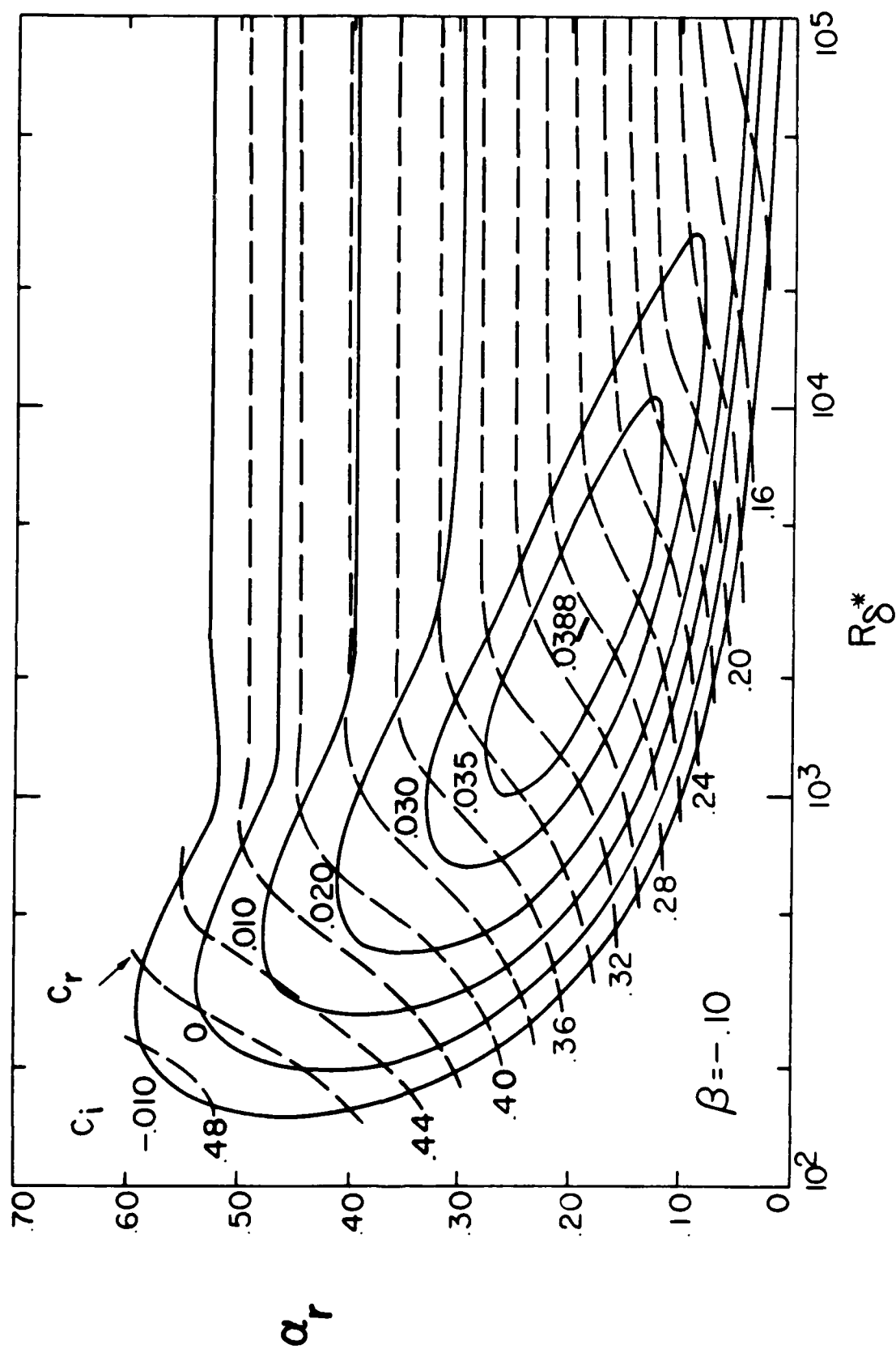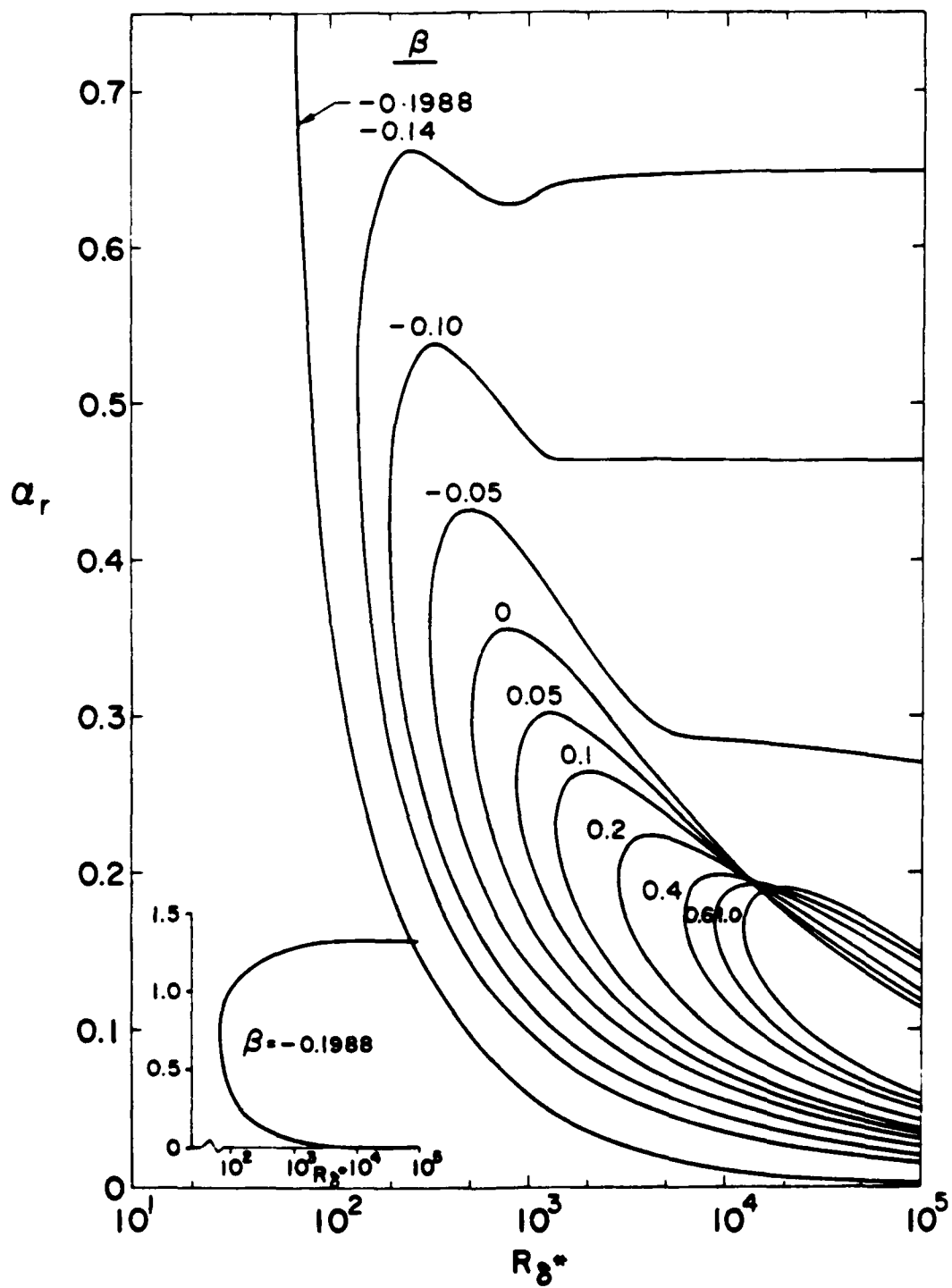
Fig 0-17   Neutral curves for Falkner-Skan boundary layers .
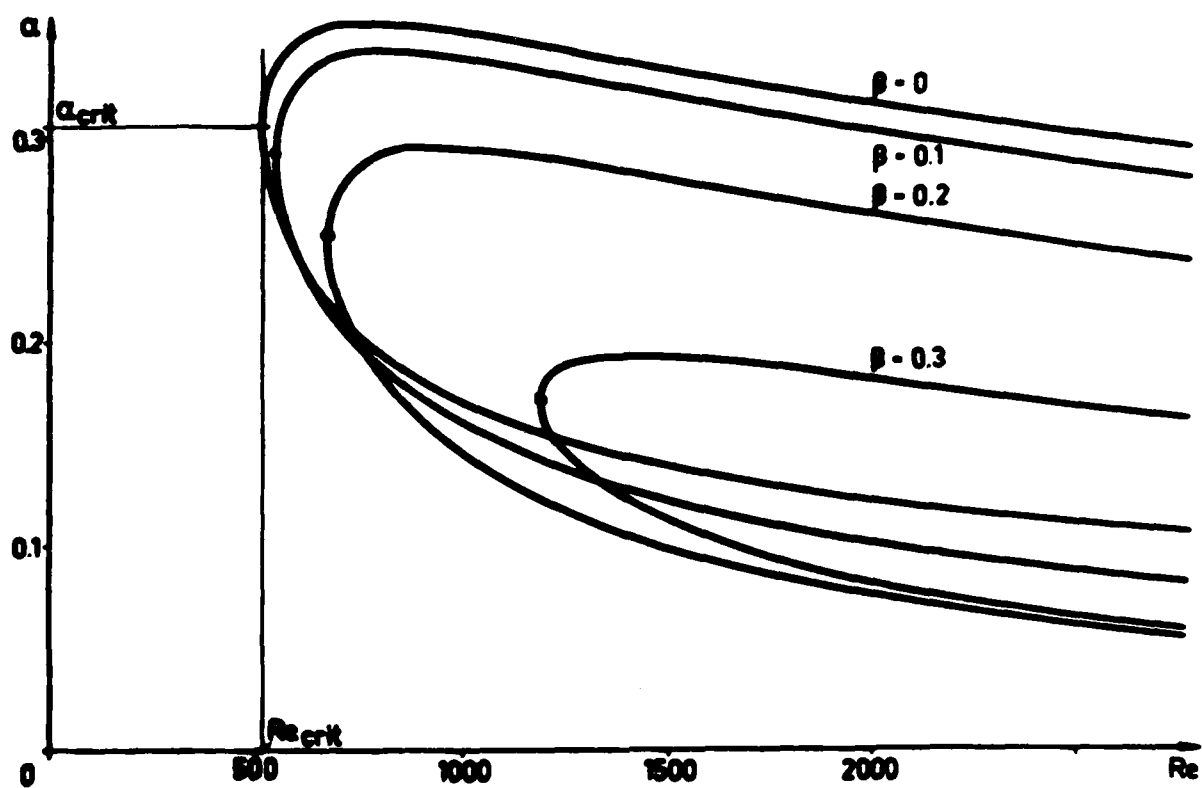
Fig 0-18   Flat-plate neutral curves for oblique waves with wave fronts

$$\alpha x + \beta z - \omega t = \text{const.}$$
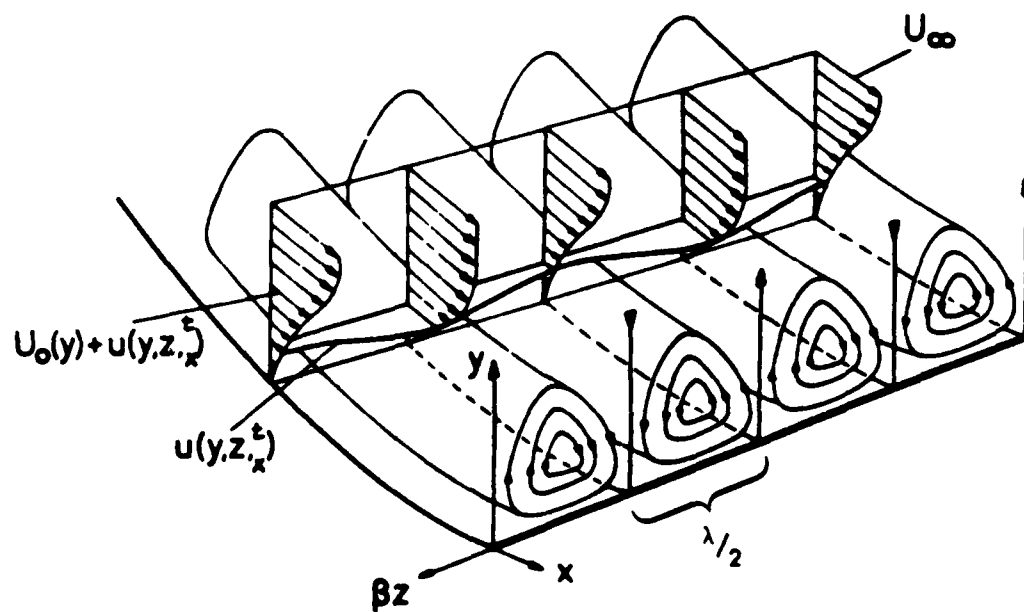
Fig 0-21 Görtler   instability pattern in concave boundary layers.
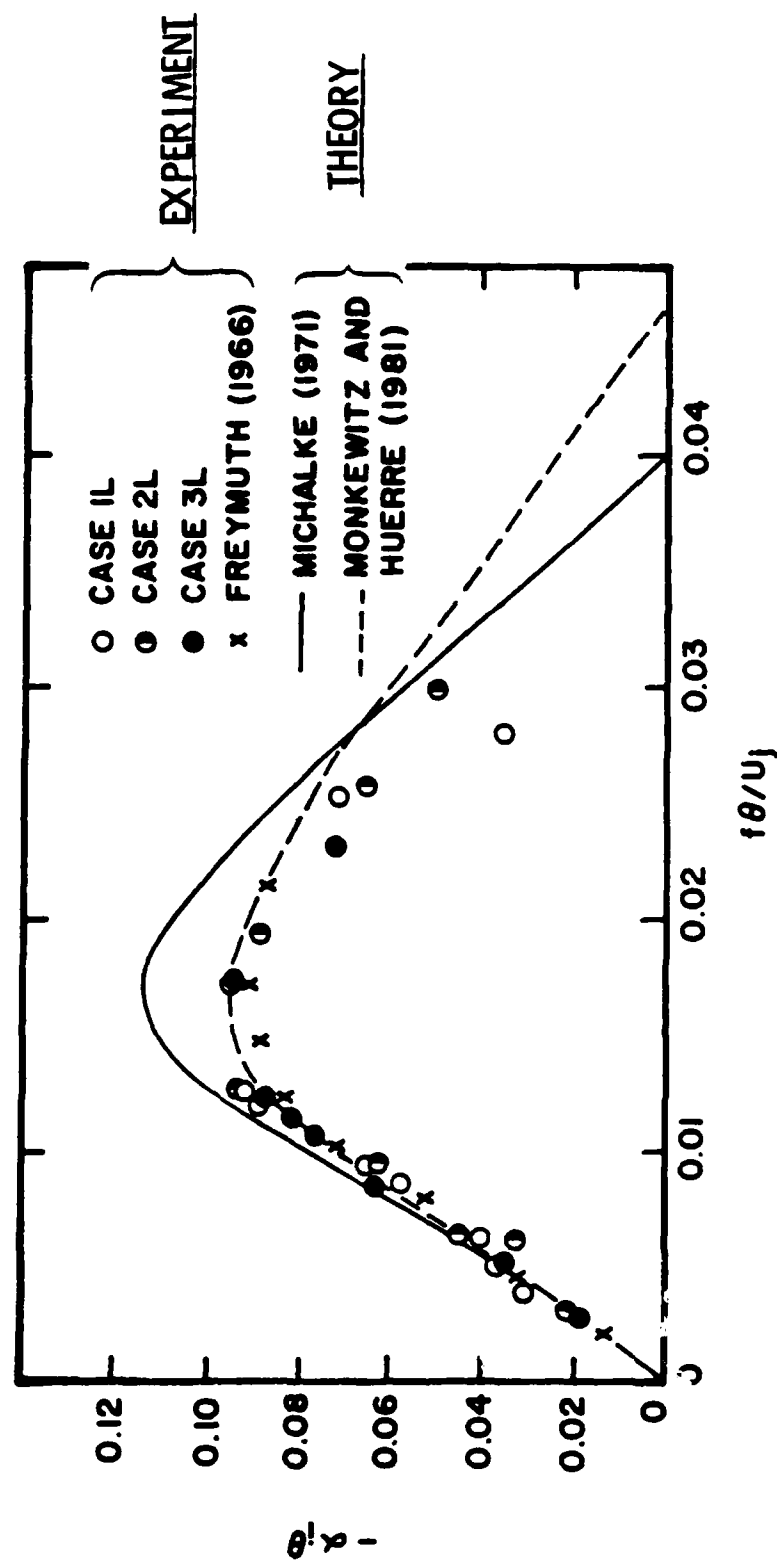
Fig 0-19 Experimental spatial growth rates in mixing layers:
quasi-parallel theory for $U = a \tan h\, y$: ———
and Blasius profile: - - -
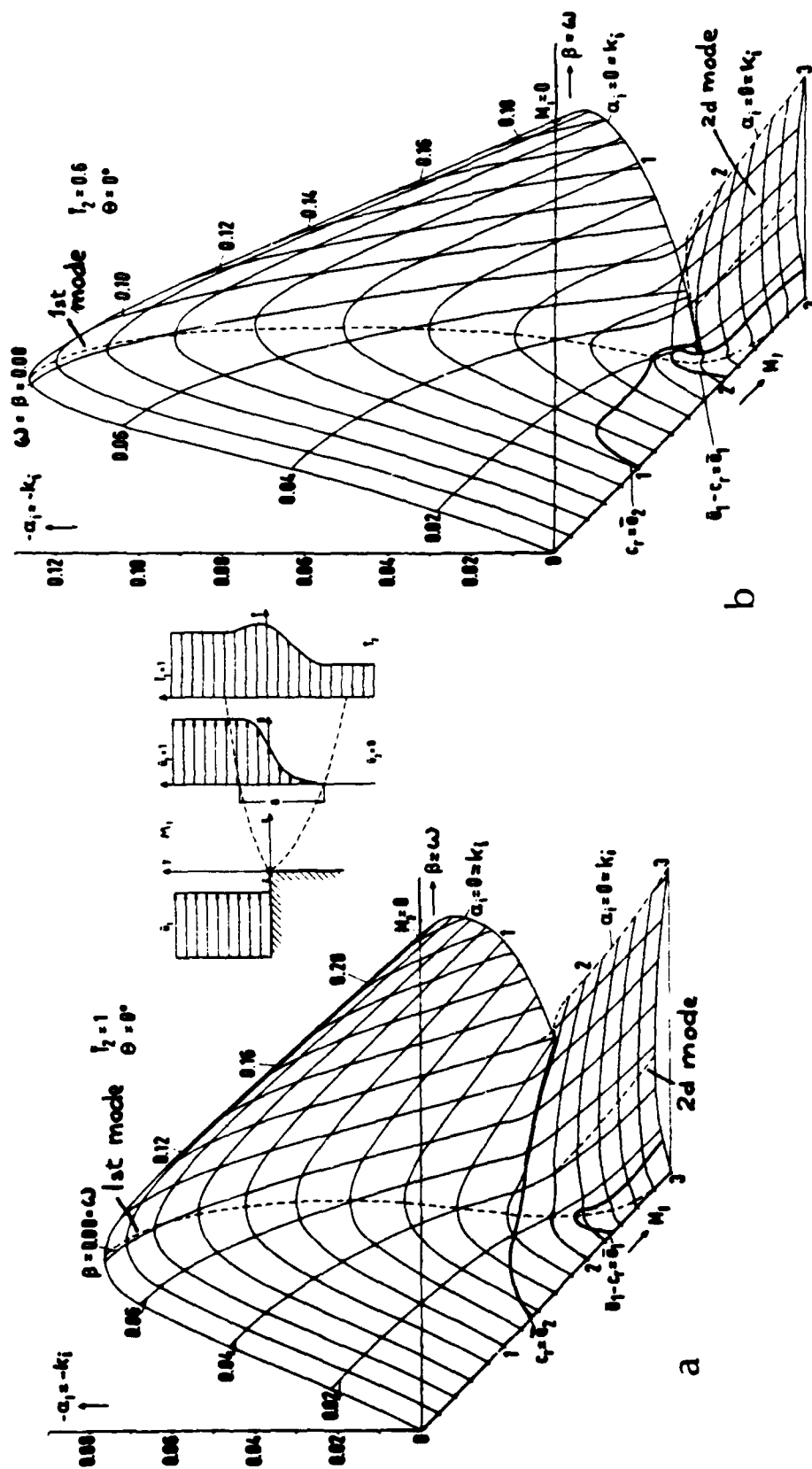
Fig 0-20   Gropengiesser's spatial amplification of inviscid instabilities for laminar
mixing layers: (a) without cooling, $T_2/T_1 = 1$;   (b) with cooling, $T_2/T_1 = 0.6$
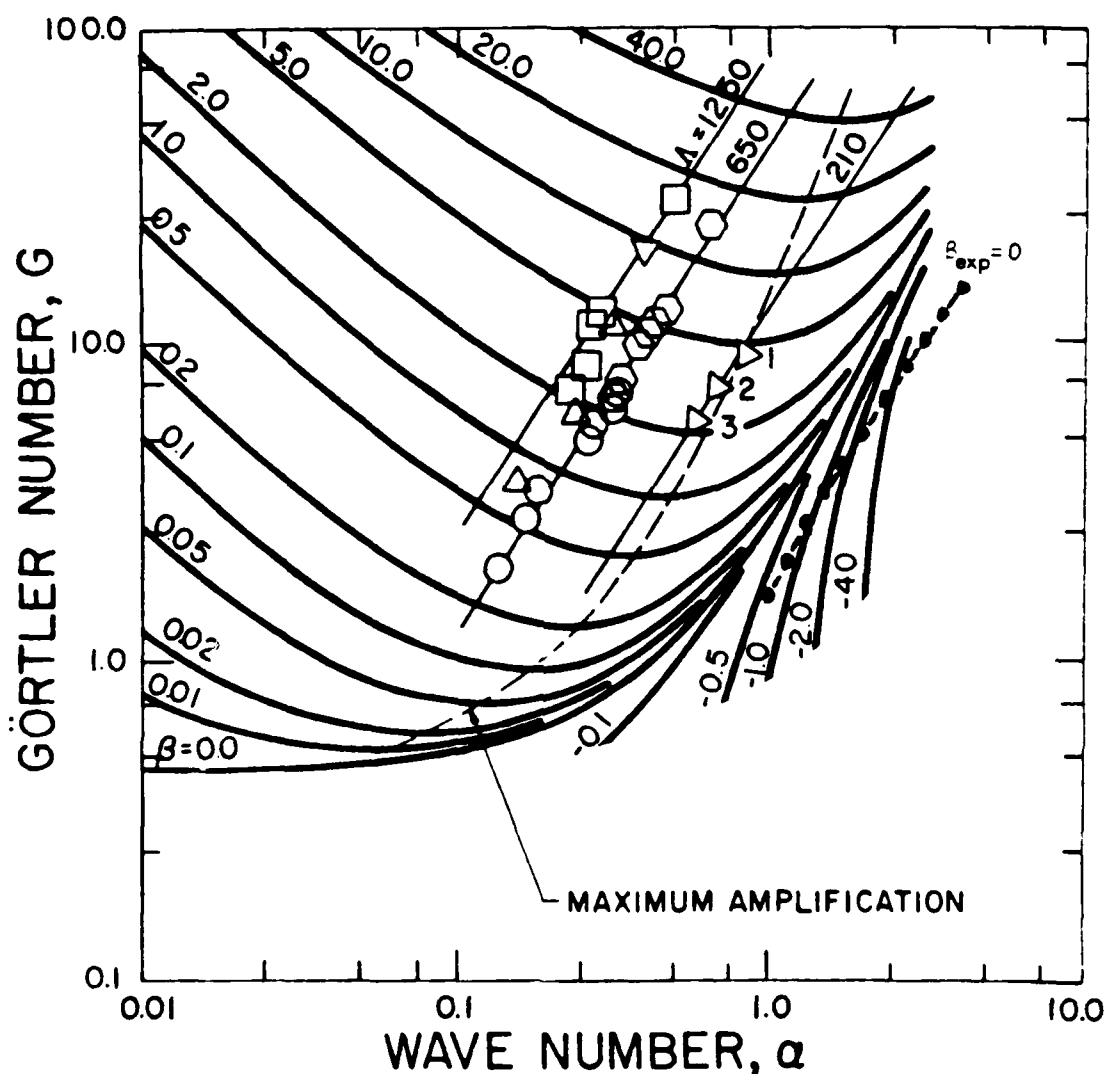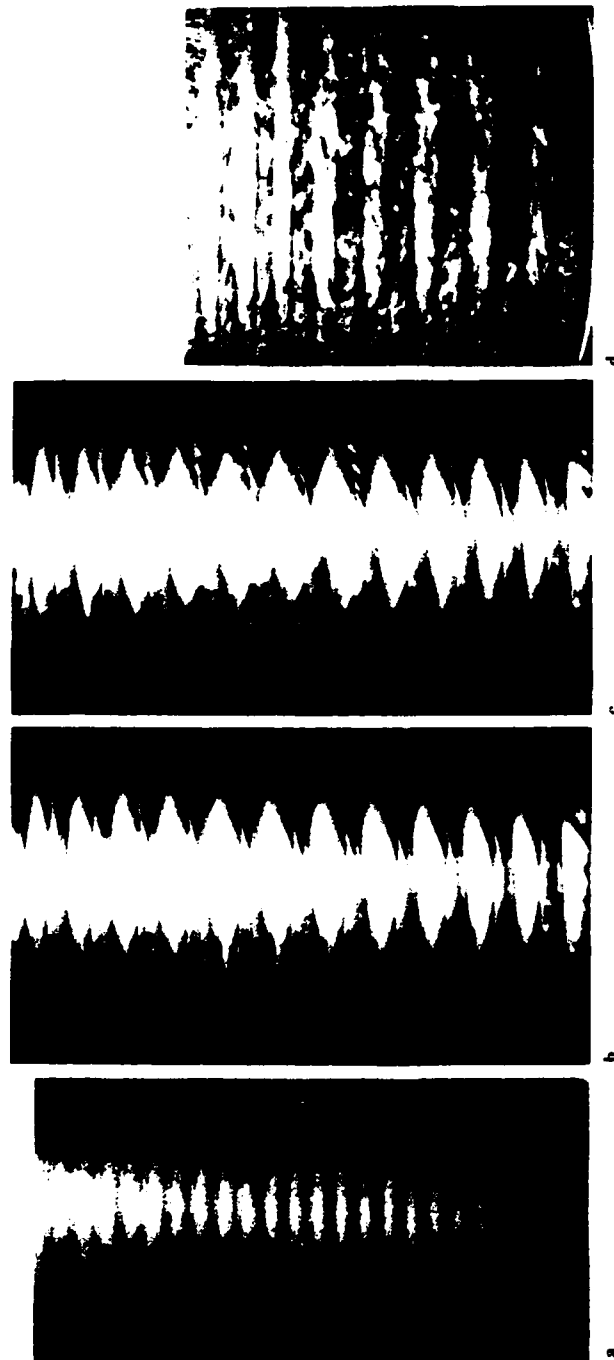
Fig 0-22 Curves of constant amplification rate as a function of Görtler number, $G = U_\infty \delta_r / \nu \sqrt{\delta_r/R}$, and wavenumber, α, for the Blasius boundary layer.   Comparison of theory with experiments: Experimental points due to Tani & Sakagami : $\bigcirc$ - U_∞ = 11 m/s, R = 10 m; $\square$ - U_∞ = 7 m/s, R = 5 m; $\bigcirc$ - U_∞ = 7 m/s, R = 3 m; $\triangle$ - U_∞ = 16 m/s, R = 10 m; ∇ - U_∞ = 7 m/s, R = 1 m. Experimental points due to Bippes : $\triangleright$ 1 - U = 0.3 m/s, R = 0.5 m; $\triangleright$ 2 - U = 0.075 m/s, R = 0.5 m; $\triangleright$ 3 - U_∞ = 0.075 m/s, R = 1.0 m.

Photographs of the flow between concentric cylinders with the inner cylinder rotating. (The radius ratio is 0.88.) **(a)** $R > R_c$: Taylor vortex flow. **(b)** $R/R_c = 10.4$: wavy vortex flow. **(c)** $R/R_c = 12.3$: the "first appearance of randomness" in wavy vortex flow. **(d)** $R/R_c = 23.5$: the azimuthal waves have disappeared and the flow is turbulent, although the axial periodicity remains. The visualization of the flow in these experiments was achieved by suspending small flat flakes in the fluid; the flakes align with the flow, and variations in their orientation are observed as variations in the transmitted or reflected intensity.
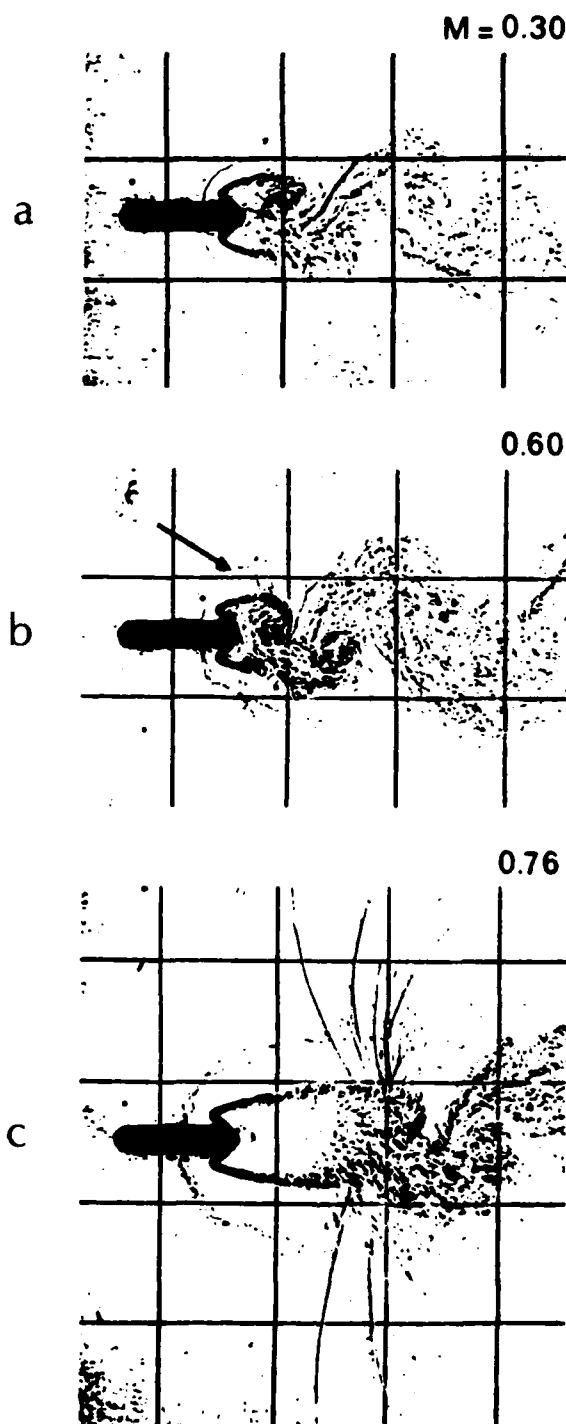
Fig 0-23 Visual evidence of successive instabilities collated by R.C.DiPrima and H.L. Swinney from E.L. Koschmieder(a); D. Coles (b,c); and P.R. Fenstermacher, H.L. Swinney, and J.P. Gollub (d). (Courtesy of Springer Verlag)

Fig 0-24   Mach number inhibition of upstream influence in a self-excited wake
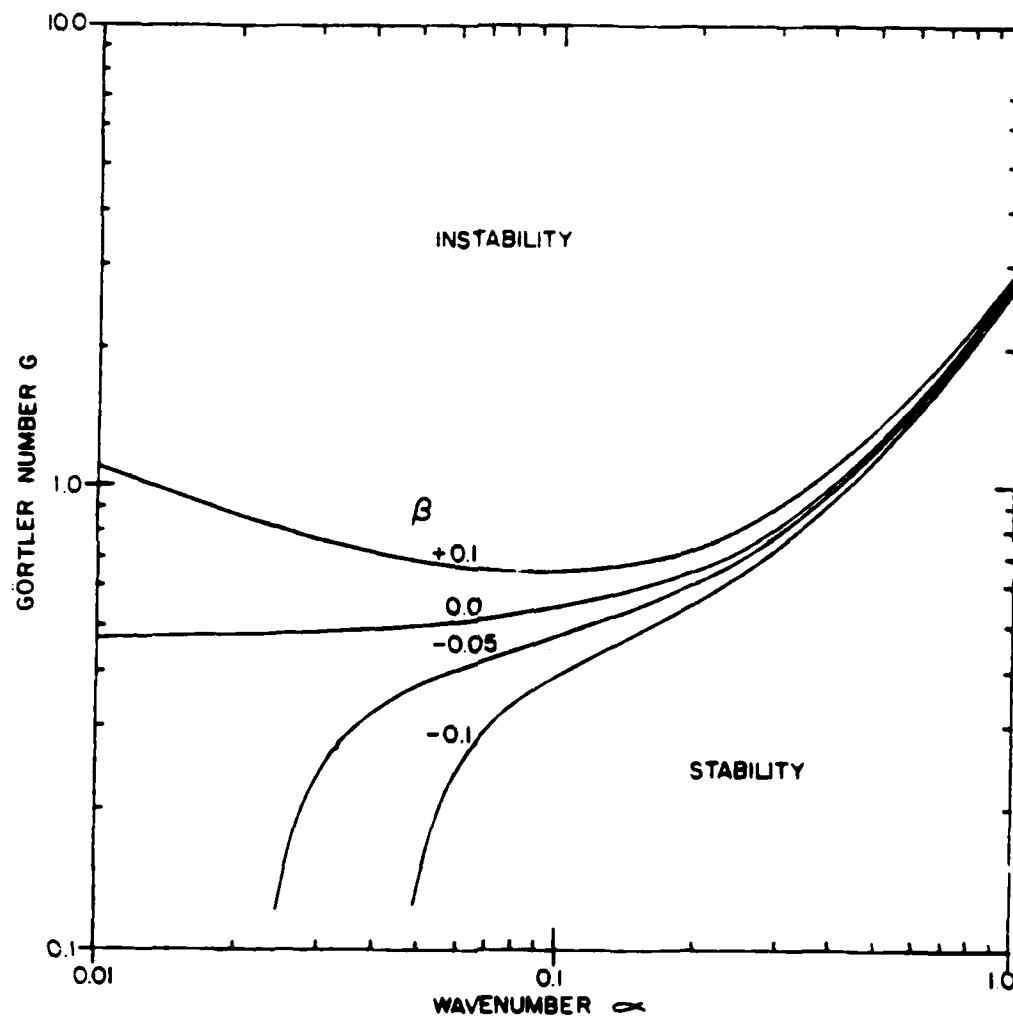generated by a flat plate normal to the stream.

M = 0.30

a

0.60

b

0.76

c

Fig 0-25   Neutral curves of Görtler instability for the
            Falkner-Skan boundary layers with parameter β.

END

FILMED

12-83

DTIC